Exploring Uranium Hexafluoride Material Distributions in 30B Cylinders with Center of Gravity Measurements

A Dissertation Presented for the

Doctor of Philosophy

Degree

The University of Tennessee, Knoxville

Scott Lawrence Stewart

May 2020

© by Scott Lawrence Stewart, 2020
All Rights Reserved.

Acknowledgments

I would like to thank the many researchers who have been involved in and supported this work. In particular, I would like to call attention to the significant intellectual contributions of James R. Garner. Mr. Garner is an unattended systems expert who has been a mentor to me the past 5 years. He was primarily responsible for the hardware, mechanical, and electrical design of the weight measurement system. Mr. Garner is also a load cell expert and contributed to and frequently discussed viable approaches to correct for zero load shifts over the course of time with me. This dissertation would not be possible without his guidance and support.

Other researchers have advised me on best practices and technical considerations for various portions of this project. Dr. Stephen Croft is a physicist with significant experience handling uncertainty quantification in measurement systems, and he provided suggestions on the best approaches to take in quantifying the uncertainty for a platform scale. Dr. Bonnie Canion is a nuclear engineer who has performed an extensive review of the historical record of UF_6 material distribution inside a cylinder, and she was willing to discuss her work and point me toward additional resources. Mark Adams is a computer scientist who provided suggestions on the design of the data analysis pipeline that I created for this work, and Nathan Martindale is a computer science graduate student from Tennessee Tech University who wrote a data analysis dashboard in Jupyter notebook that has helped significantly with data exploration.

I would also like to thank my committee members who graciously sacrificed their personal time to listen to me present, offer advice and suggestions, and aid in the completion of my dissertation work. This includes my committee chair, Dr. Jamie Coble,

as well as members Dr. Lawrence Heilbronn, Dr. Pradeep Ramuhalli, and Dr. Catherine Schuman.

Finally, I would like to thank my spouse, Elena Stewart. My pursuit of a doctoral degree while continuing to work full-time has required patience from her when I'm working on homework or making up hours for work at home. She has been a source of encouragement throughout this process and has provided continuous support ranging from food prep to bribery with baked goods or ice cream to help me stay the course as I worked through this dissertation.

Abstract

The nuclear industry commonly uses uranium hexafluoride (UF_6) in uranium conversion plants, uranium enrichment plants, and fuel fabrication plants. This chemical form of uranium is typically stored in 48Y and 30B cylinders while awaiting processing and in transit between facilities. The behavior of nuclear material inside 48Y and 30B cylinders while they are stored outside for long periods of time is an open question in the nuclear community. This is a difficult thing to measure because of the hazards associated with handling UF_6, particularly its violent reaction with water.

This work uses a force measurement to explore the behavior of UF_6 inside a 30B cylinder over time. A platform scale system with four individually instrumented load cells was used to measure the force applied by the cylinder at each load cell. This information was then used to calculate the center of gravity in two dimensions. The validity of this approach was demonstrated in a laboratory setting, and corrections for sources of uncertainty (e.g., cylinder positioning and rotation) were developed to improve the ability to compare measured values.

The experimental measurements collected by the platform scale system showed that UF_6 does move over time inside a 30B cylinder sitting outside in a storage yard. The data also demonstrated that material movement appears to occur as a result of temperature, providing evidence that sublimation and desublimation occur in a cylinder while it is sitting outside.

Table of Contents

1 Introduction **1**

1.1 Problem Statement 2

1.2 Original Contribution 4

1.3 Organization of the Document 4

2 Background **5**

2.1 Transportation and Storage Cylinders for Uranium Hexafluoride 8

2.2 Behavior of Uranium Hexafluoride Inside 30B and 48Y Cylinders 11

2.3 Weight Measurements of Uranium Hexafluoride in a Nuclear Facility 20

2.4 Scales Used to Measure Uranium Hexafluoride Cylinders 22

2.5 Center of Gravity Measurements with Weight Measurement Systems 24

3 Method **30**

3.1 Force Measurements 32

3.2 Center of Gravity Calculation 35

4 Mathematical Model **37**

4.1 Laboratory Testing 37

4.2 Studying the Effect of Angle 45

5 Experiment **53**

5.1 Measurements 53

5.2 Uncertainty from the Platform Scale 55

5.2.1 Force Transducer Behavior 58

5.2.2 Cylinder Positioning on the Platform 59
5.2.3 Random Error from Electronics 61
5.3 Uncertainty from Differences in Empty 30B Cylinders 62

6 Analysis and Results **64**
6.1 Degree of Rotation of all the Measured Cylinders 64
6.2 Center of Gravity in Empty or Heeled Cylinders 65
6.3 Study of Repeated Cylinder Measurements 70
6.4 Study of the Large Cylinder Population 75
6.4.1 Correlations between Center of Gravity and Quantitative Cylinder Attributes 77
6.4.2 Center of Gravity Values at Different Temperatures 80

7 Conclusion **84**
7.1 Recommendations and Future Work 87

Bibliography **89**

Appendix **96**
A Detailed Plots of Repeated Cylinder Measurements 97

Vita **103**

List of Tables

2.1 Specifications for Standard UF_6 Containing Cylinders from [1] 9

4.1 Laboratory Measurements on the Platform Scale 40
4.2 Load Cell Coordinates in Laboratory Testing 41
4.3 Predicted Versus Measured Values for Laboratory Testing 42

5.1 Coordinates for Each Load Cell in the Platform Scale 54

6.1 Center of Gravity Population Description 77

List of Figures

1.1 UF_6 phase diagram from [2] 2

2.1 UF_6 crystals in a glass vial from [3] 6
2.2 Dimensions of the longitudinal section of a 30B cylinder from [1] 10
2.3 Dimensions of the longitudinal section of a 48Y cylinder from [1] 11
2.4 Probe and computer system used to explore void space inside a 10-ton UF_6 cylinder from [4] 12
2.5 Probe inside the void space of a 10-ton UF_6 cylinder showing material plating the cylinder wall from [4] 13
2.6 Probe inside the void space of a 10-ton UF_6 cylinder displaying UF_6 crystals from [4] 14
2.7 UF_6 crystals dislodged from the solid using a probe from [4] 15
2.8 Hypothetical UF_6 material distribution inside a 10-ton cylinder seen at Portsmouth Gaseous Diffusion Plant from [4] 15
2.9 Reconstructed images of measurements at various locations of a 12B cylinder using APNIS from [5] 17
2.10 UF_6 Cylinder filling profiles for modeling studies expressed as an “X-Factor” 18
2.11 A recreation of a hypothetical UF_6 cylinder filling profile for liquid cooling and some desublimation cases as proposed in [6] 19
2.12 Two process systems for heating UF_6 20
2.13 Two examples of platform scales 22
2.14 Schematic of a load cell system for use under an overhead crane from [7] . 23

2.15 A traditional three-point platform scale design for measuring center of gravity as explained in [8] . . . 27

3.1 Top-down view of a 30B cylinder with reference axis shown for positive x and positive y and nomenclature for each corner of the cylinder . . . 31
3.2 Front view of a 30B cylinder with an angle, θ, shown as the angle between a line perpendicular to the ground and the bottom edge of the cylinder nameplate from [9] . . . 31
3.3 Top-down schematic of the platform scale used to measure 30B cylinders with load cells indicated by blue circles . . . 32
3.4 Wheatstone bridge circuit . . . 34

4.1 Laboratory testing scale with cutaway 30B cylinder on top . . . 38
4.2 Laboratory testing scale with test weights stacked at two locations . . . 39
4.3 MDM mass segmentation scheme used for modeling laboratory testing . . . 40
4.4 Laboratory testing results compared to predicted values for center of gravity in the x and y axes . . . 43
4.5 Cylinder filled through desublimation from gaseous UF_6 to solid UF_6 rotated about θ . . . 46
4.6 Cylinder filled through liquid UF_6 cooling to solid UF_6 rotated about θ . . . 46
4.7 The 40% void space of a cylinder bounded by an isosceles triangle . . . 48
4.8 30B cylinder rotated about ϕ . . . 50
4.9 Plot of the relationship between y and θ from 0° to 360° of rotation . . . 52

6.1 Distribution of θ in measured full 30B cylinders . . . 65
6.2 Center of gravity in x and y for empty and heel cylinders . . . 66
6.3 Measured θ for empty and heel cylinders . . . 68
6.4 Empty and heel cylinders from one manufacturer . . . 69
6.5 x and y center of gravity measurements for the same cylinder over 45 min. 71
6.6 Changes of the center of gravity in x over 4 months for four cylinders . . . 73
6.7 Changes of the center of gravity in y over 4 months for four cylinders . . . 74

6.8 Center of gravity values for the entire cylinder population 76
6.9 Heat map of correlations of known quantitative cylinder parameters 79
6.10 Center of gravity in x and y for temperatures from -3.0 to 13.0°C 81
6.11 Center of gravity in x and y for temperatures from 13.0 to 21.0°C 81
6.12 Center of gravity in x and y for temperatures from 21.0 to 27.0°C 82
6.13 Center of gravity in x and y for temperatures from 27.0 to 41.0°C 82
6.14 Standard deviation in x and y plotted versus the temperature midpoint for each subpopulation 83

A.1 Short-term repeat measurements of cylinder 13 98
A.2 Long-term repeat measurements of cylinder 26 99
A.3 Long-term repeat measurements of cylinder 65 100
A.4 Long-term repeat measurements of cylinder 66 101
A.5 Long-term repeat measurements of cylinder 67 102

Chapter 1

Introduction

Uranium hexafluoride (UF_6) is a material commonly found in the nuclear fuel cycle, specifically at uranium conversion plants, uranium enrichment plants, and fuel fabrication facilities. Typically, 30B cylinders are used to store "product" uranium that has been enriched up to 4.95% of ^{235}U content by an enricher, whereas 48Y cylinders are used to store both natural and depleted UF_6. 30B and 48Y cylinders are certified pressure vessels that can withstand both extremely high and low temperatures needed to convert the UF_6 in the cylinder from a mostly solid form to a gaseous state before it is used in a process. New cylinders are constructed according to the American National Standards Institute (ANSI) N14.1-2012 standard, although it is common for older 30B and 48Y cylinders manufactured to earlier versions of the ANSI standard to be present at a nuclear facility [1].

Nuclear experts speculate about the distribution of UF_6 in both 30B and 48Y cylinders. The distribution of UF_6 in 30B cylinders can depend on a variety of factors including the process used to place UF_6 in the cylinder as well as where the cylinders have been stored. The speculation in the community revolves around the behavior of the material inside these cylinders while they are stored outdoors in cylinder yards and are subject to wide swings in ambient temperature during the year. In some facilities, these cylinders could reasonably be subjected to a range of temperatures from freezing to well over 100°F. Based on the phase diagram in Fig. 1.1, it has been theorized that some of the UF_6 inside the cylinder would sublime and desublime over the course of the year as the

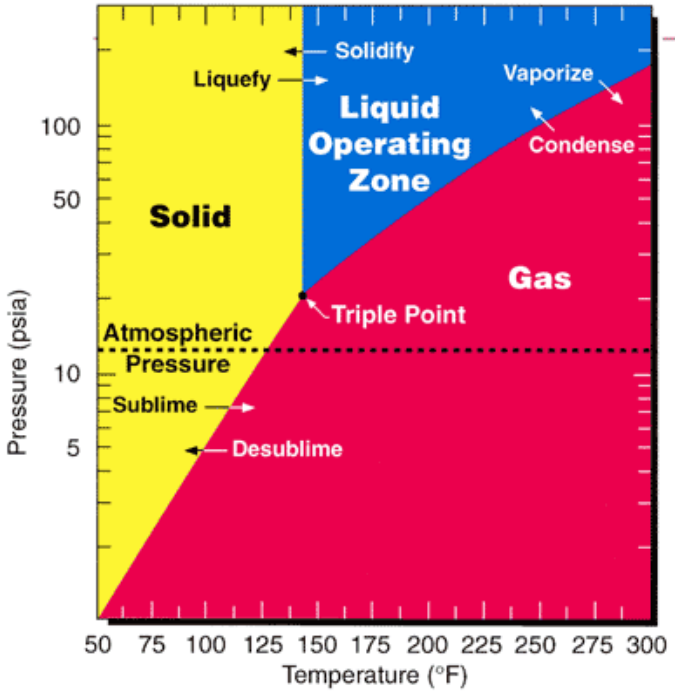


Figure 1.1: UF_6 phase diagram from [2]

ambient temperature changes. There is also speculation that a cylinder might sublime and desublime over the course of a day as the cylinder is heated by direct sunlight. This could result in the distribution of the UF_6 inside the cylinder changing from when it is initially filled to when that material is eventually used in another process or converted to a different chemical form of uranium.

Although there are several hypotheses about the distribution of UF_6 within 30B and 48Y cylinders, as well as about how the distribution may behave over time when stored outside, very little measured data exists to support any single theory. Understanding how UF_6 is distributed in 30B and 48Y cylinders over time would improve the accuracy of nondestructive assay measurements used to quantify the uranium in the cylinder and might provide additional information that could be useful for facility operations.

1.1 Problem Statement

This work uses a weight measurement system to ascertain information about the distribution of UF_6 in a 30B cylinder. Specifically, four load cells were individually

instrumented to measure values proportional to the force applied to each load cell so that the center of gravity in one plane of a 30B cylinder could be calculated. Weight measurement systems are commonly used in nuclear facilities to perform gross weight measurements. Facility operators use that information in conjunction with the tare weight of the 30B cylinder to calculate the net weight of UF_6 in each cylinder. This information is tracked to help a facility account for all of its nuclear material; to maintain the safety basis of the facility, which helps operators avoid criticality safety accidents; and for commercial accounting purposes. Weight measurement systems are not the ideal way to determine the distribution of UF_6 in a cylinder. Placing a borescope through the cap of the cylinder to capture images or using an active interrogation radiation measurement system to reconstruct an image of the inside of the cylinder would provide information about the distribution of material in all three dimensions. However, weight measurement systems are commonly used by facility operators and exist at every nuclear facility, so it is easier to gain operator acceptance to use weight measurement systems, and existing scales at nuclear facilities could plausibly be modified to measure the center of gravity of each cylinder.

By using a weight measurement system, we will answer the following research question:

> *What information can we learn about the distribution of UF_6 in a 30B cylinder by instrumenting a weight measurement system to get information about the force applied to each load cell?*

This effort includes using a mathematical model in conjunction with laboratory testing with known weights to better understand how the center of gravity relates to the distribution of material inside a cylinder. Then, data collected from 240 30B cylinders measured over several months will be analyzed to better understand what trends or patterns might be discerned. This research question is also relevant for 48Y cylinders, but this work focuses on 30B cylinders because that cylinder type is the only type that was measured during the measurement campaign.

1.2 Original Contribution

This work makes two original contributions to the nuclear field related to measuring 30B cylinders and understanding the distribution of UF_6 inside the cylinder. This project

- creates a center of gravity data set that gives some information on the UF_6 distribution inside a 30B cylinder for a large population of cylinders and
- analyzes the center of gravity data to understand what it might indicate about how the distribution of material inside 30B cylinders changes over time.

1.3 Organization of the Document

Chapter 2 of this document reviews the relevant background literature for this project including a discussion of different types of storage cylinders for UF_6, a review of published information on the behavior of UF_6 inside 30B and 48Y cylinders, a survey of other work with weight measurement systems used to measure UF_6, and finally a review of other center of gravity measurement systems. Chapter 3 discusses the physical mechanism used to quantify the force applied to a load cell as well how to compute the center of gravity. Chapter 4 demonstrates that the center of gravity can be used to find the material distribution in 30B cylinders by comparing a mathematical model for finding the center of gravity with laboratory measurements. This chapter also derives a correction factor for the rotation of a cylinder. Chapter 5 discusses the experimental 30B cylinder measurements as well as various sources of uncertainty. Finally, Chapter 6 discusses the center of gravity analysis results.

Chapter 2

Background

Uranium hexafluoride, UF_6, is a chemical form of uranium that is primarily found at enrichment plants in the nuclear fuel cycle, but it is also found at uranium conversion plants and fuel fabrication plants. This is the preferred chemical form of uranium for use at enrichment plants because fluorine only has one natural isotope, so all the isotopic separative capacity of the enrichment process of the plant can be used to enrich the uranium concentration from 0.711% ^{235}U in natural uranium to around 3% typically needed for light water reactors to operate. [10], [11]

UF_6 is also desirable for enrichment plant operators because it is possible to change the phase of the material at relatively low temperatures and pressures, which reduces the energy required to use UF_6 in processing operations when compared to other chemical forms of uranium. Specifically, this attribute allows operators to use less energy to change the phase of UF_6 from solid while in storage to liquid or gas for feeding into the start of a process, and reduces the energy cost of converting the process gas back to a solid. [10]

The appearance of UF_6 can change depending on the process used to convert the substance from another phase to the solid phase. It will appear as seen in the vial in Fig. 2.1 when it is formed by freezing UF_6 from the liquid phase. If it is desublimed from the vapor phase instead, the UF_6 will be a solid formless mass without any noticeable irregularly shaped grains. [10]

When at room temperature, UF_6 gas reacts with water vapor in humid air according to the reaction in Equation 2.1 [12]. The resulting products from this reaction are a water

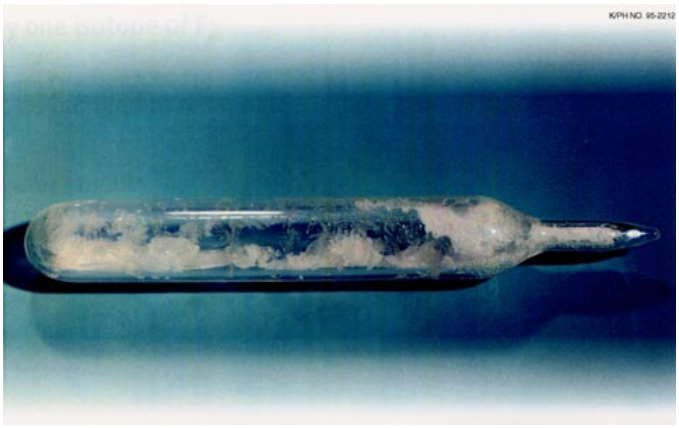


Figure 2.1: UF_6 crystals in a glass vial from [3]

soluble yellow solid containing UO_2F_2 and a visible white cloud that contains water and HF [10], [12].

$$UF_6 + 2H_2O \rightarrow UO_2F_2 + 4HF \uparrow \tag{2.1}$$

The uncontrolled release of UF_6 gas to the atmosphere is a significant health hazard to both plant personnel and the general public if it occurs. HF gas can cause burns on the skin and damage the lungs and kidneys, and the UO_2F_2 particulates are a heavy metal compound that is toxic to the kidneys if it is inhaled or ingested [10]. UF_6 can also react violently with hydrocarbon oil at elevated temperatures, and it is very corrosive to some metals. Once a fluoride film develops on the metal, UF_6 does not react with Al, Cu, Monel, Ni, and aluminum bronze.

UF_6 will react with steel, but using steel containers for transportation and storage of UF_6 is considered safe because the reaction is limited to only the internal layers of the cylinder [12]. One study destructively analyzed two different 30A steel storage cylinders to determine whether or not this hypothesis was correct. Tokens taken from the inside of these steel cylinders showed that the deposition of residual uranium can be significant over the entire cylinder (up to 5.5 kg in one cylinder), but the deposits typically only impacted steel on the inside cylinder from around 10 µm of depth in the newer cylinder to around 100 µm of depth in the older cylinder. The study also observed that poor washing

practices for a cylinder over time would increase both the residual deposit size of uranium in the cylinder as well as the depth of the UF_6 penetration of the inside wall of steel. [13]

Other than criticality safety concerns, UF_6 handling in a facility is done in a manner consistent with the handling of other corrosive or toxic chemicals [12]. Safety practices for UF_6 in a facility include always processing the material in leak-tight containers, equipment, or piping to limit the possibility of any interactions with water or hydrocarbons. Leak-tight containers do not contain view ports, which it would introduce more seals that might allow water to leak into the process piping, so images or videos of UF_6 in various states inside process equipment or storage cylinders are not very common. These handling restrictions also mean that discovering material distributions of UF_6 inside both process equipment or storage containers requires specific procedures and controls to ensure that the material inside the container is not exposed to anything it might react with. [10]

There have been accidents involving UF_6 in nuclear facility process equipment. One accident occurred in 1987 at the German Reaktor-Brennelement Union uranium conversion facility in Hanau, Germany. A small leakage of UF_6 in the valve of an evaporation autoclave at the facility started the accident sequence. This eventually lead to UF_6 reacting with water in an evacuation pump and creating a buildup of UO_2F_2. Eventually this buildup caused pressure to increase enough in a flexible tube that the tube ruptured and released UF_6 into the plant. In this incident, all of the UF_6 that was released was contained within the process building, and there was no injury to personnel or exposure to the public, although all the components in the building were covered with UO_2F_2 after the release. [14]

Several cylinder handling accidents also occurred at U.S. gaseous diffusion plants when they were operational. One accident occurred when hydrocarbon oil was introduced into a 30A cylinder containing hot liquid UF_6 by a faulty vacuum pump at the Oak Ridge Diffusion Plant. This resulted in a release of energy that blew the nameplate off the cylinder and released a small amount of UF_6. Another incident occurred when a 48 in. diameter cylinder with liquid feed material was being moved between a sampling area and a cooling yard at the Portsmouth Gaseous Diffusion Plant in Pike County, Ohio. The

weight inside the cylinder shifted as it was being lowered, and the cylinder was dropped about 10 in. This resulted in the release of all of the UF_6 inside the cylinder. [12]

2.1 Transportation and Storage Cylinders for Uranium Hexafluoride

When not in process, UF_6 is commonly stored in certified pressure vessels made of steel, nickel, or a nickel–copper alloy [10]. ANSI standard N14.1 defines the specifications for a set of certified cylinder types, details how to construct them, and states important limits on the maximum amount of material allowed in each type of cylinder as well as the maximum enrichment of the material [1]. Table 2.1 is taken from Table 4 of ANSI N14.1-2012 with weights converted to kilograms to illustrate the different types of UF_6 cylinders as well as the full range of sizes, enrichments, and amounts of material allowed in each type [1].

Cylinder safety limits for quantity of material and enrichment of the material are imposed to prevent criticality accidents or cylinder ruptures. Cylinder ruptures are possible because there is a large expansion in the amount of space a given mass of UF_6 occupies as it transitions from the solid to liquid phase [12]. A cylinder could be overfilled if filling occurs by desublimation of the material from the vapor phase. Subsequent heating of the cylinder would then result in the mass of solid UF_6 increasing in volume by 53% once it fully transitions to the liquid phase, which could result in a hydraulic deformation and rupture of the cylinder [10].

30B and 48Y cylinders are the most commonly transported cylinder types today and make up a majority of the cylinders at most nuclear facilities with UF_6, although the ANSI standard does specify designs for other cylinder types to carry small samples or higher enrichments of UF_6. Other cylinder types might still be present at older nuclear facilities, in particular at the United States Enrichment Corporation gaseous diffusion plants that are currently being decommissioned. At these facilities it is common to see older 48 in. diameter cylinders containing depleted uranium, specifically types 48G, 48H, 48X, 48O,

Table 2.1: Specifications for Standard UF_6 Containing Cylinders from [1]

Model no.	Diameter (in.)	Material of construction	Approximate tare weight (kg)	Maximum enrichment (wt % ^{235}U)	Maximum fill limit (kg UF_6)
1S	1.5	Ni or Ni–Cu alloy	0.79	100	0.5
2S	3.5	Ni or Ni–Cu alloy	1.9	100	2.2
5A	5	Ni or Ni–Cu alloy	25	100	24.9
5B	5	Ni	25	100	24.9
8A	8	Ni or Ni–Cu alloy	54	12.5	116
12A	12	Ni	84	5	209
12B	12	Ni or Ni–Cu alloy	84	5	209
30B, 30C	30	Steel	635	5	2,277
48A, 48X	48	Steel	2041	4.5	9,539
48F	48	Steel	2,359	4.5	12,261
48Y	48	Steel	2,359	4.5	12,501
48T	48	Steel	1,111	1	9,390
48O	48	Steel	1,202	1	11,825
48OM Allied	48	Steel	1,383	1	12,261
48OM	48	Steel	1,202	1	11,825
48H, 48HX	48	Steel	1,474	1	12,261
48G	48	Steel	1,202	1	12,175

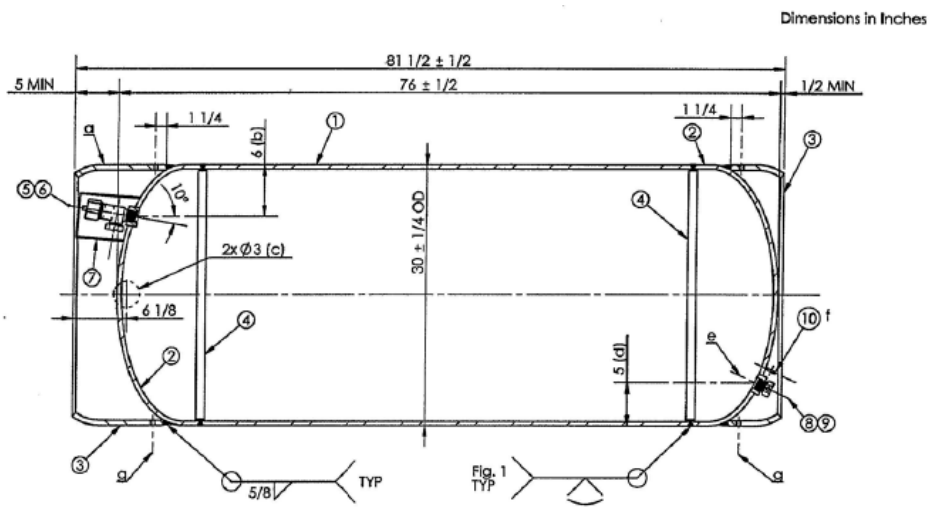


Figure 2.2: Dimensions of the longitudinal section of a 30B cylinder from [1]

and 48OM [15]. Other cylinder types, such as the 30A cylinder, may exist at older nuclear facilities but have been removed from the 2012 version of the ANSI standard [16].

One reason why older cylinders tend to continue to store material at nuclear facilities is because of how the ANSI N14.1 standard defines its inspection requirements. In the standard, all UF_6 cylinders must be inspected every 5 years "except those already filled at the 5 year expiration date [1]." This means that older cylinders commonly stay in use for long periods of time because they can continue to sit in cylinder storage yards for many years without receiving a certification inspection if they are not being shipped or used in the facility process.

The dimensions of the longitudinal side of a 30B cylinder typically used for the product materials after UF_6 has been enriched can be seen in Fig. 2.2. In this figure, the 1 is pointing to the shell of the pressure vessel, which is $1/2$ in. thick steel. The internal dimensions of the cylinder from this figure are the other main feature to note. Generally a $1/16$ in. tolerance is allowed on the dimensions shown in the figure other than on the dimensions of the pressure envelope. Also, angles in the figure have to be accurate within 2°.

The longitudinal section of the other main cylinder in use in facilities today, the 48Y, can be seen in Fig. 2.3. These cylinders are typically used to hold either feed material

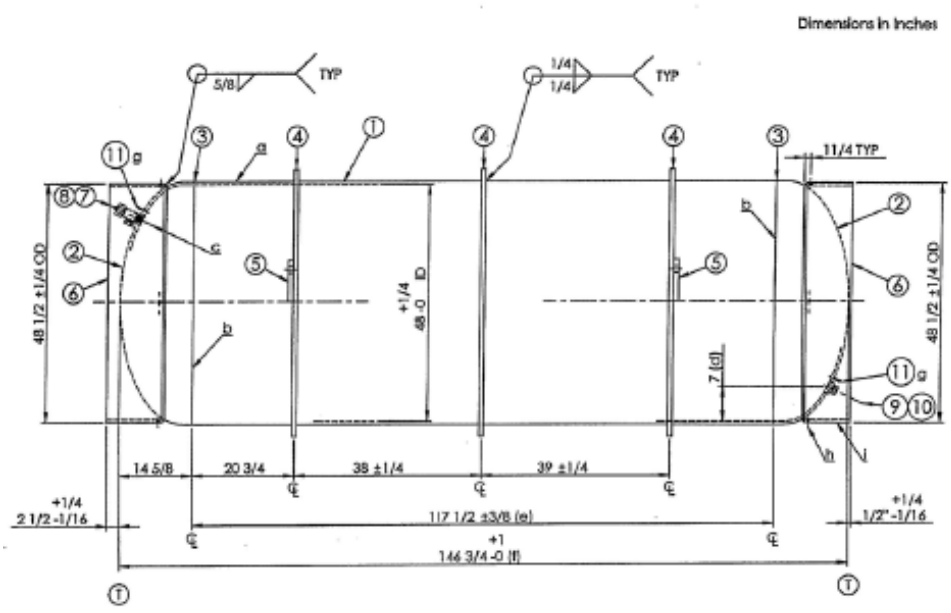


Figure 2.3: Dimensions of the longitudinal section of a 48Y cylinder from [1]

at natural enrichments or depleted uranium that has a reduced isotopic concentration of ^{235}U. Some facilities also use 48Y cylinders to hold product material enrichments, but this is not allowed for shipping off-site. These cylinders have a shell that is $5/8$ in. of steel. The final cylinder can be built to within a tolerance of $1/16$ in. or 2° again with the exception of the pressure envelope thickness, which must be as specified within the ANSI standard.

2.2 Behavior of Uranium Hexafluoride Inside 30B and 48Y Cylinders

Because UF_6 is a corrosive, toxic chemical, special handling procedures are required to examine the inside of a UF_6 cylinder. These restrictions have severely limited the number of studies that have taken measured data on the distribution of UF_6 inside 30B and 48Y containers, especially over time. However, it is known that the appearance of solid UF_6 depends on the method used to create that solid, as the solid tends to have irregularly shaped grains when it is formed by freezing UF_6 from the liquid phase and is known to



Figure 2.4: Probe and computer system used to explore void space inside a 10-ton UF_6 cylinder from [4]

have no noticeable irregularly shaped grains when it is desublimed from the vapor phase [10].

One notable study was performed at the Portsmouth Gaseous Diffusion Plant in 1993. As part of this effort, material handlers inserted a special camera into a full 10-ton UF_6 cylinder to examine the distribution of the solid material. This feed cylinder was created by filling 95% of the interior volume of the cylinder with liquid UF_6 at 160°F. After freezing, the cylinder was cooled for 5 days before it was shipped from the Paducah Gaseous Diffusion Plant in Paducah, Kentucky, to Portsmouth. Once at Portsmouth, a special camera was used to examine the void space above the cooled solid inside the cylinder after it had cooled for 31 days. This camera system is shown in Fig. 2.4. [4]

Once inside the cylinder, the researchers found that there was a continuous "snow-storm" of UF_6 inside the cylinder. They postulated that this was caused by the fact that the inside temperature of the cylinder had not yet fully reached equilibrium with the outside ambient temperature even after 31 days of cooling time, so a small amount of UF_6 was still being vaporized from the surface of the solid and transitioning to the gas phase. It was also hypothesized that the void space tended to be cooler than the surface temperature



Figure 2.5: Probe inside the void space of a 10-ton UF_6 cylinder showing material plating the cylinder wall from [4]

of the solid, so the warmer gas rising from the surface of the solid would eventually cool sufficiently to freeze to a solid UF_6 "snowflake" before settling. [4]

Researchers also found that as the material cooled, it would plate out against the side of the cylinder in a solid line along the walls of the cylinder, but at the head of the cylinder where the valve cap is located, it would have a more irregular shape. They also demonstrated that the material plated against the sides of the cylinder wall was somewhat loose as they were able to dislodge it by hitting the side of the cylinder with a hammer. Fig. 2.5 is an image that was captured inside the cylinder that shows the material plated against the cylinder wall. While inspecting the top of the solid UF_6 in the cylinder, researchers found crystals that were similar to those present on the walls of the cylinder, which led to the hypothesis that crystals are frequently dislodged during cylinder handling. Fig. 2.6 shows some of the UF_6 crystals that were seen inside the cylinder. [4]

Researchers also tested the top of the solid in the UF_6 cylinder to determine whether or not it was soft or hard. To conduct the test, they pulled the camera back in the tube they had inserted into the cylinder and tested whether or not the front portion of the tube could



Figure 2.6: Probe inside the void space of a 10-ton UF_6 cylinder displaying UF_6 crystals from [4]

be used to dislodge some of the solid. They concluded that the material was soft because it could be dislodged with the tube. An image of this experiment is shown in Fig. 2.7. [4]

Based on these experiments, the Portsmouth Gaseous Diffusion Plant researchers hypothesized that the bottom of a cylinder is generally filled with solid UF_6. This solid layer encompasses about 65% of the total internal volume of the cylinder. Typically, the top of this solid layer would contain loose UF_6 crystals that have been dislodged from the walls during handling and/or that have been created based on the heating and cooling effect that created the "snowstorm" seen when the probe was inserted into the void space of the cylinder. The graphic drawn to represent this hypothetical distribution is shown in Fig. 2.8. [4]

One issue with using this video as a basis for hypothesis of cylinders in use today is that the cylinder model was not explicitly stated beyond mentioning it was a 10-ton cylinder. Criticality safety studies performed around the time of this video indicate that the maximum amount of UF_6 inside a so-called 10-ton cylinder was 9,555 kg [17]. Based on Table 2.1 from the ANSI N14.1 standard and the fact that the material under examination

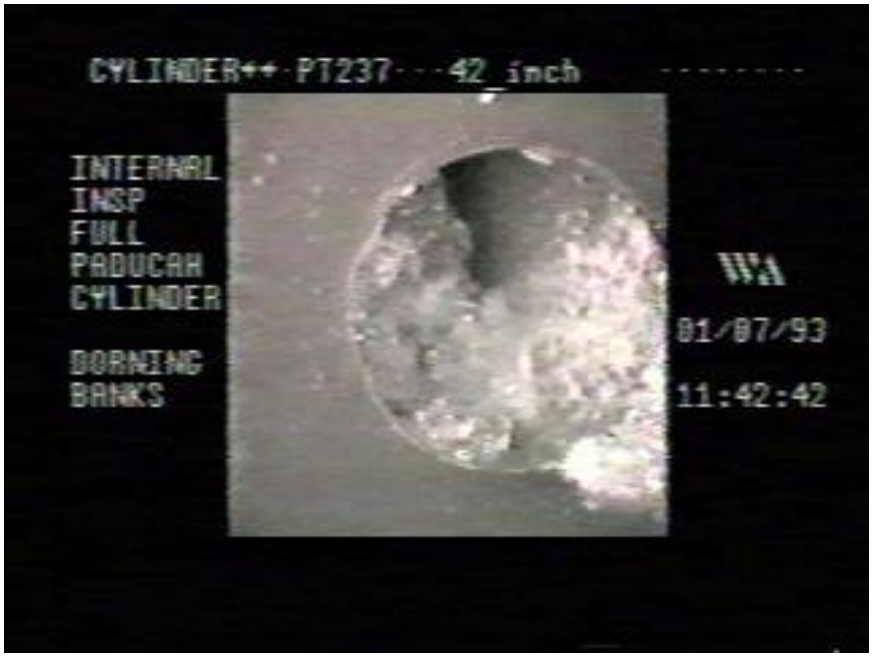


Figure 2.7: UF_6 crystals dislodged from the solid using a probe from [4]

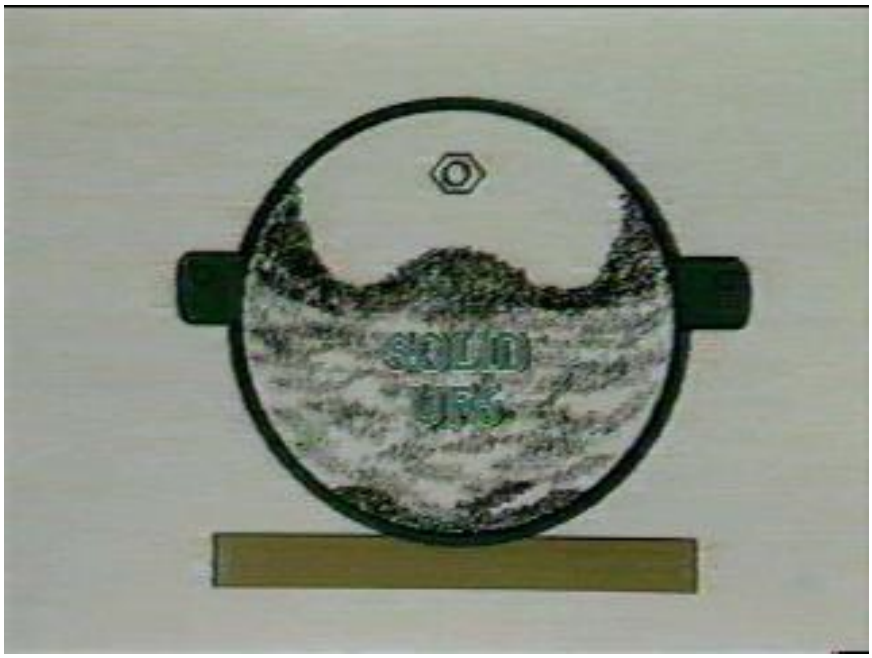


Figure 2.8: Hypothetical UF_6 material distribution inside a 10-ton cylinder seen at Portsmouth Gaseous Diffusion Plant from [4]

had already been slightly enriched at Paducah, it is likely that the cylinder in the video was either a model 48A or a 48X [1].

Another challenge for more broadly applying the findings of this video is that at least some gas centrifuge enrichment plant operators today desublime UF_6 gas directly to the solid phase rather than freezing it from the liquid phase into a cylinder [18], [19], [20], [21]. At a minimum, based on what has been seen in laboratory experiments, it seems reasonable to hypothesize that this would impact the formation of the solid crystals inside the cylinder [10].

There do not appear to be any other publications or videos that use cameras to explore the inside of steel cylinders containing UF_6; however, there is a publication about a fast neutron transmission tomography system that could be used to explore these cylinders without the need to penetrate the void space with a camera. This system, the Advanced Portable Neutron Imaging System (APNIS), interrogates an object with 14 MeV neutrons from a neutron generator. The neutrons incident on the object under interrogation then pass through the item and are scattered or absorbed. Finally, neutrons are measured by an array of neutron scintillators to construct a density map, also called a transmission image, of the object being measured. [5], [22]

As a proof-of-concept demonstration, the APNIS system was used to measure several locations on a 12B cylinder that had been filled and then later drawn down. The 12B cylinder was filled with the long axis of the cylinder pointed in the vertical direction and appears to have been stored that way. Also material in this cylinder was drawn down periodically for use in processing. The resulting cross-sectional images from the study show UF_6 material on the sides of the cylinder but not in the center of the cylinder toward the top of the 12B. In the bottom $1/3$ of the cylinder, material seems to fill more of the center of the cylinder, but a void is still visible (the study authors note that due to the preliminary nature of the study, there is no way to know for certain if this void is real or if it is an artifact of the reconstruction process). Finally, a cross-sectional image from the bottom 10–15% of the cylinder shows that solid UF_6 fills the entire cylindrical space. The reconstructed images at various heights of the 12B taken from this study are shown in Fig. 2.9. [5]

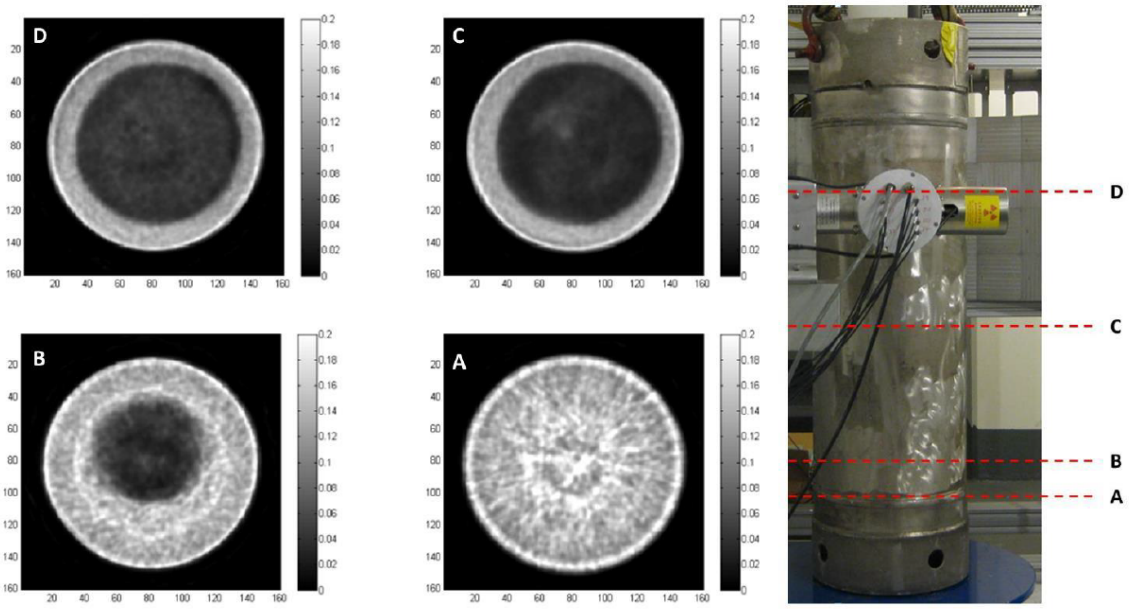


Figure 2.9: Reconstructed images of measurements at various locations of a 12B cylinder using APNIS from [5]

This study is interesting because it seems to confirm that UF_6 has a tendency to plate on the sides of a cylinder, but it is hard to draw any definitive conclusions about the behavior of material in 30B or 48Y cylinders from this work because the handling practices for the cylinders would be rather different. In particular, while a 30B or 48Y cylinder might be filled with the long axis of the cylinder pointed in the vertical direction, it would always be rotated to point the long axis in the horizontal direction with respect to the ground for storage or transport between facilities. Based on the Portsmouth study, this seems likely to cause the material inside the cylinder to redistribute, with some of the material falling from the top to the bottom of the cylinder.

Finally there are a number of modeling studies of UF_6 cylinders, which have been performed in support of the development of nondestructive assay instruments [6], [23], [24]. These studies generally postulate a number of hypothetical material distributions inside a cylinder to explore the sensitivity of the technique to the range of distributions. Fig. 2.10 shows a recreation of the typical mock filling factors used in these studies expressed as a function of "X-Factor."

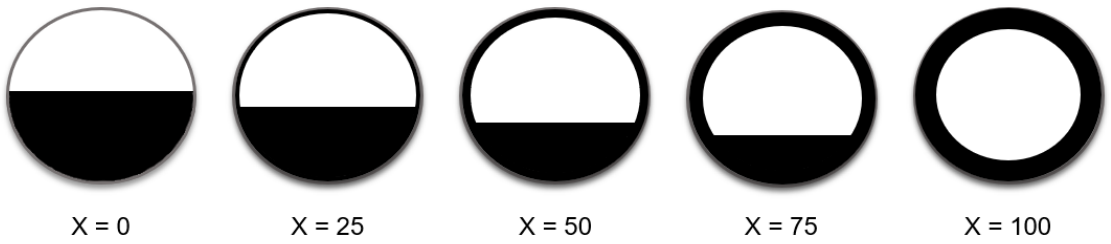


Figure 2.10: UF_6 Cylinder filling profiles for modeling studies expressed as an "X-Factor"

This set of fill profiles was first proposed by Berndt, Franke, and Mortreau. The authors justified this set of representative fill profiles by noting that "the distribution of the material within the cylinder depends on how it was filled, on the last operation made on it (for instance, sampling in the liquid phase after homogenization) or how long and under which conditions (temperature, sunshine) it was stored" [6]. The authors derived these different representative fill profiles by studying three different mechanisms for filling cylinders.

The first possible fill profile is a large annular ring of solid UF_6, as represented by the $x = 100$ case from Fig. 2.10. This ring is formed when a container is filled by desublimation with the cylinder at -25°C. As this cylinder is moved during routine operations, some of the material will flake off the sides and gradually collect at the bottom of the cylinder. [6]

Another way to fill the cylinder through desublimation is to fill a container at 15°C with UF_6 gas at 80°C. Initially, this fill method will also result in a large annular ring, but over time the formed solid will continue to increase in temperature and will transition to a liquid. The $x = 75$, $x = 50$, and $x = 25$ cases are supposed to represent various stages of material relocating from the annular ring configuration to the bottom of the cylinder depending on the method of desublimation used and how the cylinder was handled in the facility. [6]

Finally, the $x = 0$ profile represents the case where some material might be coated on the walls of the cylinder but a majority of the material is at the bottom. This fill profile can be created when the cylinder is filled with liquid UF_6 and allowed to cool to a solid. This method for filling a cylinder can be used to fill cylinders during the enrichment process, but may also be used to homogenize the cylinder before taking a sample or before shipping a product cylinder to a fuel fabrication plant [25]. [6]

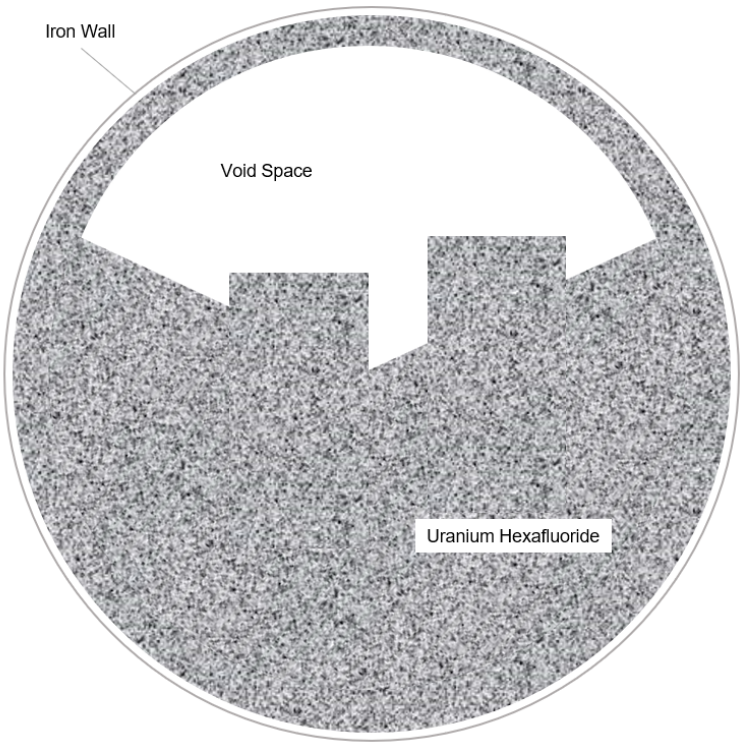
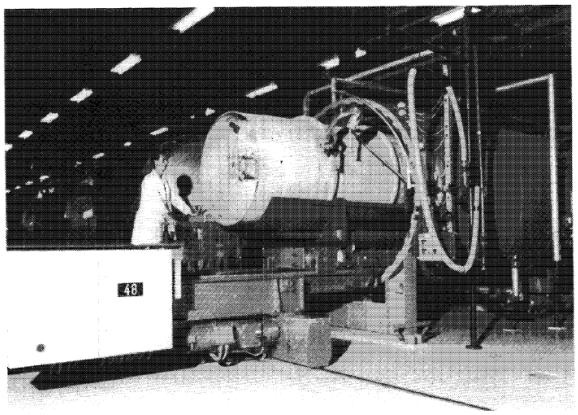


Figure 2.11: A recreation of a hypothetical UF_6 cylinder filling profile for liquid cooling and some desublimation cases as proposed in [6]

Based on these different fill profiles, Berndt, Franke, and Mortreau hypothesized that the inside of a typical UF_6 cylinder might look something like Fig. 2.11. This fill profile is somewhat similar to the one proposed by Portsmouth researchers in Fig. 2.8 based on the images they captured from inside the void space of a 10-ton cylinder.

Berndt, Franke, and Mortreau also hypothesized that changing ambient temperatures over the course of a day will change the fill profile in the cylinder. In particular, they claim that the UF_6 coating of the cylinder will sublime from the cylinder wall to the cooler areas within the cylinder thereby decreasing the thickness of UF_6 on the wall. This, they speculate, will be a minor effect that causes “no important modification.” [6]

Although Berndt, Franke, and Mortreau provide insightful commentary on a range of filling mechanisms and hypothesized fill distributions based on logical behavior of the UF_6 material in different temperature domains, they do not present measured quantitative data from a cylinder to support their hypothesis as part of their paper or reference another study that presents these kind of results.



(a) Image of an autoclave from [30]



(b) Animation of a hot box from [31]

Figure 2.12: Two process systems for heating UF_6

2.3 Weight Measurements of Uranium Hexafluoride in a Nuclear Facility

Weight systems are frequently used to measure the gross weight of UF_6 cylinders in nuclear facilities. These measurements are generally made to accommodate nuclear material accountability at the site or process control and monitoring [26].

One example of using load cells in process control measurements is their integration into feed and withdrawal stations at gas centrifuge enrichment plants [27], [28]. Fig. 2.12 shows two different process methods for heating UF_6. Fig. 2.12a shows a photo of an autoclave that is used to heat up UF_6 in a 48Y cylinder for feeding into the enrichment process, and Fig. 2.12b shows an animation of a hot box that can also be used to heat up UF_6. Load cells in withdrawal stations can also be used to monitor the filling rate of a cylinder. This type of monitoring is common at facilities that fill cylinders with liquid UF_6 to prevent overfilling [29], [30].

Accountability scales, on the other hand, are used to support nuclear material control and accountability programs at the nuclear facility. For commercial nuclear facilities in the United States, the requirements for maintaining a nuclear material control and accountability program are articulated in 10 CFR Part 74: Material Control and Accounting of Special Nuclear Material [32]. This includes the requirement that “all licensees . . . maintain records showing the receipt, inventory, acquisition, transfer, and disposal of

all SNM in its possession regardless of its origin or method of acquisition [33]." U.S. Nuclear Regulatory Commission (NRC) guidelines for licensees state that for UF_6 the ^{235}U concentration must be measured using a nondestructive assay system, the net weight of UF_6 must be measured, and a correction factor must be applied that represents the percentage of uranium in the UF_6 that is periodically checked by analyzing samples from the cylinder [34]. The accountability scale at a nuclear facility is often the most precise scale used to measure cylinders at a facility and is used to find the gross weight of the cylinder so that the net weight of UF_6 can be calculated [26], [35].

The process of verifying the weight of a cylinder when it arrives at a facility is explained in the NRC Regulatory Guide RG 5.41. As part of the shipping process, the shipping facility, or shipper, makes a declaration of the amount of nuclear material inside a container before sending it to the receiving nuclear facility, or receiver. When the cylinder arrives at the receiving facility, that facility must also measure the amount of nuclear material inside the cylinder and evaluate the difference between the declared shipper value and the receipt value. This difference is called the shipper receiver difference. A shipper–receiver difference is considered significant if it exceeds a certain minimum quantity or if it is twice the standard error of the measurement where the standard error is calculated using Equation 2.2. [34]

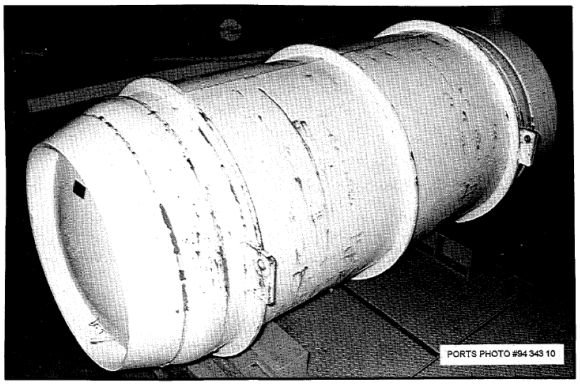
$$\sigma_{SE} = \sqrt{(\sigma_s)^2 + (\sigma_r)^2} \tag{2.2}$$

Where:

$\sigma_s =$ the shipper's measurement standard error

$\sigma_r =$ the receiver's measurement standard error

A significant shipper–receiver difference requires that a facility reconcile the difference with the shipper before it can accept the nuclear material shipment. Once a facility has accepted the shipper's declaration for the amount of nuclear material in a shipped item, it will either use the shipper's declaration as the official amount of nuclear material in the item for its own internal inventory record, or it will use the measured receipt value. [34]



(a) Image of a platform scale from [10]



(b) Animation of a weighing station from [31]

Figure 2.13: Two examples of platform scales

2.4 Scales Used to Measure Uranium Hexafluoride Cylinders

Several different types of scales are commonly used for measuring UF_6 cylinders. One type that is often used for accountability scales is a *platform scale*. Two examples of this type of scale can be seen in Fig. 2.13. A typical platform scale consists of a set of v-blocks or other style of mechanism for holding a cylinder in a stable position in the center of a scale. The v-blocks are on a load-bearing frame that rests on several load cells, usually four. This design ensures that all of the load of the cylinder is applied to the load cells and can therefore be reliably measured.

Another type of weighing system that can be used to measure UF_6 cylinders is a *under-the-hook scale* system, which is designed to hang between a crane and the load a crane is lifting so that the weight of the lifted object can be measured. Several generations of this type of system have been developed for the International Atomic Energy Agency (IAEA) so its inspectors can measure the gross weight of cylinders without any reliance on the facility operator's weight platforms. The system was designed to be portable by an IAEA inspector and compatible with the lifting equipment at a broad range of facilities. Fig. 2.14 shows a schematic of this type of load cell system. The system shown in the schematic is designed to measure a full 30B cylinder within 1 kg, whereas a traditional

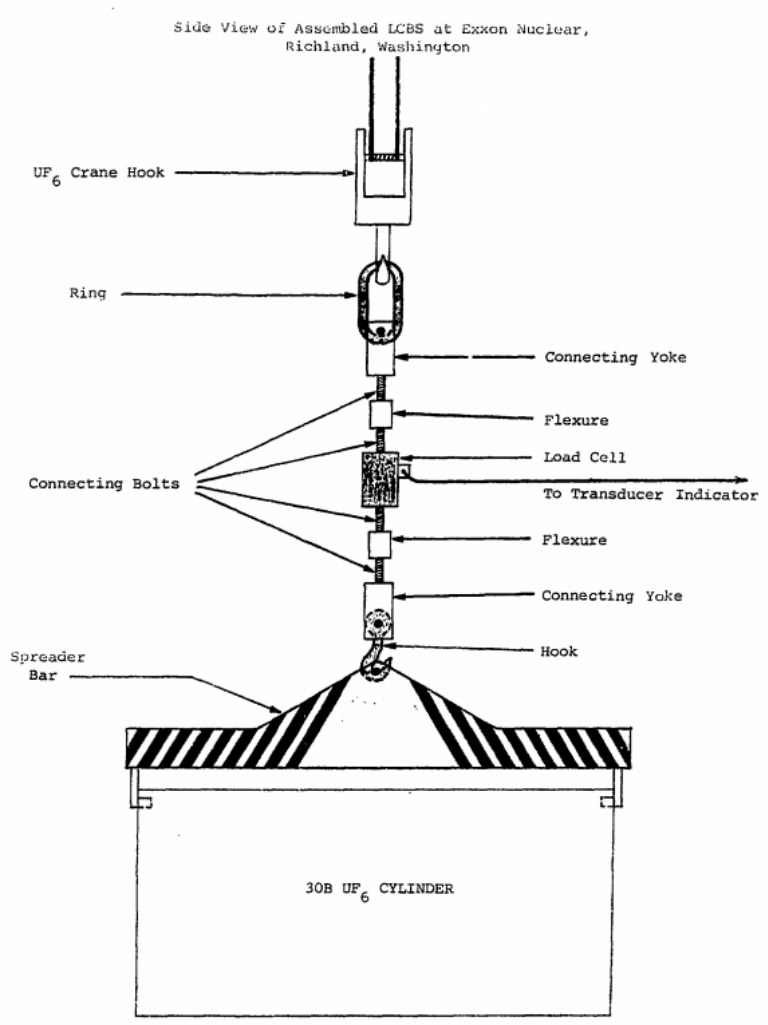


Figure 2.14: Schematic of a load cell system for use under an overhead crane from [7]

platform accountability scale would be able to measure the same full cylinder at least within 0.5 kg. [36] [7]

Some more recent work with a *floor scale* type system highlights some of the challenges that must be managed to accurately measure the weight of a UF_6 cylinder. This work aimed to develop a floor scale that could be used as part of a UF_6 cylinder portal monitoring system. The system would integrate the floor scale with gamma detectors so that an increase in the gamma count rate could be used to trigger a weight measurement. A testing report for this system indicates that the system had issues measuring weight accurately due to temperature fluctuation in the laboratory during measurements. Although the overall impact of this effect was not substantial, the authors

noted that it illustrates the importance of zeroing the scale between measurements, which is a typical practice of IAEA inspectors in the field when using the hanging load cells. [37]

2.5 Center of Gravity Measurements with Weight Measurement Systems

There is no evidence in literature that weight systems have previously been used to measure the center of gravity of a UF_6 cylinder. However, it is common to use a load cell system to find the center of gravity of an object under measurement. Center of gravity is often measured because it can help predict the performance of vehicles such as aircraft, cars, and space vehicles when they are in motion. [38]

Various methods have been used to estimate the center of gravity during the design phase for these types of vehicles. For aircraft, one method used is the *mass distribution management* method, or MDM. With this method, the center of gravity of an airplane is calculated by dividing the sections of the airplane into multiple independent segments. Segments are considered independent if their mass can be increased or decreased independently from other adjacent segments. [39]

The use of segments allows for the center of gravity to be calculated with the following system of equations [39]:

$$m_i = m_{i_S} + m_{i_{FE}} + m_{i_F} + m_{i_{PL}} \tag{2.3}$$

and

$$m = \sum_{i=1}^{n} m_i \tag{2.4}$$

and

$$X_{cg} = \frac{\sum_{i=1}^{n} m_i x_i}{\sum_{i=1}^{n} m_i} \tag{2.5}$$

and

$$Y_{cg} = \frac{\sum_{i=1}^{n} m_i y_i}{\sum_{i=1}^{n} m_i} \tag{2.6}$$

and

$$Z_{cg} = \frac{\sum_{i=1}^{n} m_i z_i}{\sum_{i=1}^{n} m_i} \tag{2.7}$$

Where:

$n =$ the number of segments

$m =$ the current mass of the aircraft

$m_{i_S} =$ the contribution of the structural mass to the segments

$m_{i_{FE}} =$ the contribution of the fixed equipment mass to the segments

$m_{i_F} =$ the contribution of the fuel mass to the segment

$m_{i_{PL}} =$ the contribution of the payload mass to the segment

$X_{cg} =$ the center of gravity in x

$Y_{cg} =$ the center of gravity in y

$Z_{cg} =$ the center of gravity in z

The authors of this approach note that the segments will be drawn differently for each aircraft, and the number of segments should increase until the mathematical algorithm and experimental measurement techniques converge. As an example, the authors divided a Boeing 747-100 into 29 segments to simulate it using this methodology while the aircraft was in a cruising flight meeting Level-I flying quality requirements (i.e., flying qualities that are adequate for a flight phase with no adverse circumstances [40]). [39]

Generally, modeling approaches for aircraft, including the MDM method, are focused on finding all of the inertia parameters of the aircraft in motion including the mass, center of gravity location, and inertia tensor rather than just the properties of the mass and center of gravity. These methods are prone to errors on the order of 15% because of issues with geometric tolerances or uncertainties in understanding mass properties, such as the density, of the components being modeled. Therefore, it is common to pair modeling of

the mass distribution of these objects with controlled laboratory measurements to better understand the system. [38]

Load cells are one common way that both mass and center of gravity of a system are measured. Typical accuracies in these systems are around 0.02–0.05%. Custom systems are commonly built that also take a measurement based on force restoration technologies (like a load cell) that can achieve accuracies of around 5E-6%. There are two general categories of these measurement systems: static and dynamic. Static measurement systems include reaction force measurement methods, suspension methods, and balancing methods. [38]

The most commonly used static method is the reaction force method. The reaction force method uses a measurement system like a load cell to measure the mass of an object as well as the center of gravity of the object in the horizontal frame of reference. The object must then be rotated to at least two different positions on the instrument and measured to determine the center of gravity in the third axis as well as the inertial tensor. The accuracy of the measurement of the inertial tensor as well as the third center of gravity axis is dependent on the tilting angle, with a greater tilting angle resulting in a better accuracy. The accuracy of the measurement in the third axis will always be worse than the two horizontal axis measurement since it is being measured by the same reaction force instrument but with an added source of uncertainty due to the measurement of the angle. [38]

One common example of a reaction force measurement system is a system similar in design to a platform load cell system that has three force transducers. A schematic of this system is shown in Fig. 2.15. The force transducers in this figure are shown in blue and labeled A, B, and C, and the center of the A load cell is (0,0). A center of gravity point is shown using a center of gravity notation with lines drawn to demonstrate directions in the horizontal plan to that location. [8]

The following system of equations from [8] is used for calculating center of gravity given that A is at (0,0):

$$W = W_A + W_B + W_C \tag{2.8}$$

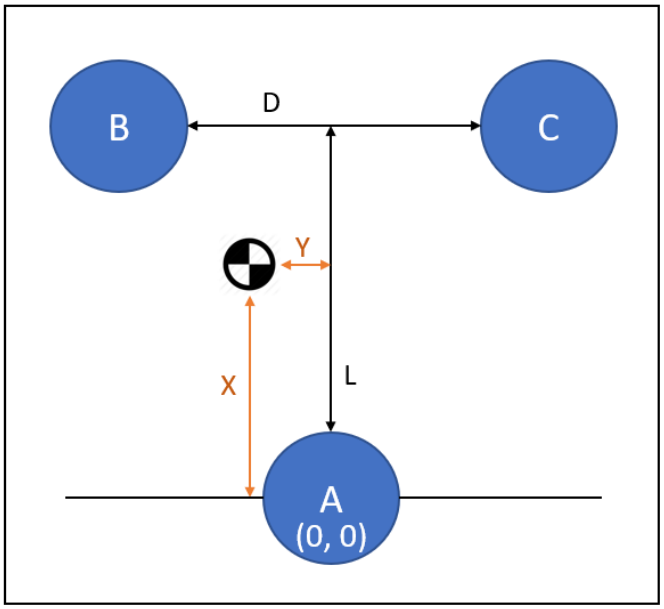


Figure 2.15: A traditional three-point platform scale design for measuring center of gravity as explained in [8]

and

$$X_{cg} = \frac{(W_B + W_C)L}{W} \tag{2.9}$$

and

$$Y_{cg} = \frac{(W_C - W_B)D}{2W} \tag{2.10}$$

Where:

$W =$ the sum of the force applied to all three load cells

$W_A =$ the force applied to load cell A

$W_B =$ the force applied to load cell B

$W_C =$ the force applied to load cell C

$L =$ the distance from A to line D

$D =$ the distance from the center of B to the center of C

A typical measurement procedure with this type of system would involve measuring the tare weight of the fixture that is going to hold the object being measured, then measuring

the object of interest in the fixture. Once both of these measurements are made, the tare values are subtracted from the measurement with the object of interest and the system of equations from above are used to calculate X_{cg} and Y_{cg}. One example of this type of three-point measurement system is a load cell system that can be installed on the landing gears of a plane to measure the horizontal center of gravity of the plane before it takes off so that its handling properties when in motion can be predicted [41]. [8]

An interesting perturbation of a reaction force method system is the use of a truck scale to measure the mass and center of gravity of a truck with a full load to understand if the load should be better positioned to prevent accidents. The truck scale system measures the axle weight and the wheel base length to calculate the center of gravity while the truck is in motion. The wheel base length is difficult to directly measure, so it is estimated using the position of the truck as a function of time as it drives over the load cells. This motion creates an eccentric load for the load cells, changing the measured output over time. An eccentric load is a load that is applied parallel to the principal axis of the load cells and results in either an increase or a decrease in the output of the load cell for the same load [42]. [43]

Also, the number of force transducers used can be reduced if it is only important to understand the center of gravity in a single dimension. One example of this type of system is a platform that is used to measure the center of gravity and wheel resistance of a patient in a wheelchair so that a clinician can evaluate their stability and make adjustments to the wheelchair configuration if needed. This application uses a platform scale system with a single scale on one end of the platform and a pivot point on the other. [44].

Suspension methods offer another way to measure the center of gravity of an object. These systems measure the center of gravity by suspending an object by a single connection point and capturing where the vertical line passes through the object. This measurement is repeated three times using different suspension points on the object. The center of gravity is then calculated by finding the point inside the object where all the measured vertices intersect. [38]

The third static measurement approach for center of gravity is the balancing method. For this approach, the object under measurement is positioned on an edge then the center

of gravity is located by finding either the equilibrium position of the object or by balancing the tilting beam with counterweights. This system only measures one axis at a time, and the object must be rotated to measure the third axis, but it has a high degree of accuracy. [38]

The main dynamic measurement method is the pendulum method. Dynamic methods are typically less accurate than static methods but can be used to identify all three dimensions of the center of gravity of an object that cannot easily be rotated. The pendulum method relies on the use of a classic pendulum. To measure the center of gravity, an object is placed on the classic pendulum with a known cable length. While the object is on the pendulum, the frequency of the pendulum can be measured. This measurement is repeated with different known cable lengths to find the center of gravity of the object. [38]

Because vehicles are difficult to rotate, their center of gravity is commonly measured using the pendulum method. There have been various efforts to reduce the number of measurements required by the classic pendulum method. One such effort involves a test rig with three or four bar pendulums that hold the object being measured. The object is then rotated around three axes near the estimated center of gravity, and the resulting motion is recorded. A simulation built from a first-principals model is then run to generate a predicted motion path based on estimated inertial tensor. The inertial tensor estimate is then refined by running the simulation iteratively with different values for the tensor until the error between the measured and computed motion is minimized. [45]

Chapter 3

Method

This study uses a static reaction force measurement system, as discussed in Section 2.5, to measure the force applied to a platform scale and calculate the center of gravity. This calculation gives the center of gravity of a UF_6 cylinder in two dimensions, x and y, as shown in Fig. 3.1. The internal dimensions of a 30B UF_6 cylinder are 179 cm by 76.2 cm, so based on the reference frame in Fig. 3.1, the nameplate of the cylinder would be at approximately -89.5 cm in x not considering the thickness of the steel of the cylinder and assuming the nameplate is centered.

The front face of the cylinder with the cylinder nameplate is shown in Fig. 3.2. This figure shows an angle θ that will be used to discuss the degree to which a cylinder is rotated. For this work, a normally placed cylinder is assumed to have a θ of 90°. Measuring the third vertical axis, z, would be possible with the static reaction force measurement system used in this work if three measurements were made per cylinder with θ at 60°, 90°, and 120°. However, cylinders are not allowed to be rotated during routine handling operations at the facility where measurements were made. Operators at this facility are supposed to limit the angle θ such that it never varies more than 10° from its normal 90°.

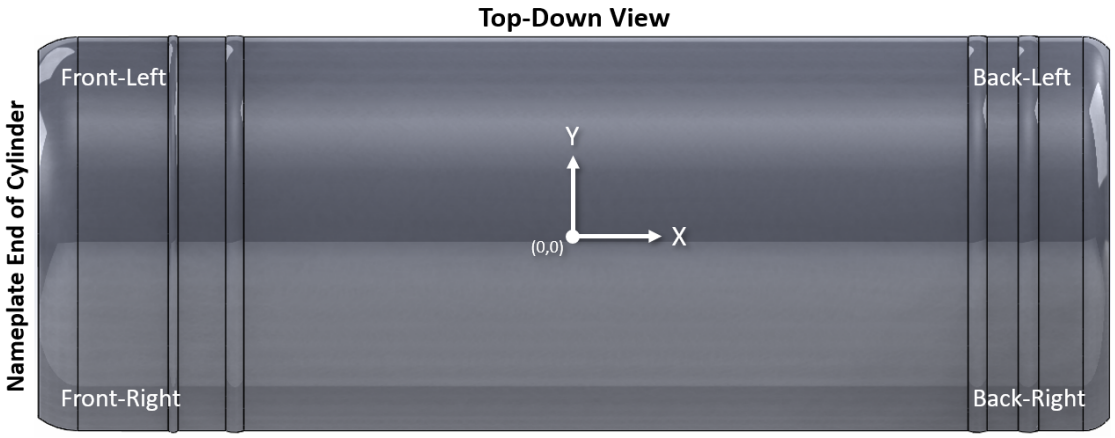


Figure 3.1: Top-down view of a 30B cylinder with reference axis shown for positive x and positive y and nomenclature for each corner of the cylinder

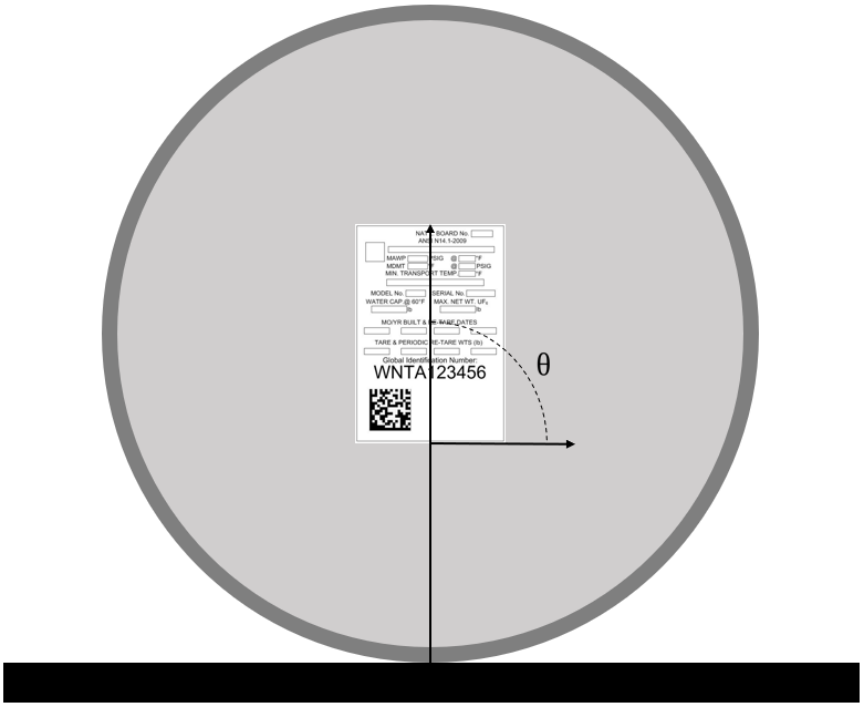


Figure 3.2: Front view of a 30B cylinder with an angle, θ, shown as the angle between a line perpendicular to the ground and the bottom edge of the cylinder nameplate from [9]

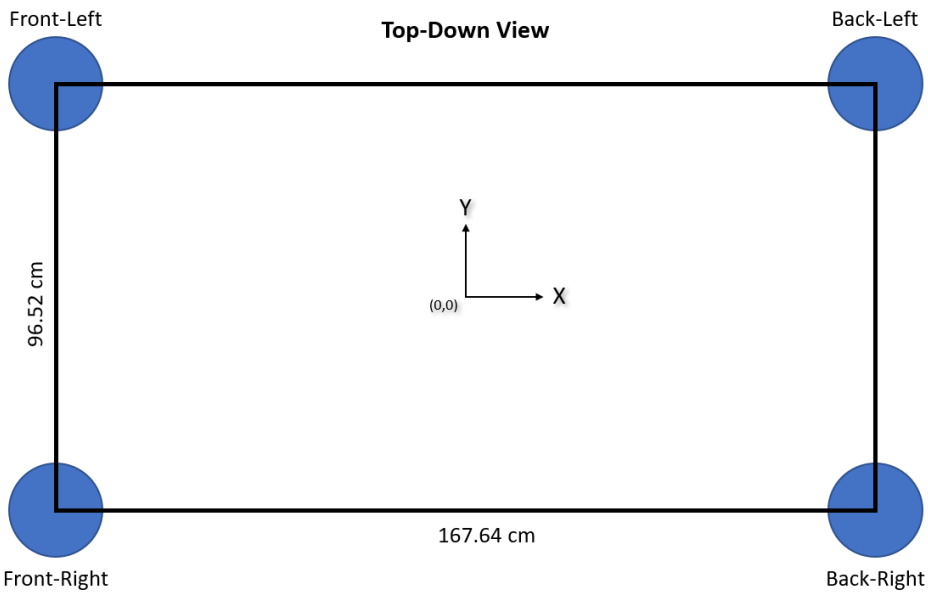


Figure 3.3: Top-down schematic of the platform scale used to measure 30B cylinders with load cells indicated by blue circles

3.1 Force Measurements

The static reaction force measurement system used in this study is a platform scale designed to hold UF_6 cylinders centered in the y axis using v-blocks. The platform scale has four digital load cells with one load cell in each corner of the platform. A schematic of this platform is shown in Fig. 3.3.

It is still common to find both analog and digital load cells in many different measurement applications. The main difference between analog and digital load cells is digital load cells convert the analog signal measured to a digital format using a microcontroller installed on the load cell module. In contrast, fully analog systems will transmit analog values to a junction box where they are summed and then sent to the weight indicator for conversion to a digital value. [46]

Digital load cells were chosen for this work because a digital signal is more resistant to sources of interference (e.g., electronic interference or temperature) during transmission than analog signals. Also, digital load cells can be hermetically sealed to prevent dust or other particulates from damaging sensitive components, which enhances their longevity. Finally, since digital load cells are designed to work without a junction box, it is possible

to read and record individual values that are equivalent to the force applied to each load cell. [46]

The digital load cells in this experiment are compression style load cells that measure the force applied using a strain gauge. A strain gauge typically contains a thin foil resistor that is bonded to an elastic material, such as a metal, which is deformed based on an external stress. The resistance of the foil changes proportionally with the strain of the elastic material from the external force. [47]

The difference in material strain typically results in very small changes in resistance. For this reason, a Wheatstone bridge circuit is used to measure the resistance changes. The relationship between these resistances and the strain of the material is shown by the following equation from [48]:

$$\frac{\Delta R}{R_o} = k * \epsilon \tag{3.1}$$

Where:

$\Delta R/R_o =$ the relative change of resistance of the strain gauge

$k =$ the experimentally measured gauge factor

$\epsilon =$ the applied strain

A full Wheatstone bridge circuit is shown in Fig. 3.4 and has four resistors as well as a bridge input voltage, U_E, and a bridge output voltage, U_A. The governing equation for this circuit from [48] then becomes:

$$\frac{U_A}{U_E} = \frac{R_1}{R_1 + R_2} - \frac{R_4}{R_3 + R_4} \tag{3.2}$$

Strain gauges are typically made such that the circuit can be set to be balanced at the zero, or initial, state of the instrument [48]. When the circuit is balanced (either $R_1 = R_2 = R_3 = R_4$ or $R_1 : R_2 = R_4 : R_3$), then the ratio of the bridge input voltage, U_E, to the bridge output voltage, U_A, is

$$\frac{U_A}{U_E} = 0. \tag{3.3}$$

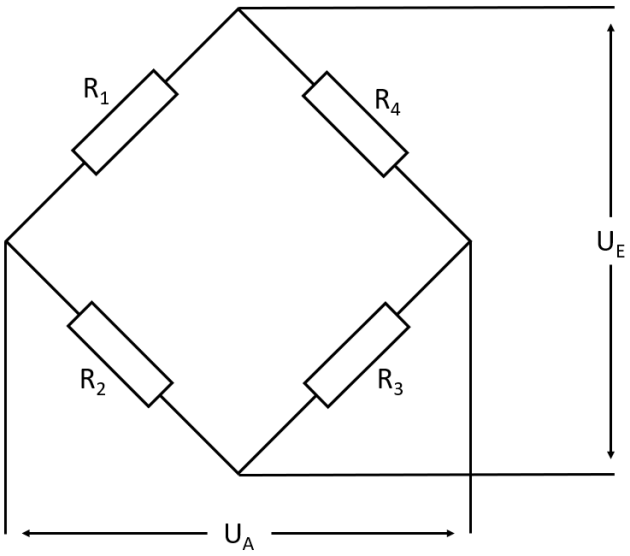


Figure 3.4: Wheatstone bridge circuit

When stress is applied to the strain gauge, the resistors will vary and an output voltage will appear. Assuming that the resistance variation ΔR is much smaller that the resistance itself, the following equation from [48] is true with load applied:

$$\frac{U_A}{U_E} = \frac{1}{4}\left(\frac{\Delta R_1}{R_1} - \frac{\Delta R_2}{R_2} + \frac{\Delta R_3}{R_3} - \frac{\Delta R_4}{R_4}\right) \tag{3.4}$$

The resistors are typically chosen such that $R_1 = R_2 = R_3 = R_4$ when the input voltage is constant so that changes in each of the bridge arms are proportional to the change in the output voltage. This characteristic allows for Equation 3.1 to be substituted into Equation 3.4 resulting in the following from [48]:

$$\frac{U_A}{U_E} = \frac{k}{4} * (\epsilon_1 - \epsilon_2 + \epsilon_3 - \epsilon_4) \tag{3.5}$$

The load cells used in this work are bending beam load cells. Bending beam load cells are designed so that the strain values measured by each resistor have the same magnitude but opposite sign from each other. Therefore, using Equation 3.5 from [48], we convert the signs:

$$\frac{U_A}{U_E} = \frac{k}{4} * (\epsilon_1 - (-\epsilon_2) + \epsilon_3 - (-\epsilon_4)) = k * |\epsilon| \tag{3.6}$$

Simplifying this equation then shows that the magnitude of the strain can be determined by measuring the ratio between the input and the output voltage from the load cell. This is demonstrated here, where k is an experimentally measured constant of the strain gauge:

$$|\epsilon| = \frac{U_A/U_E}{k} \tag{3.7}$$

The strain can then be correlated to engineering values for weight using standard calibration procedures for scales described in procedures released by the National Institute of Standards and Technology (NIST) [49]. However, this type of calibration will not be needed to calculate the center of gravity.

3.2 Center of Gravity Calculation

The center of mass for a system can be calculated using this equation from [50]:

$$R = \frac{1}{M}\int rdm \tag{3.8}$$

Where:

$R =$ the center of mass

$M =$ the total mass of the system

$r =$ the location of a particle in the system

$dm =$ the contribution to the mass at a particle in the system

The difference between the center of mass of a system and the center of gravity is the center of mass is the point at which the distribution of mass is equal in all directions, and the center of gravity is the point at which the distribution of weight is equal in all directions. This point is the same when an object is in a uniform gravitational field, which is a reasonable approximation for the UF_6 cylinder being measured on the platform scale in this work. Also, since scales measure weight not mass, the result of the measurement

with the force measurement system described in the previous section is the center of gravity.

Assuming that the object is in a uniform gravitational field and that we are using a discrete number of measurement points to calculate the center of mass rather than a large number, Equation 3.8 becomes a sum rather than an integral resulting in the following equation:

$$\overrightarrow{R_{cg}} = \frac{1}{M} \sum_{1}^{N} \overrightarrow{r_i} m_i \tag{3.9}$$

Where:

$\overrightarrow{R_{cg}} =$ a vector pointing to the center of gravity location

$M =$ the total weight measured by the system

$\overrightarrow{r_i} =$ a vector for a specific measurement point

$m_i =$ the mass measured at a specific measurement point

$N =$ the total number of measurement points

From Equation 3.9, it is clear that a calibration for the scale is not needed to calculate the center of gravity as the units for mass will cancel out of the center of gravity equation. Instead it is sufficient that values being measured by the force measurement system are proportional to the weight across the range of the system.

Chapter 4

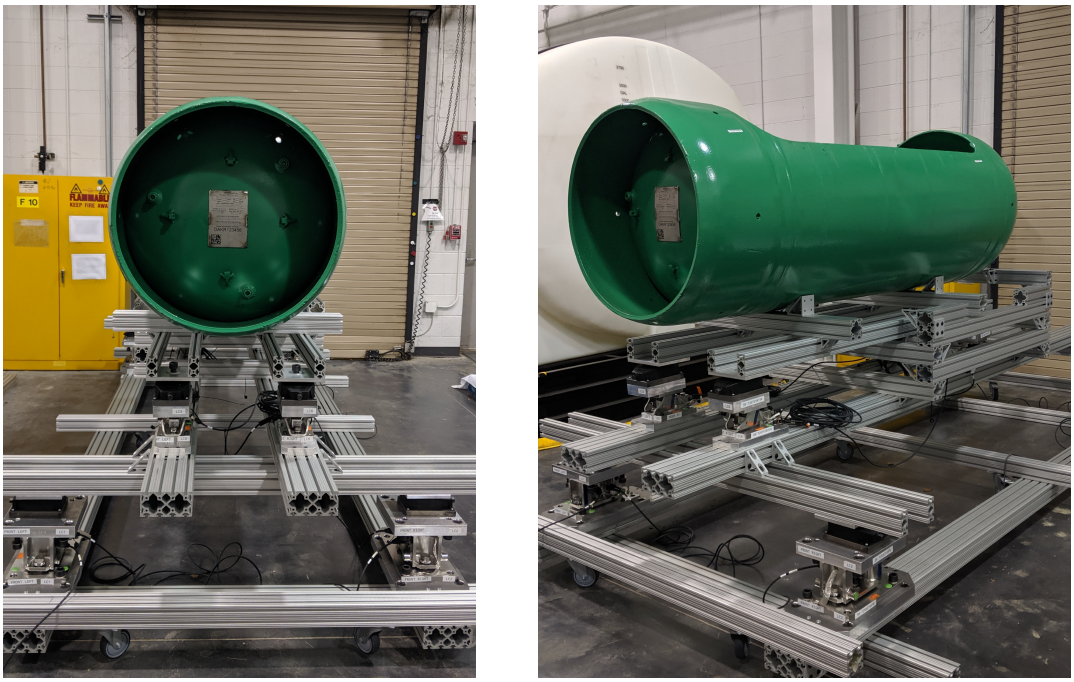
Mathematical Model

This section will explore the center of gravity measurement using a mathematical model and compare that model to laboratory testing to better understand how the movement of weights impacts the center of gravity value. This section will use the first part of the MDM approach described in Section 2.5 from [39] to segment the masses used in laboratory testing. The mathematical model will focus on the x and y dimension of the system as shown in Fig. 3.1. z is not considered because as mentioned in [8], three measurements are required at different angles to determine the center of gravity in the z axis. The raw data collected on 30B cylinders used in this work was restricted to a single measurement per cylinder at a single angle due to cylinder handling restrictions, so the center of gravity in z could not be calculated.

After this discussion, the impact of the rotation of the 30B cylinder on the center of gravity in y will be explored. Specifically, a mathematical approach to correct for variations in θ (defined in Fig. 3.2) will be derived.

4.1 Laboratory Testing

Laboratory testing was performed using a stacked platform scale system built out of 80/20 aluminum pieces and eight different load cells [51]. The top portion of the scale was assembled to replicate a typical 30B platform scale, and so the load cells that are part of this platform are the only ones considered in this work. A cutaway steel cylinder was



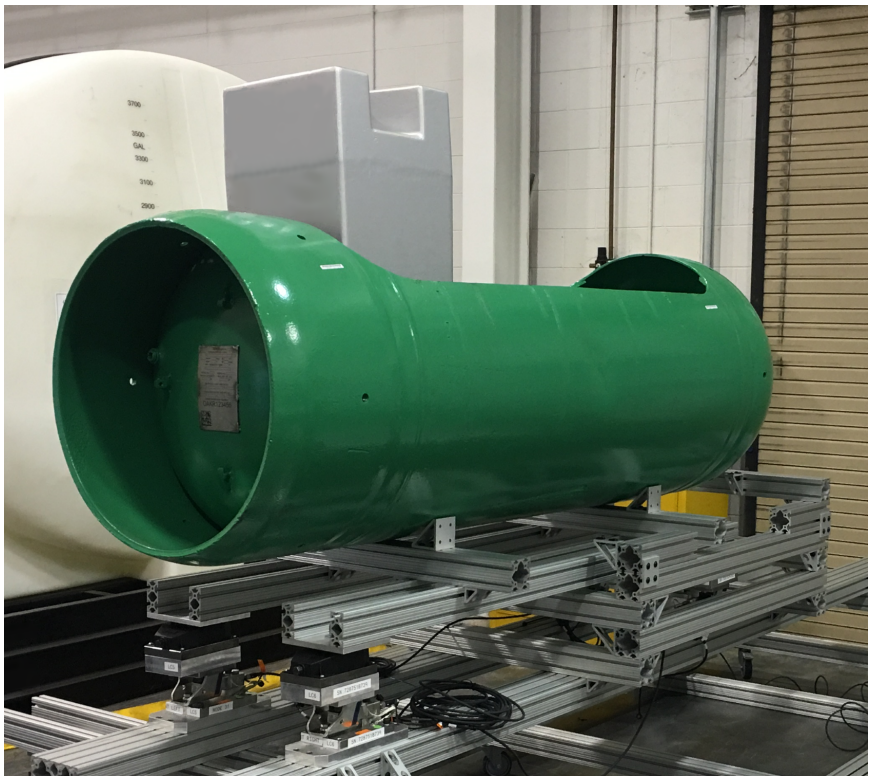
(a) Front **(b)** Side angle

Figure 4.1: Laboratory testing scale with cutaway 30B cylinder on top

placed on top of the 30B platform scale to allow for known weight standards to be loaded at different locations. The steel cylinder was designed to have the same dimensions as a 30B as well as a similar weight to an empty cylinder. A steel plate was welded inside the cylinder to support the loading of weight standards. This testing apparatus is shown in Fig. 4.1.

For this test, the front, left, back, and right are defined with respect to the face of the cylinder nameplate as seen in Fig. 3.1. Two 1,000 lb. test weights were used to examine the center of gravity response of the overall system. The 1,000 lb. weights were varied between two measurement locations, A and B, where location A was very close to the front end of the cylinder and location B was very close to the back end of the cylinder. Fig. 4.2a shows two 1,000 lb. test weights stacked on top of each other at location A, and Fig. 4.2b shows the two weights stacked at location B. There were six measurements made using this test apparatus. The specific measurements are described in Table 4.1.

The MDM method calls for dividing a complex object into multiple independent segments where each segment can have its mass increased or decreased independently



(a) Test weights at location A



(b) Test weights at location B

Figure 4.2: Laboratory testing scale with test weights stacked at two locations

Table 4.1: Laboratory Measurements on the Platform Scale

No.	Description
1	Cutaway cylinder with one test weight in location A
2	Cutaway cylinder with two test weights in location A
3	Cutaway cylinder with one test weight in location A and one in location B
4	Cutaway cylinder with one test weight in location B
5	Cutaway cylinder with two test weights in location B
6	Cutaway cylinder with no test weights

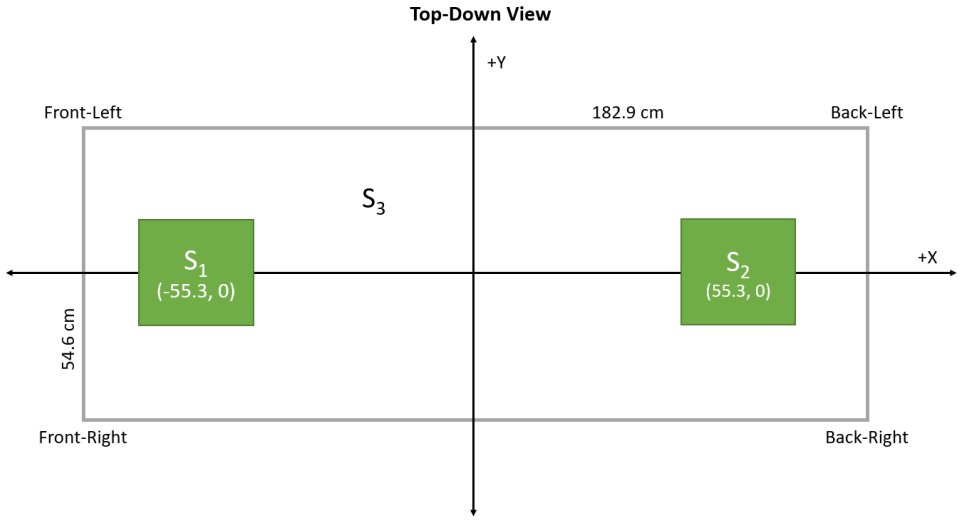


Figure 4.3: MDM mass segmentation scheme used for modeling laboratory testing

from other adjacent segments [39]. So, for this work, the inside of the cutaway cylinder has been broken into three different segments, S_1, S_2, and S_3, as shown in Fig. 4.3. In Fig. 4.3, S_1 and S_2 represent the rectangles in x and y that are centered on the locations A and B, respectively, where either one or two 1,000 lb. test weights were loaded in the laboratory. S_3 represents the rest of the cutaway cylinder and can be represented as having zero mass.

This mass segmentation scheme can be used in conjunction with the center of gravity formula for a system of discrete points to predict the value for the center of gravity in x and y. This approach predicts that when either one or two test weights are loaded on either location A or location B, the center of gravity should be equal to the coordinates for either S_1 for location A or S_2 for location B. As an example, this approach would yield the following system of equations when two of the weights are loaded onto position A:

Table 4.2: Load Cell Coordinates in Laboratory Testing

Load cell position	x (cm)	y (cm)
Front-left	-91.5	27.3
Back-left	91.5	27.3
Front-right	-91.5	-27.3
Back-right	91.5	-27.3

$$X_{cg} = \frac{\sum_{i=1}^{n} m_i x_i}{\sum_{i=1}^{n} m_i} = \frac{2,000\ lb * -55.3\ \text{cm}}{2,000\ lb} = -55.3\ \text{cm} \tag{4.1}$$

and

$$Y_{cg} = \frac{\sum_{i=1}^{n} m_i y_i}{\sum_{i=1}^{n} m_i} = \frac{2,000\ lb * 0.0\text{cm}}{2,000\ lb} = 0.0\ \text{cm} \tag{4.2}$$

Therefore, with two test weights at position A, this method suggests a center of gravity of (-55.3 cm, 0.0 cm). When one weight is loaded on location A and one weight on B, the system of equations changes to

$$X_{cg} = \frac{(1,000\ lb * -55.3\text{cm}) + (1,000\ lb * 55.3\ \text{cm})}{2,000\ lb} = 0.0\ \text{cm} \tag{4.3}$$

and

$$Y_{cg} = \frac{(1,000\ lb * 0.0\text{cm}) + (1,000\ lb * 0.0\text{cm})}{2,000\ lb} = 0.0\ \text{cm}. \tag{4.4}$$

So the center of gravity in this case would be at the origin of the coordinate system, (0.0 cm, 0.0 cm). To compare this with experimental data collected in the laboratory, Equation 3.9 was used in conjunction with the force response of each load cell as well as the location of each load cell in a two dimensional coordinate system to calculate the center of gravity for each measurement. The load cell locations for the laboratory testing were based on the coordinate system outlined in Fig. 4.3 and are detailed in Table 4.2.

Since the empty cutaway cylinder was also measured in the laboratory, the response of each load cell to the empty cylinder is subtracted from the response of that load cell to every other measurement configuration to ensure that the result only represents the

Table 4.3: Predicted Versus Measured Values for Laboratory Testing

No.	Predicted	Measured
1	(-55.3 cm, 0.0 cm)	(-56.2 cm, 5.0 cm)
2	(-55.3 cm, 0.0 cm)	(-55.9 cm, 7.0 cm)
3	(0.0 cm, 0.0 cm)	(2.1 cm, 2.9 cm)
4	(55.3 cm, 0.0 cm)	(60.0 cm, 0.6 cm)
5	(55.3 cm, 0.0 cm)	(60.1 cm, 2.5 cm)

location of the weight standards inside of the cutaway cylinder. This is important for comparisons to the mass segmentation approach used in Fig. 4.3 because S_3 is assumed to have zero mass. With this subtraction added, Equation 3.9 becomes

$$\overrightarrow{R_{cg}} = \frac{1}{M^{weights}} \sum_{1}^{N} \overrightarrow{r_i} (m_i^{weights} - m_i^{cylinder}). \tag{4.5}$$

The results from the laboratory measurements compared to the values predicted by the mathematical modeling approach are shown in Fig. 4.4. The figure shows three different plots of results. The top plot shows the measured results versus the predicted values in both the x and y axes for the reference frame presented in Fig. 4.3. The bottom two plots show the x and y center of gravity values versus the measurement number from Table 4.1 for both the measured and predicted values to give a sense of how well the experimental values agree with the model prediction. The measured and predicted values for each measurement are also shown in Table 4.3.

The results show that the model predicted the measured results in the x axis fairly well. For measurements 1 and 2, the measured values are within 1 cm of the predicted values. Also, as expected, the measured value for x does not change significantly between measurements 1 and 2 because one weight is stacked on top of the other. Measurements 4 and 5 do not align nearly as well with 1 and 2 with the predicted value in x, but they do not change substantially as one weight is stacked on top of the other. This discrepancy is likely due to the relative imprecision of trying to hit a mark with a 1,000 lb. weight using an overhead crane as well as error introduced when trying to create the target mark location for B using tape measures and tape. The lack of symmetry between measurement locations A and B would also explain why measurement 3 is off-center in x. This can

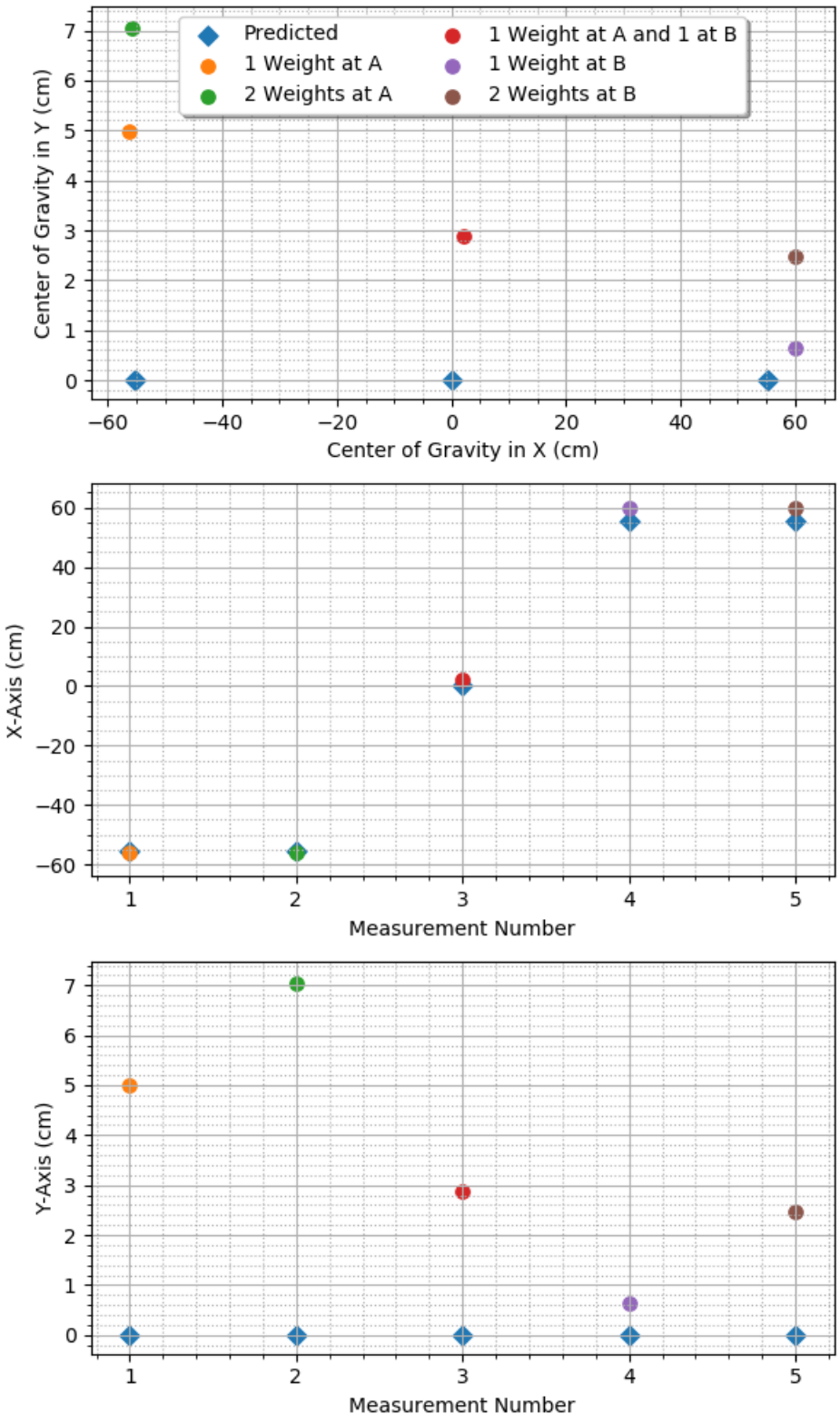


Figure 4.4: Laboratory testing results compared to predicted values for center of gravity in the x and y axes

be checked for consistency with the mathematical model by modifying Equation 4.3 to use the measured center of gravity values for the 1,000 lb. test weights in measurements 1 and 4:

$$X_{cg} = \frac{(1,000\ lb * -56.2\text{cm}) + (1,000\ lb * 60.0\text{cm})}{2,000\ lb} = 1.9\ \text{cm} \tag{4.6}$$

The result is within 0.2 cm of the measured center of gravity in the x axis, which indicates that the measured laboratory values and the mathematical model generate consistent predictions in the laboratory setting. The y axis center of gravity measurements, however, are not at all consistent with the model predictions. One potential indicator for why can be seen by comparing measurements 1 and 2 and measurements 4 and 5. In both cases, the pairs of measurements should be consistent, so measurements 1 and 2 should be comparable in their y center of gravity location and measurements 4 and 5 should be comparable. Instead these pairs of measurements have differences of 2 cm and 1.9 cm, respectively.

Although it is not apparent in Fig. 4.2, there was clearly a slight angle to the second weight when it was loaded onto the first weight at both position A and position B in the laboratory. Since the cylinder was loaded onto the platform scale such that the bottom of the cylinder nameplate was approximately perpendicular to the ground, the fact that the weights tilted at an angle when loaded into the cylinder likely indicates that the welded piece of sheet metal inside the cylinder is not level with respect to the bottom of the cylinder nameplate. This, in turn, means that the force applied by the weights would not be centered on points S_1 and S_2 as used in the MDM model.

There are two interesting implications of this discrepancy between the mathematical model and the laboratory measured values. First, it is apparent that the angle of the cylinder with respect to the ground can be a significant source of systematic error for the center of gravity measurement. Second, it seems that this systematic error more directly impacts the y axis center of gravity value rather than the x axis center of gravity value. The relationship between the cylinder angle and the center of gravity values will be more fully explored in the next section.

4.2 Studying the Effect of Angle

This section will consider the effect of measuring a cylinder at different angles θ, the angle of the nameplate with respect to a vertical line perpendicular to the ground, on the center of gravity measurement. Two different cylinder configurations from Fig. 2.10 will be considered: 1) the $x = 0$ case, which represents when a cylinder is filled with liquid UF_6 and allowed to cool and 2) the $x = 100$ case, which represents when a cylinder is filled with gaseous UF_6 and desublimed directly to a solid.

For this theoretical study, the origin of the cylinder will be defined as the geometric center of the cylinder. The direction of the y axis will be the same as in Fig. 3.1, and the z axis will be defined to be positive when pointing up and negative when pointing toward the ground. Note, this definition means that the direction of y with respect to the front face of the cylinder is opposite of what is typical for an axis definition, meaning positive y is toward the left and negative y is toward the right. This study only examines the center of gravity in the y and z axes because the two theoretical material distributions presented are symmetric about the x axis, and changes in θ would not affect this symmetry.

This study also makes a few assumptions. First, while a 30B cylinder is not perfectly cylindrical, this study will approximate a 30B cylinder as a geometrically cylindrical volume. This study will also assume that the UF_6 inside the cylinder does not redistribute as the cylinder is rotated in θ.

Figure 4.5 shows a cylinder with UF_6 desublimed from the gaseous state to the solid state. The figure clearly illustrates that all the material is symmetric about the origin of the cylinder no matter the rotation in θ. Since the material is symmetric, the center of gravity of the cylinder will be located at the geometric center of the cylinder, which is defined as $(0, 0)$ in the y and z axes.

Figure 4.6 shows a cylinder that has been filled with liquid UF_6 and allowed to cool to solid UF_6 as it is rotated about θ. It is clear that the center of gravity in both the y and z axis will change as a function of θ for material in this configuration. To find the functional relationship between θ and the center of gravity in y and z, it is important to first find the typical UF_6 fill level in a 30B cylinder.

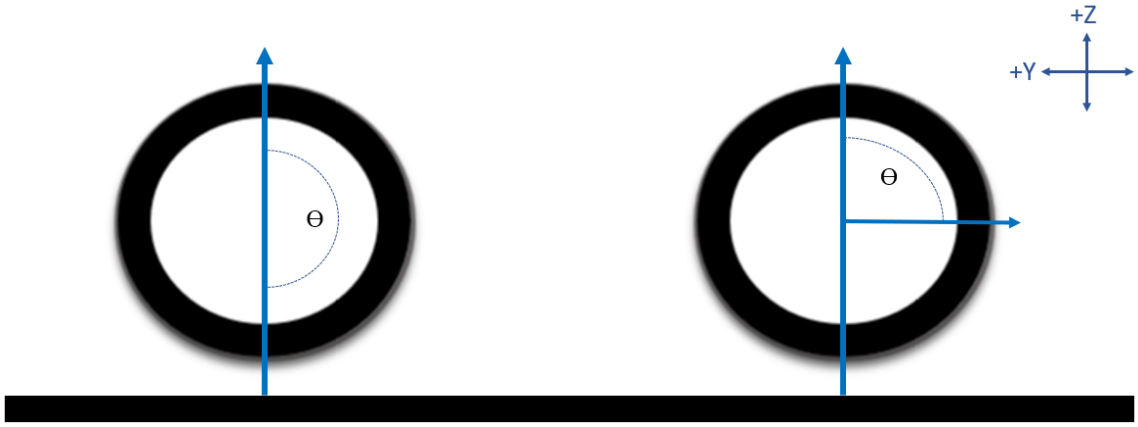


Figure 4.5: Cylinder filled through desublimation from gaseous UF_6 to solid UF_6 rotated about θ

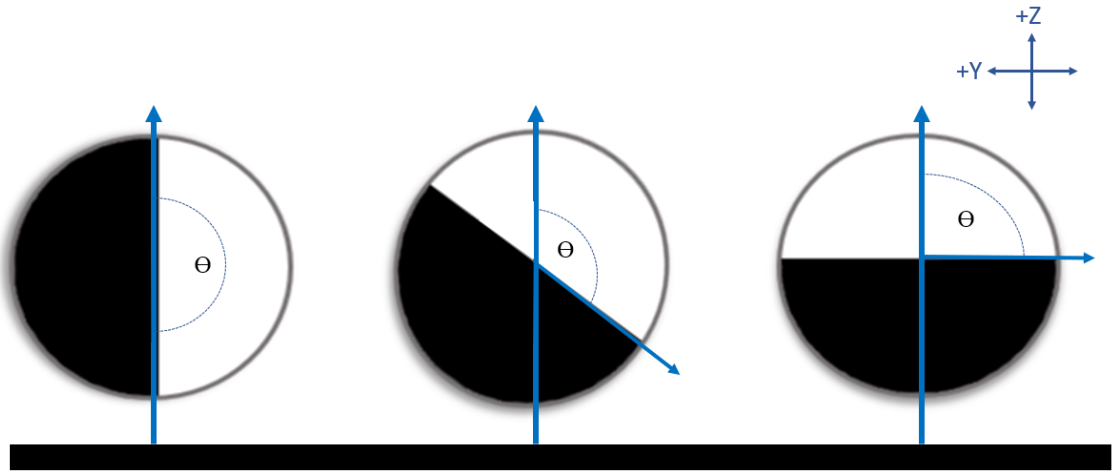


Figure 4.6: Cylinder filled through liquid UF_6 cooling to solid UF_6 rotated about θ

If we assume that all the UF_6 is in a solid state, it should have a uniform density of 5.1 g/cm^3 [10]. Also, per Table 2.1, the maximum amount of UF_6 allowed in a 30B cylinder is 2,277 kg. This means that this amount of material would take up the following volume:

$$\rho = \frac{M}{V} \rightarrow V = \frac{M}{\rho} = \frac{2,277 \text{ kg}}{.0051 \text{ kg/cm}^3} = 4.5\text{e}5 \text{ cm}^3 \tag{4.7}$$

According to [10], the internal volume of a 30B cylinder is 26 ft.^{3} or 7.4e5 cm^3. So, a 30B cylinder filled with the maximum amount of UF_6 would be filled approximately

$$\frac{4.5\text{e}5 \text{ cm}^3}{7.4\text{e}5 \text{ cm}^3} \approx 60\%. \tag{4.8}$$

With this information it is possible to solve for the center of gravity of the cylinder in one orientation. Finding the center of gravity of the 60% full cylinder is equivalent to solving for the center of gravity of a completely full cylinder and subtracting the center of gravity of the 40% empty half cylinder [52]. If the cylinder is oriented such that the material is symmetrical in the y axis, the following equations apply:

$$m_1 z_1 = m z_0 - m_2 z_2 \tag{4.9}$$

and

$$m = m_1 + m_2 \tag{4.10}$$

Where:

$m_1 =$ the mass of the 60% of the cylinder filled with UF_6

$m_2 =$ the mass of the 40% void space

$z_0 =$ the center of gravity of a completely filled cylinder

$z_1 =$ the center of gravity of the 60% of the cylinder filled with UF_6

$z_2 =$ the center of gravity of the 40% void space

Given that the center of gravity for a full symmetric cylinder is 0 in z, this series of equations becomes

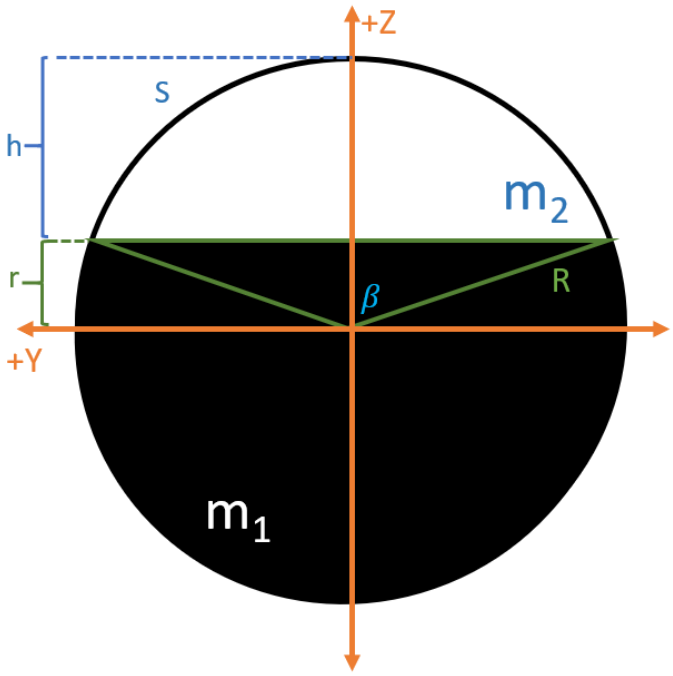


Figure 4.7: The 40% void space of a cylinder bounded by an isosceles triangle

$$z_1 = \frac{-m_2 z_2}{m_1}. \tag{4.11}$$

If we assume that the material is uniformly solid, both m_1 and m_2 will be proportional to the area of the geometric objects they represent in two dimensions. The area of m_2 then can be thought of as a circular segment bounded by an isosceles triangle of angle β as seen in Fig. 4.7, where R is the radius of the 30B cylinder, r is the distance from the origin to the side of the triangle opposite angle β, h is the distance from the far side of the triangle to the top of the 30B cylinder, and s represents the arc length of the 40% void space [53].

For this figure, $R = 38.1$ cm, which is the radius of a 30B cylinder, and h must represent 40% of the diameter of the 30B cylinder, or 30.48 cm. r then can be found from

$$r = R - h = 7.62 \text{ cm}. \tag{4.12}$$

Because the void space is a circular segment, the area can be defined as

$$A = A_{sector} - A_{triangle} = \frac{R^2(\beta - \sin(\beta))}{2}. \tag{4.13}$$

Where β is:

$$\beta = 2 \arccos \frac{r}{R} = 2.7389 \tag{4.14}$$

This then lets us solve for the mass ratio using the following equation:

$$\frac{m_2}{m_1} = \frac{\frac{R^2(\beta - \sin(\beta))}{2}}{\pi R^2 - \frac{R^2(\beta - \sin(\beta))}{2}} = 0.5963 \tag{4.15}$$

The last step required for finding z_1 is to find z_2. This is equivalent the geometric centroid of the circular segment, which can be found with the following equation:

$$z_2 = \frac{4R \sin \frac{\beta}{2}^3}{3(\beta - \sin \beta)} = 20.3592 \text{ cm} \tag{4.16}$$

z_1 is then:

$$z_1 = -0.5963 * 20.3592 \text{ cm} = -12.1 \text{ cm} \tag{4.17}$$

As a cylinder with this material distribution is rotated about the origin, the center of gravity with respect to the material inside the cylinder will not change. Instead, the values of the y and z axes will change as a function of the angle of rotation. The relationship between y and this angle along with the length, L, of the center of gravity with respect to the material can then be solved for using trigonometry.

Figure 4.8 shows a 30B cylinder rotated about ϕ. In this figure, L is the location of the center of gravity with respect to the material in the cylinder. For $\phi = 0°$, this is equivalent to z_1 that was solved for previously. Here, the original location of the center of gravity and the new location of the center of gravity after the cylinder has been rotated form an isosceles triangle. The new locations of y and z can then be thought of as a right triangle attached to the side, c, of the isosceles triangle.

y can then be solved for using this equation:

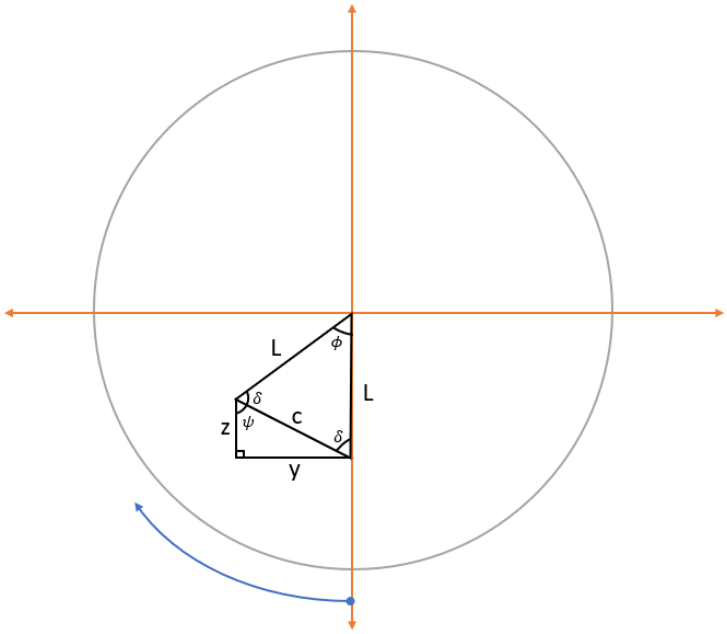


Figure 4.8: 30B cylinder rotated about ϕ

$$y = -\sin(\psi)c \tag{4.18}$$

ψ can be expressed in terms of ϕ using the following relationships between the angles:

$$2\delta + \phi = 180 \rightarrow \delta = 90 - \frac{\phi}{2} \tag{4.19}$$

and

$$\psi = 90 - (90 - \delta) = 90 - \frac{\phi}{2} \tag{4.20}$$

c can then be expressed in terms of L using the law of cosines:

$$c^2 = L^2 + L^2 - 2L^2\cos(\phi) = 4L^2\sin(\frac{\phi}{2})^2 \rightarrow c = 2L\sin(\frac{\phi}{2}) \tag{4.21}$$

Finally, 4.20 and 4.21 can be plugged back into Equation 4.18 to get the following solution for y in terms of L and ϕ:

$$y = -2L\sin(90 - \frac{\phi}{2})\sin(\frac{\phi}{2}) = -2L\sin(\frac{\phi}{2})\cos(\frac{\phi}{2}) \tag{4.22}$$

Measuring θ as depicted in Fig. 3.2 is much easier than measuring ϕ because the nameplate serves as a reasonable reference point, so it is useful to express Equation 4.22 in terms of θ rather than ϕ. When the material in the cylinder is fully distributed on the bottom of the cylinder, ϕ will be at 0° and θ will be 90°, so:

$$\phi = \theta - 90 \tag{4.23}$$

Therefore, Equation 4.22 becomes

$$y = -2L\sin(\frac{\theta - 90}{2})\cos(\frac{\theta - 90}{2}) = L\cos(\theta). \tag{4.24}$$

The cosine function behaves as expected given the assumption that the material in the cylinder does not move as θ changes. The center of gravity in y is 0 cm when the cylinder is at 0° and 270° because the material is symmetric about the y axis by either being at the bottom or the top of the cylinder. The center of gravity in y also approaches L as material is distributed entirely on the left side of the cylinder at 180° and approaches $-L$ as the material is entirely on the right side of the cylinder at 0°. Again, note that the reference frame for the top-down view of the cylinder defined in Fig. 3.1 means that y is positive to the left when looking at the cylinder nameplate and negative to the right. Fig. 4.9 shows a plot of the cosine function using the value found for z_1 earlier, -12.1 cm, as L.

In practice, the fill height assumption in this section is a reasonable assumption for full 30B cylinders that have been filled to near the maximum amount of material allowed in the cylinder. Also, the assumption that material does not redistribute in the cylinder with respect to θ likely holds true for a range of θ near 90°. Once the cylinder has been rotated to near 180°, the crystalline structure of UF_6 would likely be unable to support the weight of the material, and at least some of it would fall back toward the bottom of the cylinder. This hypothesis is partially based on the Portsmouth study of the inside of a UF_6 cylinder, which demonstrated how easily solid UF_6 crystal could be separated from other

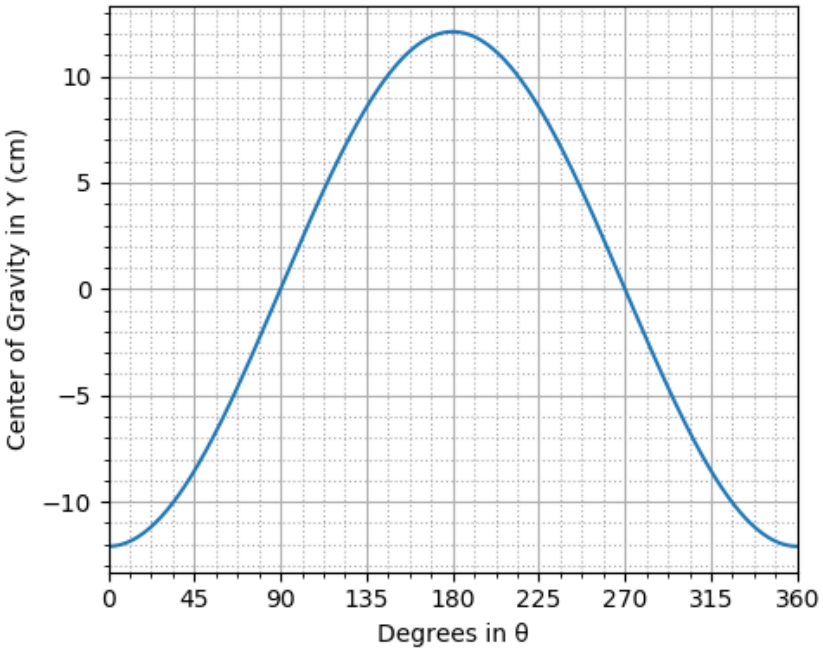


Figure 4.9: Plot of the relationship between y and θ from 0° to 360° of rotation

solid UF_6, as well as the commentary throughout the existing literature that material inside the cylinder shifts with operator handling [4], [6].

Chapter 5

Experiment

This chapter discusses how measurements were collected, how calculations using experimental data were made, and how the environment where the data was collected varied over time. This section also discusses sources of measurement uncertainty and some of the methods that were used to control and correct for sources of systematic error. Finally, the formulas used to propagate random uncertainty in the measurement system are derived.

5.1 Measurements

The data used for the center of gravity study in this work originated from a platform scale system at a nuclear facility that was instrumented so that values representing the force applied to each individual load cell could be recorded. Data was collected for 1 min. on each cylinder measured by the platform scale while the cylinder was stable on the platform. The zero value for each individual load cell before the cylinder was loaded was also measured for approximately 1 min. so that zero drift over time and differences in scaling of the force values from each load cell could be corrected for.

The center of gravity calculation with this system is very similar to what was used in the laboratory setting, except that instead of subtracting the weight of the empty cylinder, the zero weight of the scale is subtracted. This results in the following equation for the center of gravity:

Table 5.1: Coordinates for Each Load Cell in the Platform Scale

Load cell position	X (cm)	Y (cm)
Front-left	-83.82	48.26
Back-left	83.82	48.62
Front-right	-83.82	-48.62
Back-right	83.82	-48.62

$$\overrightarrow{R_{cg}} = \frac{1}{M^{cylinder}} \sum_{1}^{N} \overrightarrow{r_i}(m_i^{cylinder} - m_i^{zero}) \tag{5.1}$$

Where:

$R_{cg} =$ a vector pointing to the center of gravity location given the coordinate system defined in Fig. 3.1

$M^{cylinder} =$ the average total force applied by the cylinder to all four load cells over the 1 min. measurement

$N =$ the number of load cells in the system, which is four for this platform scale

$\overrightarrow{r_i} =$ a vector pointing to the location of an individual load cell, i, shown in Table 5.1 given the system frame of reference from Fig. 3.1

$m_i^{cylinder} =$ the average force applied to the individual load cell i for 1 min.

$m_i^{zero} =$ the average force applied to the individual load cell i for 1 min. before the cylinder was loaded on the platform scale

The platform scale system was used to collect measurements on 240 30B cylinders filled with UF_6 over about 4 months. Unless otherwise noted, each of these cylinders was filled with approximately 2,200 kg of UF_6. Each of the full cylinders had been homogenized, which is a process that converts all the solid UF_6 in a cylinder to a liquid state before allowing it to cool again. The cylinders then had sufficient time to cool before they were measured, and a majority of the UF_6 could reasonably be expected to be in the solid state. Based on the literature in chapter 2, it is reasonable to postulate that the typical material distribution of the cylinders measured during this data collection effort should most resemble the $x = 0$ case presented in Fig. 2.10.

During the measurement campaign, the platform scale was outside and subjected to ambient temperature swings, but it was somewhat protected from the elements by a roof. The overall ambient temperature range over all the measurements was -9 °C to 41 °C. During this time, the system encountered rain, high winds, and snow/ice conditions.

5.2 Uncertainty from the Platform Scale

Most of the literature on capturing the uncertainty in a scale system is based on using the scale to find the weight of an object in engineering units. This section explores some of the considerations for quantifying uncertainty for this use case and then details which of those are applicable to the center of gravity calculation using measured force values applied to each load cell.

Since force transducer systems like the platform scale do not have an absolute internal reference for the measurement of force, they are all highly dependent on a calibration and calibration procedure to achieve high accuracy measurements. NIST finds the combined standard uncertainty of a force transducer system like the platform scale by solving the following equation from [54]:

$$u_c^2 = u_f^2 + u_v^2 + u_r^2 \tag{5.2}$$

Where:

u_f^2 = the standard uncertainty associated with the applied force. This value is impacted by uncertainties in the mass calibration, uncertainties in the air density, and uncertainties in the acceleration of gravity.

u_v^2 = the standard uncertainty in the calibration of the voltage ratio measurement instrumentation.

u_r^2 = the standard uncertainty calculated according to ASTM 74-04 [49]. This value is impacted by differences between the individual measured responses and the calibrated response.

Because center of gravity measurements use a ratio of the force response of each individual load cell weighted by their position to a summation of the force response of all the load cells, the calculation does not require a mass calibration. Therefore, the standard uncertainty associated with the force applied to the system is not important to consider in this experiment because it only applies to uncertainties of a standard weight used for calibration.

The standard uncertainty in the calibration of the voltage ratio measurement instrument also does not apply to this system per NIST guidance because the platform scale incorporates an indicating instrument directly into the load cell by performing the analog-to-digital conversion within the load cell itself [54]. The digital values from the load cell are then transmitted to the weight indicator for readout.

The contribution to the uncertainty of the measurement from the difference between individual measured responses and the calibrated response is the primary uncertainty component that affects the center of gravity measurement. Again, a calibration to engineering units is not needed for the center of gravity calculation, but the center of gravity calculation does assume a linear response of the load cells to an applied load. This term captures factors that may cause load cells to deviate from that assumption including random errors associated with the electronics, creep, hysteresis, temperature response, zero drift, and any sensitivity of the scale response to where an object is placed on the scale [54], [42]. The scale may also exhibit a nonlinear response if the system is not level with respect to the ground [55].

NIST does not attempt to quantify the impact of each of these effects using a bottom-up approach. Instead it outlines a procedure for measuring the combined impact of these sources of uncertainty using a series of known reference forces in sequence. The recorded responses from this procedure are used to create a quadratic calibration curve using the following equation from [54]:

$$R = A_0 + \sum A_i F_j \tag{5.3}$$

Where:

$R =$ the transducer response

$F =$ the applied force

$A_i =$ are coefficients characterizing the transducer that are typically carried to the order of 2 or 3 for load cells. These coefficients are derived by applying a least squares fit to the calibration data.

NIST fits a quadratic response function because force transducers do not, in fact, have a linear response to applied load. This is, however, a reasonable assumption for commercial load cells because they have been compensated to have a fairly linear response to force under a range of operating conditions by the manufacturer.

Once the response function is fit, the uncertainty due to the variation of the measured data from the fitted calibration curve can be found using the standard deviation with this equation from [54]:

$$u_r^2 = \frac{\sum d_j^2}{n - m} \tag{5.4}$$

Where:

$d_j =$ the differences between the measured responses R_j and the calculated responses from the calibration curve

$n =$ the number of individual measurements in the calibration data set

$m =$ the order of the polynomial plus one

NIST's approach to quantifying this component of the scale uncertainty would be useful for the calculation of the center of gravity because it could be used to find the uncertainty of each load cell's response to an applied load, which could then be propagated through the center of gravity calculation. Unfortunately, a known set of representative weights were not available at the nuclear facility used for data collection, so this calibration could not be performed. Also, this procedure would not fully capture the uncertainty due to changes in ambient temperature because the scale is sitting outside, and the calibration would happen at a certain point in time with a certain ambient temperature. Instead, the approach taken in this work is to control some of the

contributors to this uncertainty term with procedure and to quantify the other sources of uncertainty to the extent possible. The approach used to control for each of these different uncertainty components is discussed in the next few sections.

5.2.1 Force Transducer Behavior

There are many different potential sources of error related to force transducer behavior. These effects typically cause the force transducer to respond to force in a nonlinear way, change the slope of the linear response, or change the zero point of transducer. Some of these effects include creep, hysteresis, response changes due to temperature, and zero drift over time [54].

Creep refers to the change of the response of a force transducer while it is under a constant load. This can be thought of as a "relaxing" of the spring-like elastic material in the load cell. This effect can be measured by keeping the load cells under constant load for around 30 min. in constant environmental conditions [42]. The effect of creep in this work is minimized by using a short measurement time of 1 min. and taking the average of the measurements collected during that time.

Hysteresis refers to the difference in the output reading of the load cells for the same applied load depending on if the reading was obtained by increasing the load from the minimum load of the cell or if it was obtained by decreasing the load from the maximum load of the cell [42]. Hysteresis is one of the reasons why a load cell might respond in a nonlinear manner to applied load. This effect is not much of a concern in this work because the loads being measured are all at approximately the same gross weight, and the scale always starts from a near zero load before a cylinder is measured.

Changes in ambient temperature can also cause the slope of the load cell response to translate up or down, or it might increase or decrease the angle of inclination of the response. Ambient temperature changes may also cause the zero point of the scale to drift over time [42]. Very little can be done to account for changes in the load cell response due to changes in ambient temperature. All four of the load cells in the platform scale are high-precision commercial load cells that are supposed to be compensated for

temperature from -10 °C to 40 °C, which is almost identical to the range of temperatures experienced by the platform scale over 4 months. Zero drift due to temperature is corrected for by capturing 1 min. of data from the platform scale before the cylinder is loaded to use as the zero point for the subsequent measurement.

Because each of these metrics is either compensated by the commercial load cell or controlled using measurement procedures, these sources of uncertainty are not considered when propagating uncertainties.

5.2.2 Cylinder Positioning on the Platform

Uncertainties of the force response due to the placement of a cylinder in different locations on the scale was controlled by limiting the ability of the operator to place the cylinder in different locations. Given the frame of reference from Fig. 3.1, the consistent placement of the cylinder in the y axis on the platform scale was guaranteed by using v-blocks to hold the cylinder in a fixed location during measurements. Variations of the cylinder placement in x were also minimized by giving the operators a target to aim the "front" end of a cylinder toward during loading.

The target limited gross deviations in cylinder placement, but there were still small differences that could impact the results of the center of gravity calculation. These variations were measured using a laser distance measurement system that was mounted a fixed distance from the platform scale. This measured value was then used to correct the calculated center of gravity values to ensure that cylinders were all compared in the reference frame of the cylinder rather than in the reference frame of the platform scale system. The equation for this correction is

$$x_{cg}^{corr} = x_{cg}^{meas} - x^{laser}. \tag{5.5}$$

Where:

$x_{cg}^{corr} =$ the corrected center of gravity in x

$x_{cg}^{meas} =$ the calculated center of gravity in x before correcting for differences in cylinder placement

x^{laser} = the distance, in centimeters measured by the laser distance sensor

Also, while the positioning of the cylinder in y was consistent, the angle θ (described by Fig. 3.2) was also shown to impact y from the laboratory testing in Chapter 4. Facility handling requirements called for operators to limit the amount of rotation in θ for any cylinder filled with UF_6 at the facility. A θ of 90° is considered normal in the facility and in practice, operators would ensure that θ would not deviate by more than 10° during cylinder handling operations. However, even this degree of variation will complicate the comparisons of the y center of gravity values for different cylinders.

So, since there was no way to limit degree of cylinder rotation, a fixed focal length camera was mounted a fixed distance away from the front of the platform to capture an image of the nameplate of each cylinder measured by the platform scale. The angle θ was then measured manually in post-processing using the Fiji image processing package [56]. Fiji is a tool typically used to aid in scientific image analysis in bioimage informatics and biology and has built in tools that allow for angle measurements within an image.

The measured θ was then used in to calculate a correction factor for the center of gravity in y using the mathematical model derived in Section 4.2. This results in the following equation for correcting y:

$$y_{cg}^{corr} = y_{cg}^{meas} + 12.1\text{cm}\cos(\theta) \tag{5.6}$$

Where:

y_{cg}^{corr} = the corrected center of gravity in y

y_{cg}^{meas} = the calculated center of gravity in y before correcting for angle

For this work, the uncertainty due to the process of manually measuring the angle in the image of the cylinder nameplate was estimated to be approximately 0.25°. This results in an error of ± 0.043 cm to the y axis correction factor which will be incorporated into the variance propagation discussed in Section 5.2.3.

Another potential source of uncertainty related to cylinder positioning can be caused by a failure to ensure that the scale is completely level when it is installed. This does not

necessarily impact the linear response of the load cells, but it does change the angle of the force vector being measured by the load cell system. This, in turn, will introduce a systematic bias into the measured center of gravity values because of this angle.

5.2.3 Random Error from Electronics

The random uncertainty from electronics are captured by taking the standard deviation of multiple measurements for each sensor used in this work over the 1 min. of data collection. This standard deviation is then propagated through the calculations using the following sets of procedures and equations.

First, before calculating the center of gravity, the zero value of each individual load cell recorded during the 1 min. before the cylinder was loaded into the platform scale is subtracted from the load cell response of the loaded cylinder, as seen in the inner portion of the sum in Equation 5.1. The standard deviations of the measurement variability during each of these times is propagated as follows for each load cell:

$$\sigma_{m_i} = \sqrt{\sigma^2_{m_i^{cylinder}} + \sigma^2_{m_i^{zero}}} \tag{5.7}$$

Where:

$\sigma_{m_i^{cylinder}}$ = the standard deviation of the measurements while the cylinder is on the platform scale

$\sigma_{m_i^{zero}}$ = the standard deviation of the measurements for 1 min. before the cylinder is loaded on the scale

The resulting values are then used to compute the center of gravity per Equation 5.1. The uncertainty is propagated through the rest of that calculation as follows to find the uncertainty of the uncorrected center of gravity vector

$$\sigma_{\overrightarrow{R_{cg}}} = \overrightarrow{R_{cg}} \sqrt{\frac{\sum(\overrightarrow{r_i}\sigma_{m_i})^2}{\sum(\overrightarrow{r_i}m_i)^2} + \frac{\sum(\sigma_{m_i})^2}{\sum(m_i)^2}} \tag{5.8}$$

In x, the center of gravity value is then corrected by the average of the laser distance sensor values measured for 1 min. per Equation 5.5. The final resulting uncertainty for

center of gravity in x is the square root of the sum of squares as seen in the following equation:

$$\sigma_{x_{cg}^{corr}} = \sqrt{\sigma_{x_{cg}^{meas}}^2 + \sigma_{x^{laser}}^2} \tag{5.9}$$

The final propagation step in y also uses a square root of the sum of squares to propagate uncertainty from Equation 5.6, but here a constant value related to the estimated uncertainty of 0.25° for measuring θ is used

$$\sigma_{y_{cg}^{corr}} = \sqrt{\sigma_{y_{cg}^{meas}}^2 + (0.043)^2} \tag{5.10}$$

5.3 Uncertainty from Differences in Empty 30B Cylinders

Ideally, this work would be comparing center of gravity differences between cylinders solely caused by the UF_6 material distribution inside the cylinder. One potential source of systematic error that may complicate this comparison is that there might be a differences in the center of gravity of the 30B cylinders themselves. These differences could exist between individual cylinders or could exist in populations of cylinders from different manufacturers as a result of differences in manufacturing processes. Because the ANSI N14.1 standard has changed over time, differences might also exist based on the year the 30B cylinder was built [1].

Any differences in the center of gravity between empty 30B cylinders are likely to be fairly small. There are two main reasons for this. First, the ANSI standard does allow for tolerances in specified dimensions of the 30B cylinder, but these tolerances tend to be fairly tight. Also, things like the valves used in the cylinder that might introduce the most variation in the center of gravity between cylinders are specified in detail. Second, any difference in the center of gravity between empty 30B cylinders that is introduced by the ingress of UF_6 into the wall of the 30B cylinder over time is likely negligible based on destructive analysis studies that have shown that in the worst case, UF_6 only penetrated the first 100 µm of depth of the interior wall of the cylinder [13].

The best way to control for this source of systematic uncertainty is to take two measurements for a given cylinder: 1) when it is filled with UF_6 and 2) after the UF_6 has been removed from the cylinder and the cylinder has been washed. This approach is consistent with the approaches for measuring the center of gravity of a complex system outlined in the literature given that the center of gravity of the material inside the UF_6 cylinder is the measurement of interest [8].

Because heels of material are always left behind in a cylinder when UF_6 is removed, measuring the cylinder after removal of UF_6 would not support an accurate empty cylinder correction. The only way to be confident the heels are no longer present in the cylinder is to completely wash the inside of the cylinder. This process is commonly performed during cylinder recertification and requires special equipment. The washing process is time-consuming, and not every nuclear facility has the capability to wash cylinders. These limitations mean that true empty cylinder center of gravity measurements are not available for any of the filled cylinders measured in this data collection effort. Instead, a few empty and heeled cylinders were measured to provide an example of what the center of gravity may look like for both cases.

Chapter 6

Analysis and Results

This section discusses the results and analysis from the data collection campaign. First, a few of the sources of systematic error identified in Chapter 5 are examined. Then analysis results on repeated measurements of the same small set of cylinders over time as well as the analysis results of trends in the entire cylinder population are discussed.

6.1 Degree of Rotation of all the Measured Cylinders

One of the major sources of systematic error for the y axis center of gravity measurement that impacts the ability to compare different cylinders is the angle of rotation of the cylinder with respect to the ground when it is placed in the platform scale. Throughout this work, this angle has been measured as θ per Fig. 3.2.

This angle was measured manually for each cylinder that visited the platform scale system. The distribution of these measurements for all the cylinders measured as part of the data collection campaign is shown in Fig. 6.1. This distribution is plotted against the correction factor for the center of gravity in y over this angle range assuming that all the material is a solid inside the cylinder and fills about 60% of the bottom of the cylinder.

From Fig. 6.1, the range of θ measured in the field trial is from 84.2° to 93.7° with a mean of 89.3° and a standard deviation of 1.6°. This span of 9.5° is much smaller than what is allowable by the facility operating limits, but does illustrate that operators are attentive to this angle during cylinder handling operations. The small range of the angles

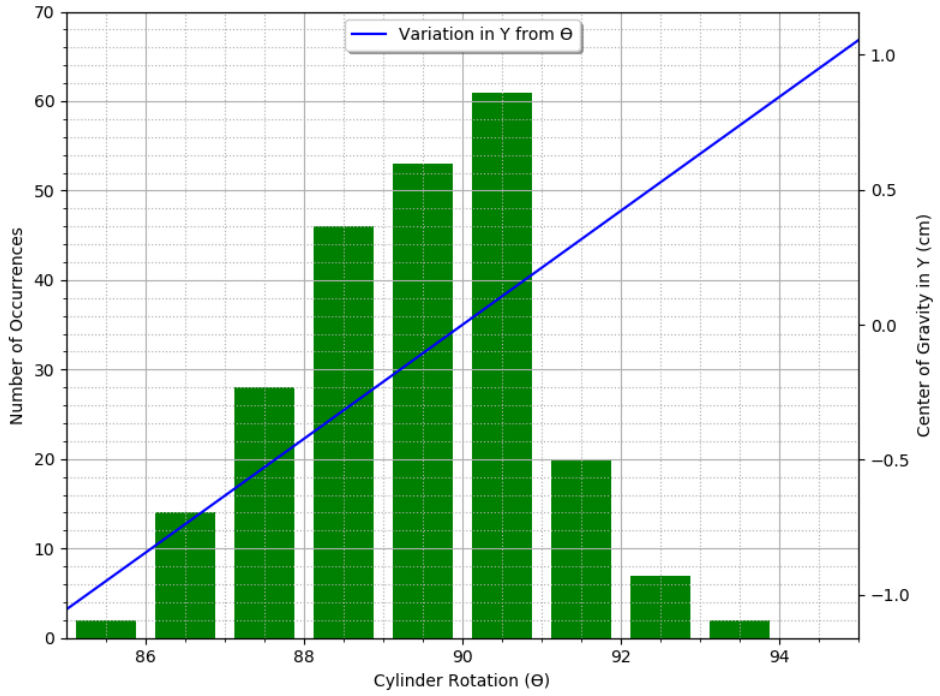


Figure 6.1: Distribution of θ in measured full 30B cylinders

measured in this field trial as well as the fact that all the cylinders are fully filled means that the assumptions made in the derivation of the correction factor for θ in Section 4.2 are reasonable for the cylinders measured in this work. So, using the correction factor to modify the y center of gravity value calculated from the platform scale should provide results that allow for better comparisons between different cylinders.

Based on the full range of different cylinder angles seen in the data collection effort, the average correction factor for y due to θ is -0.14 cm. The total range for the correction factor is from -1.22 cm to 0.77 cm with a standard deviation of 0.33 cm.

6.2 Center of Gravity in Empty or Heeled Cylinders

Three empty 30B cylinders and two 30B cylinders with heels were measured in addition to the 240 cylinders filled with UF_6. The center of gravity in x and y for these five cylinders is shown in Fig. 6.2. The top plot is this figure shows the x center of gravity value plotted against the y center of gravity value, and the bottom two plots show x and y individually

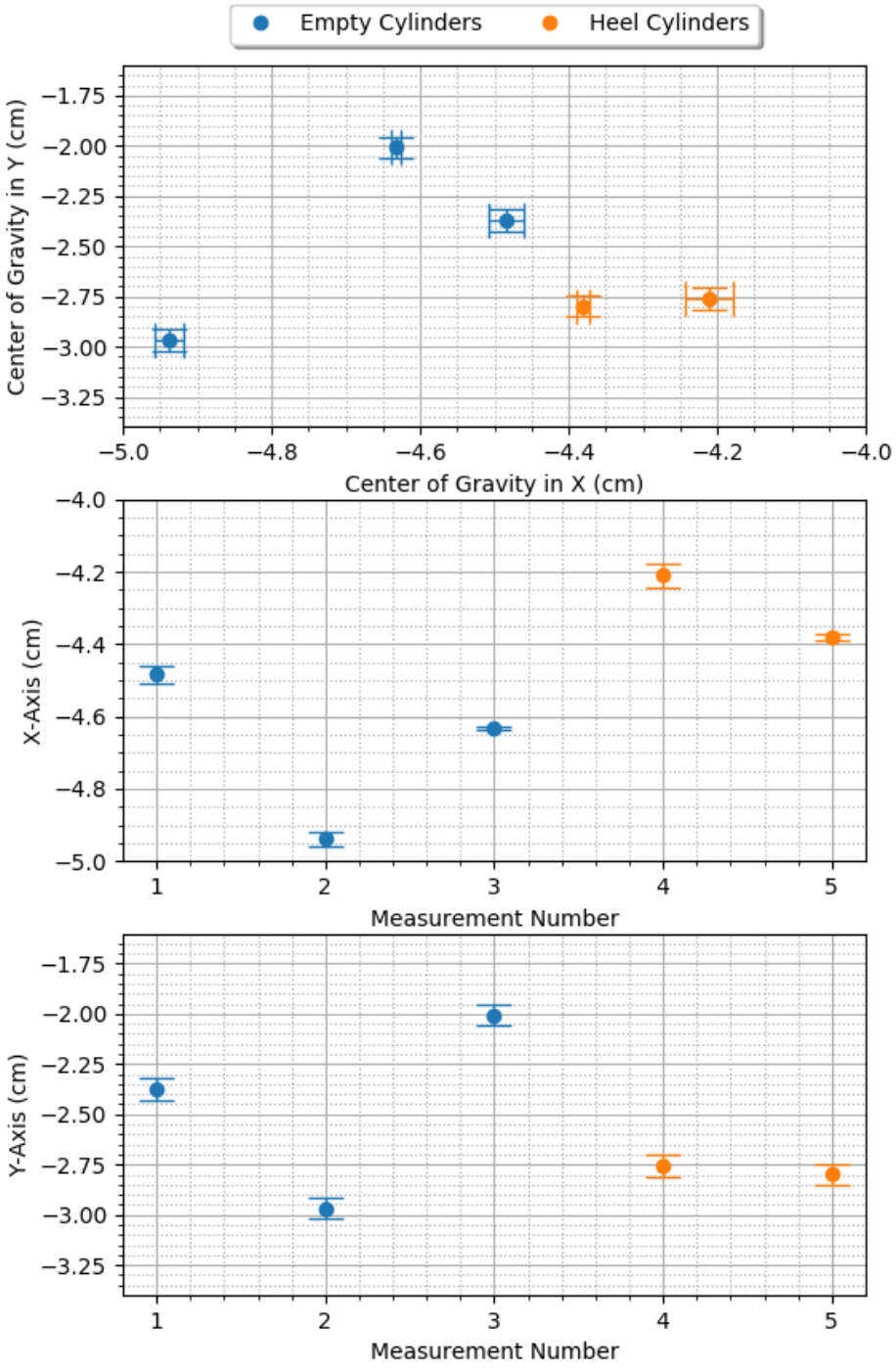


Figure 6.2: Center of gravity in x and y for empty and heel cylinders

on the y axis plotted against the measurement number on the x axis. The error bars in these plots were calculated using the approach described in Section 5.2.3.

It is common for 30B cylinders from a single enrichment company to share a serial number prefix. If it is conservatively assumed that each company buys 30B cylinders from a different manufacturer, then each unique prefix might denote a set of cylinders from a certain manufacturer. Based on this assumption, the three empty cylinders are likely from two different manufacturers, and each heel cylinder is likely from a different manufacturer. One of the heel cylinders has the same cylinder identifier prefix as two of the empty cylinders, so it is probable that these cylinders are all from the same manufacturer. Because this is such a limited data set, it is important to be careful about extrapolating any larger claims about the cylinder population from these results.

That said, a few interesting things can be noted. First, all of these measurements are in the $-x$ and $-y$ quadrant, which means their center of gravity tends to be toward the front right corner of the cylinder. The trend toward the front end of the cylinder (where the cylinder nameplate is located) makes intuitive sense because Fig. 2.2 illustrates that there is clearly more of a steel lip on the front of a 30B cylinder than the back of a 30B cylinder.

The trend toward the right, on the other hand, makes less sense. The valve on the front of the 30B, the cylinder nameplate, and the plug at the back of a 30B are all centered with respect to the y axis per manufacturing specifications. It is possible that the valve of the 30B cylinder might weigh slightly more than the plug, so as θ increases beyond 90°, there might be a slight tendency toward the right; however, this is not consistent with the distribution of the angles in Fig. 6.3, as the empty and heels population has angles both greater and less than 90°.

The trend toward the right might be indicative of a systematic bias in the scale based on the design or placement of the platform. This kind of bias might appear if, for example, the system was not well leveled when it was installed. This potential bias in y does impact the ability to find the absolute center of gravity of the UF_6 within a cylinder, but deconvolving this value from the center of gravity contribution of the 30B cylinder itself is already infeasible without two measurements for each filled cylinder (one with it full and

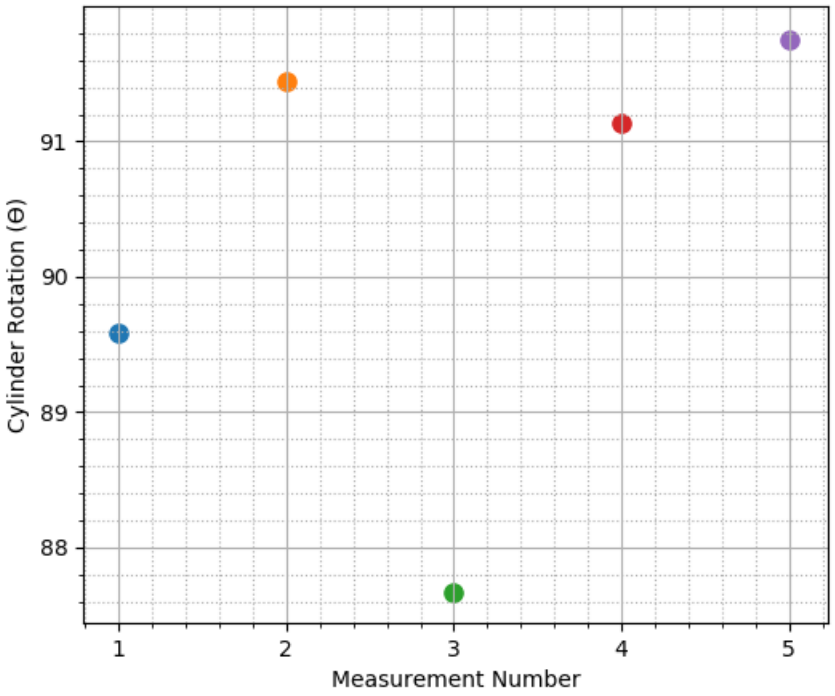


Figure 6.3: Measured θ for empty and heel cylinders

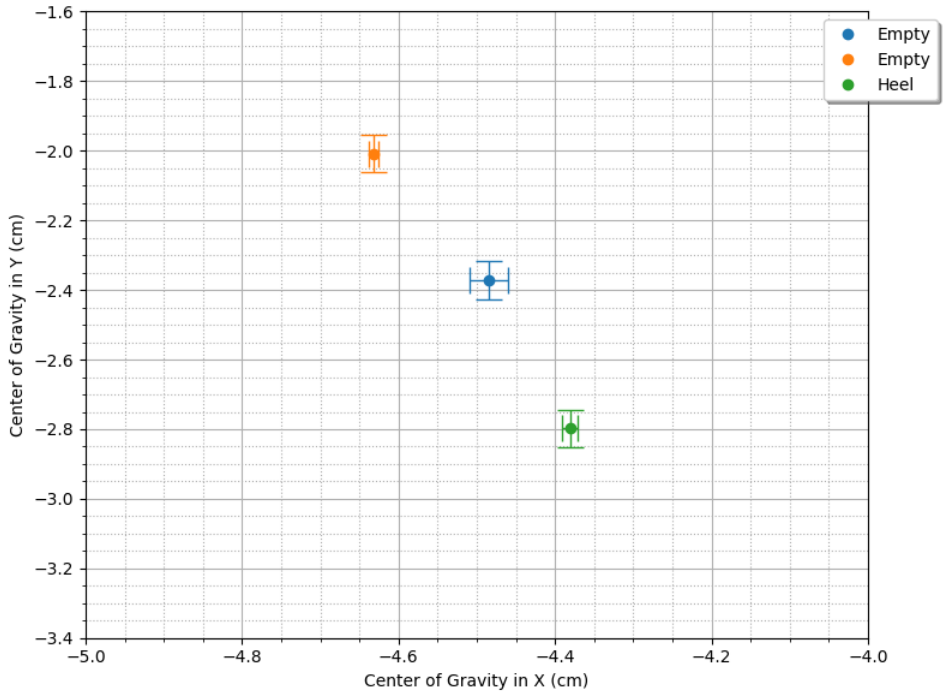


Figure 6.4: Empty and heel cylinders from one manufacturer

one with it empty). This bias does not impact the ability to compare measurements of different filled cylinders because all the cylinders were measured with the same scale.

Another interesting feature of this data is that the heeled cylinders tend to have centers of gravity that are more toward the back of the cylinder compared to the empty cylinders. This finding is consistent with the notion that some heels of material remains toward the back of a cylinder after the UF_6 has been removed.

Figure 6.4 shows just the one heel and two empty cylinders that are mostly likely from the same manufacturer. These three cylinders are measurement number 1, 3, and 5 in Fig. 6.2. The limited number of measurements on these cylinders again complicate any ability to draw broad conclusions from the data presented in this figure. The three cylinders do have the tightest grouping in x compared to the other two cylinders, but they are not the tightest grouping in y. If anything, the fact that the two empty cylinders are not distinctly grouped together compared to the third empty cylinder may indicate that the specific cylinder manufacturer might not be strongly correlated with the empty cylinder's center of gravity.

6.3 Study of Repeated Cylinder Measurements

One of the main challenges of this study is that the measurement of interest is the center of gravity of the UF_6 inside the 30B cylinder, but what is measured is a combination of the center of gravity of the UF_6 inside the cylinder as well as the empty 30B cylinder itself. There is not a reasonable way to deconvolve these two contributors to the center of gravity from each other because none of the full cylinders measured were also measured empty. Also, while there were a few empty cylinders that were measured, this is not a large enough sample size to give enough confidence to create some kind of general correction factor for an empty cylinder.

One way to mitigate this issue is to repeatedly measure the same cylinder and compare those measurements to each other. The primary purpose of this type of measurement is not to measure the absolute center of gravity of the cylinder, as that will still be influenced by the center of gravity of the empty cylinder, but to look at trends in the value over time. The data set from the platform scale contains five full UF_6 cylinders that were measured multiple times. One of these cylinders was measured within a very short time interval, but the others were measured multiple times over 4 months.

The short term repeat cylinder was measured five times within 45 min. For each measurement, the cylinder was raised vertically off the platform scale using an overhead crane before being placed back down again. Due to the fact that ambient temperature was relatively constant and cylinder handling was minimal, it is reasonable to assume that the distribution of UF_6 inside the cylinder should not change during the repeated measurements. The repeat measurements on this cylinder can then be used as a baseline to understand the random uncertainty of the platform scale system.

Figure 6.5 shows two plots of the five repeat measurements. The top plot shows the repeat measurements in x, and the bottom shows repeat measurements in y. Each individual measurement is shown with error bars that reflect the random uncertainty from the variability of the electronics during each 1 min. measurement. The y axis values also include the uncertainty associated with manually measuring the θ of each cylinder. Also drawn are one and three σ lines centered around the average of all five measurements.

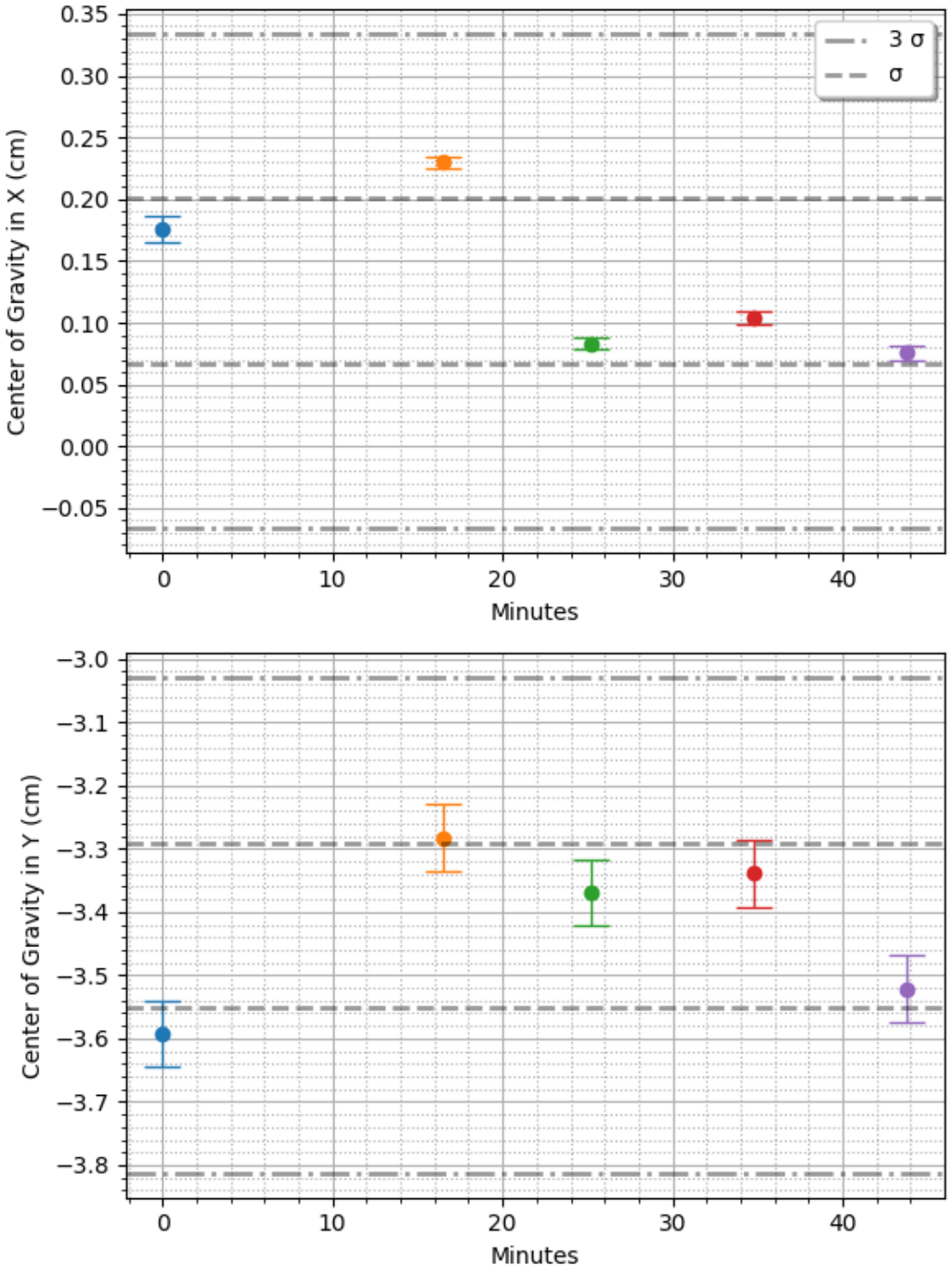


Figure 6.5: x and y center of gravity measurements for the same cylinder over 45 min.

The σ in this plot was calculated by taking the standard deviation of the five measurements.

Repeat weight measurements of the same object can reasonably be expected to eventually form a Gaussian distribution around the true value if no systematic biases exist. Given that, one interesting observation from Fig. 6.5 is that the error bars for each of the measurements in x would seem to indicate that the object under measurement has changes in the center of gravity that are significantly different from each other. On the other hand, the σ lines drawn by calculating the standard deviation of the five measurements in both x and y are within one to two σ from each other. This demonstrates that the error bars found by propagating the variance of the electronic errors and uncertainty in θ are an underestimate of the random uncertainty of the object under measurement. This finding is not particularly surprising because truly independent repeat measurements are required to quantify random uncertainty, which for load cells means the object under measurement must be fully removed and placed back on the scale.

Now that the short term repeat measurement has given a better understanding of the random uncertainty of the system, the σ from the short term repeat measurement can be used to ascertain whether or not any variation in the long term repeated measurement is significant. Figure 6.6 shows the change of the center of gravity value in x for the four cylinders that were repeatedly measured over 4 months, and Fig. 6.7 shows the results of the same set of measurements in y. Each of these plots are showing the difference between the first measurement of each of these cylinders and each subsequent measurement. If material does not move at all in the cylinder over time, then each subsequent measurement of the center of gravity should be within three σ of zero on the y axis in each plot. The one and three σ lines determined from the short term repeat measurement are plotted around 0 cm in both of these plots to aid in this determination. Also, the ambient outdoor temperature gradually increased from near freezing to around 30°C as the measurements progressed from the first measurement to the last measurement for these cylinders.

Three of the four cylinders in long term repeat measurement population show statistically significant deviations from zero over 4 months in both x and y. The fourth

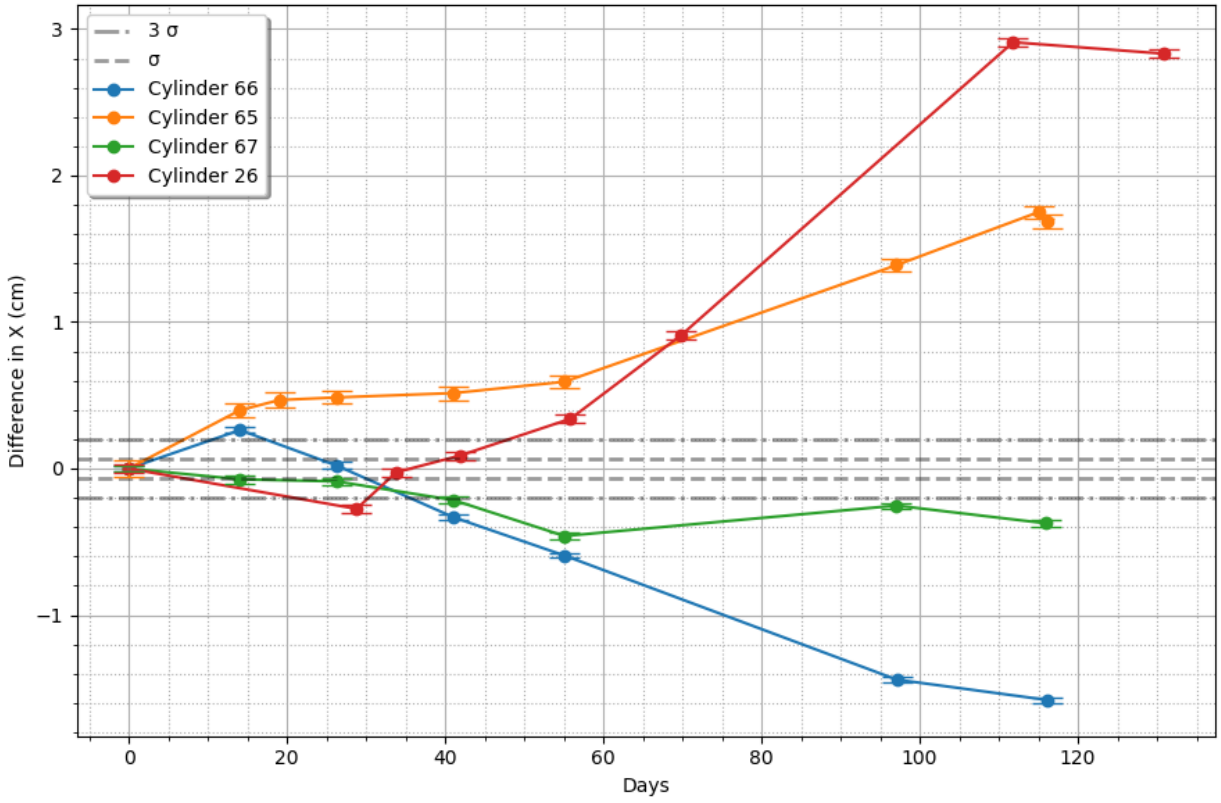


Figure 6.6: Changes of the center of gravity in x over 4 months for four cylinders

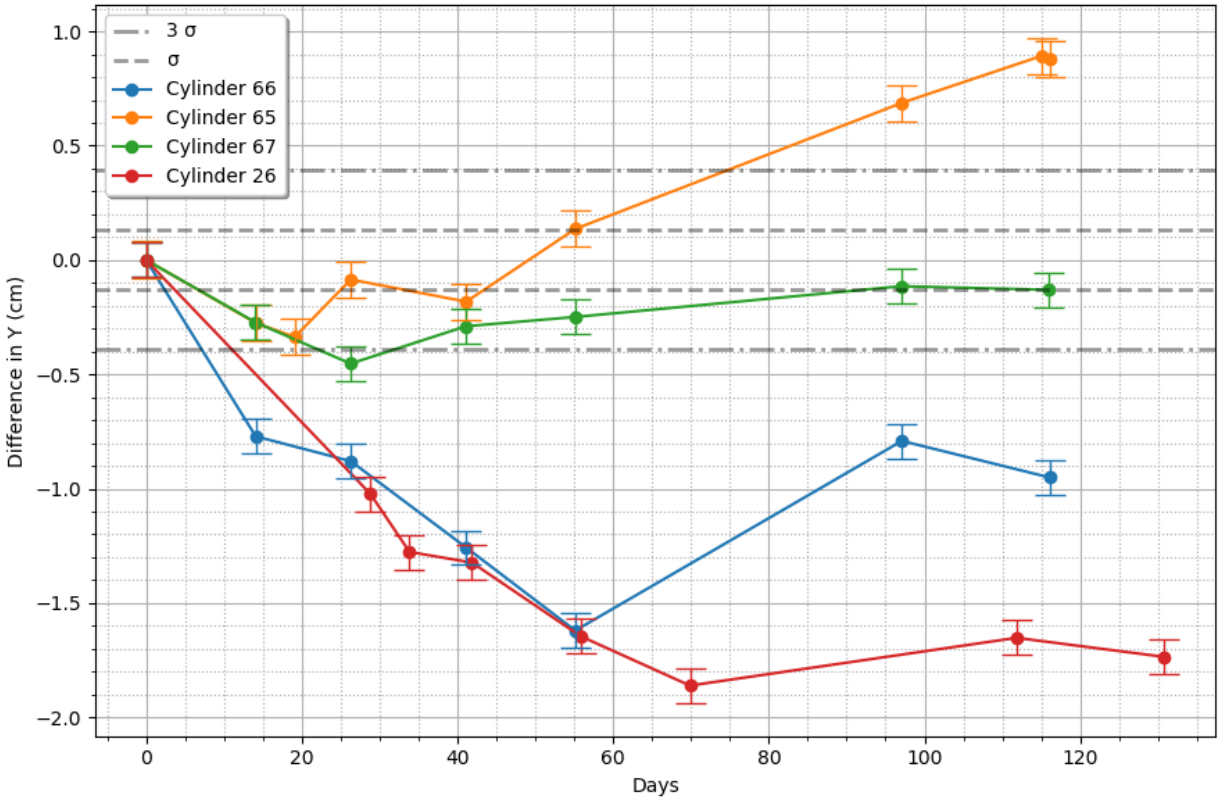


Figure 6.7: Changes of the center of gravity in y over 4 months for four cylinders

cylinder, cylinder 67, shows a statistically significant deviation from zero around 55 days into the field trial in x.

Also notable is the movement of material in the cylinder does not seem to trend in one specific direction for all four cylinders. In the x direction, material seems to be moving toward the front of the cylinder in cylinders 66 and 67, but it seems to move toward the back of the cylinder in cylinders 26 and 65.

In y, material in cylinders 66 and 26 initially goes to the right, but then material in 66 seems to move back toward the left. Material in cylinder 67 does not seem to move to the left or right in a statistically significant way over time, but then material in cylinder 65 seems to move towards the left over time.

Unfortunately, data is not available about where these cylinders were stored while outside or their orientation with respect to the sun. Also, how the cylinders were handled between repeated measurements is not known. This means that it is not possible to draw any conclusions about whether or not the material movement was caused by solid UF_6 crystals moving around in the cylinder due to handling by the operator or if the movement was from sublimation and desublimation of material in the cylinder due to radiative heating from the sun. Additional plots for the center of gravity in x and y for each of these cylinders are also available in Appendix A.

6.4 Study of the Large Cylinder Population

In addition to the smaller set of cylinders that were measured repeatedly, there were many cylinders that were measured just once on the platform scale. Figure 6.8 shows a scatterplot of all the measured center of gravity values for the entire cylinder population. It also shows a histogram of the measurements in x on the top portion of the plot, and a histogram of the measurements in y on the right side of the plot.

Values descriptive of the center of gravity for the entire population are shown in Table 6.1. A few things of interest in this table include the fact that the center of gravity in x and y only varied by 6.67% and 5.67% of the interior dimension of the 30B cylinder for the 240 full cylinders. Also, the mean for y is negative for the cylinder population, and

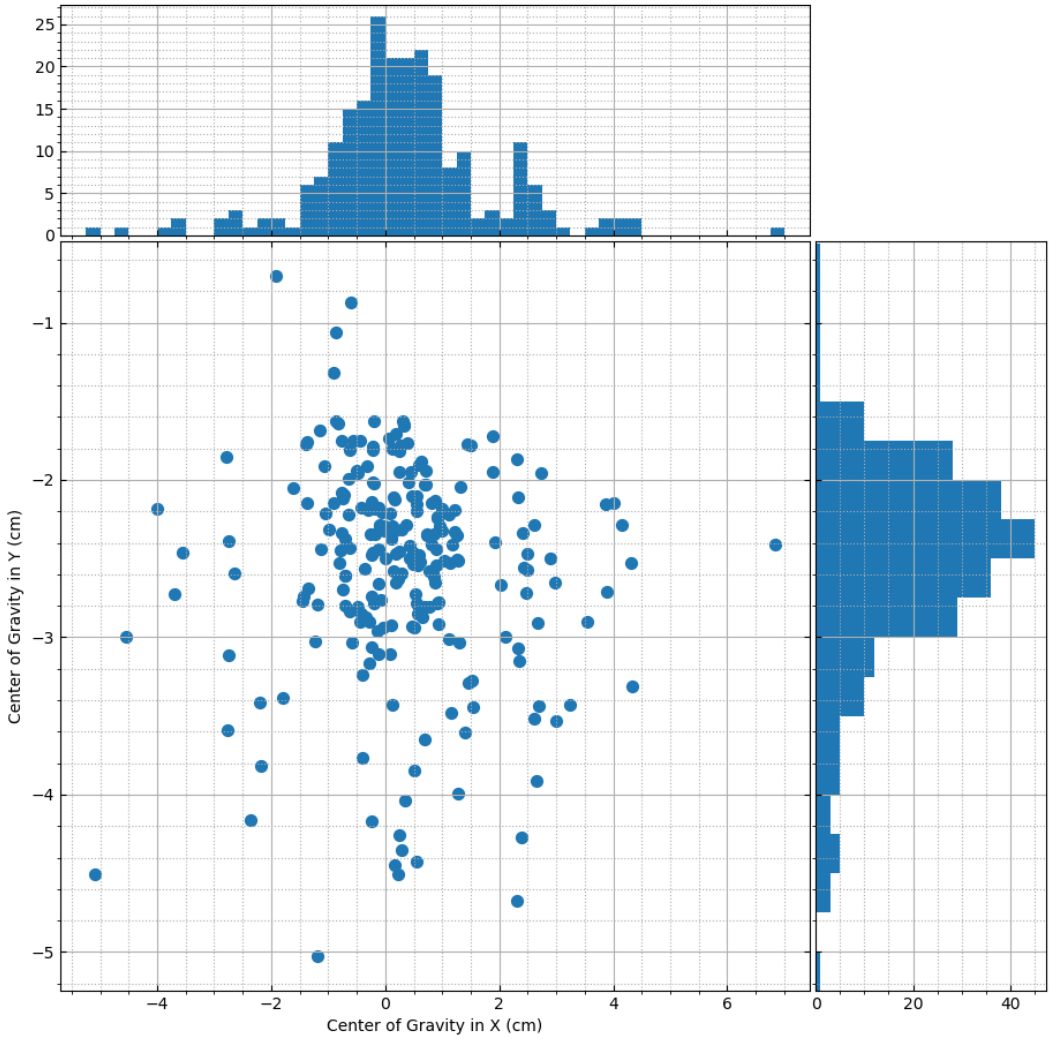


Figure 6.8: Center of gravity values for the entire cylinder population

Table 6.1: Center of Gravity Population Description

	x axis	y axis
Mean (cm)	0.32	-2.56
Standard deviation (cm)	1.53	0.68
Max (cm)	6.84	-0.71
Min (cm)	-5.10	-5.02
% of Interior Dimension	6.67%	5.67%

the maximum value of y is -0.71 cm. So, over the entire population the center of gravity of every single cylinder measured tends to be toward the right. Unfortunately, there is no additional data available from the platform scale that can indicate if this trend means that all the cylinders measured tended to have UF_6 distributed to the right, or if this is instead indicating that the platform scale is not entirely level with the ground.

Again, owing to the inability to separate the center of gravity of the UF_6 inside the cylinder from the center of gravity contribution of the 30B cylinder, it is difficult to use the measured value for the center of gravity for this population to make definitive claims about the shape of the distribution inside the cylinder. Instead, this large population will be used to analyze whether any of the known features of the cylinder seem to be strongly correlated to the measured center of gravity. This may, in turn, support what the literature has said about the movement of material within a cylinder, or this might provide attributes of a cylinder that merit further study. The cylinder population will also be broken into different populations based on temperature and studied to determine the relative dispersion of the measured center of gravity values. This study may show a relationship between the population cylinder's collective center of gravity values and ambient environmental conditions over the field trial.

6.4.1 Correlations between Center of Gravity and Quantitative Cylinder Attributes

The facility assisting with data collection made a wide variety of information available for each cylinder. This included things like destructive analysis results on a small sample of

the material in the 30B cylinder, how long the cylinder had been at the facility, and how long it had been since the cylinder was filled. Information about the ambient weather conditions during the cylinder measurement was also available.

Date and time data formats are not typically well behaved during correlation analysis. Examples of this type of data for this work include the date since the last time the cylinder was filled and the amount of time the cylinder had been at the facility. This data was parameterized by taking the amount of time in days from the given date to the start of the cylinder measurement. Also another column of information was added to the known data for the cylinder that represented the time, in days, from the start of the field trial to the time of measurement. This parameter is intended to be a proxy for the time of year.

Once all the provided data was in a proper format, it was scaled using minimum maximum scaling so that all data was in the range of (0,1) to reduce any errors that might be introduced by comparing data with different units [57]. The resulting correlation matrix can be seen in Fig. 6.9.

The center of gravity values for x and y both before and after their respective corrections for horizontal distance in x and angle in y are the first four columns on the top left of the correlation matrix. The x value is not strongly correlated with any of the other parameters available for the measured cylinders. The parameter with the largest positive correlation with x, at 0.26, is the gross weight, and the strongest negative correlation is between x and the ratio of ^{99}Tc to ^{235}U at -0.34.

There are some stronger positive and negative correlations between the y center of gravity and some of the other known parameters. Both y and corrected y have at least a weak negative correlation with both the number of days since receipt and the number of days since the cylinder was last filled. These correlations are at -0.44 and -0.43, respectively, for corrected y. The y value for center of gravity also has a weak positive correlation with several indicators that are related to the enrichment of the cylinder. These include the ratio of ^{234}U to ^{235}U, the ^{235}U enrichment, and the ^{235}U mass. All of these correlations are between 0.43 and 0.44. Another interesting feature in y is that there is a negative correlation of -0.62 between the corrected y center of gravity value and θ, which makes sense because we are using θ to correct y.

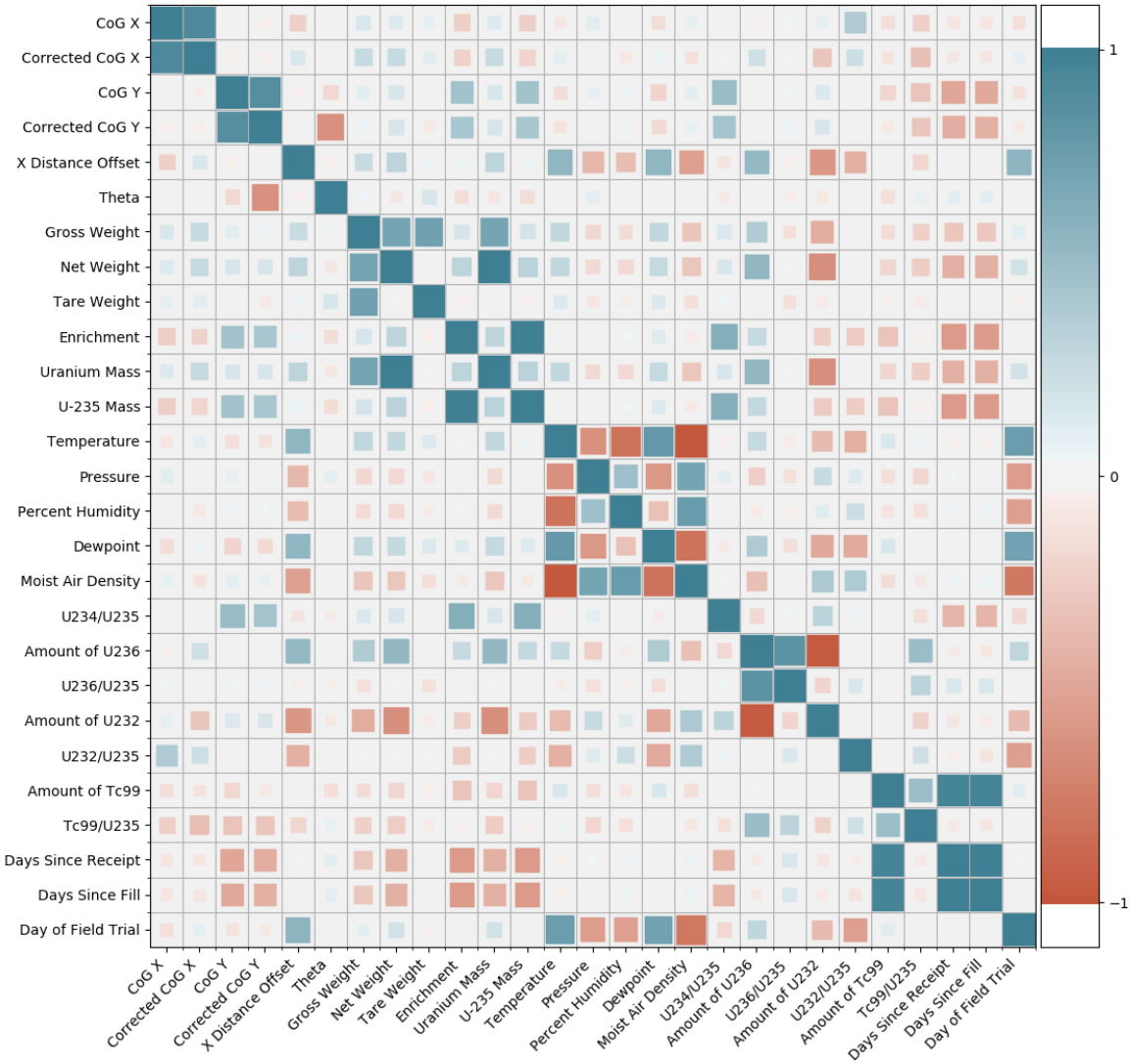


Figure 6.9: Heat map of correlations of known quantitative cylinder parameters

Overall, the results of the correlation study are as expected based on the literature review. It would be concerning, for instance, if there were a strong correlation between the center of gravity and the enrichment because the material distribution should be related to the method used to fill the cylinder, which should be completely independent of the enrichment of the uranium inside the cylinder. The only scenario this might not apply to is if this study included a population of both 30B and 48Y cylinders and the processes used to fill the cylinders were different.

It is, however, interesting that there is not at least a weak correlation between the center of gravity and the day of the field trial (standing in as a proxy for the time of year) or the ambient temperature during the measurement. This could be because material movement due to sublimation and subsequent desublimation is mostly caused by radiative heating from the sun, and so would be highly dependent on the storage orientation and location in the cylinder yard. If the cylinders in the yard were stored in different orientations, this change would manifest as a greater dispersion of the center of gravity values for certain times of year rather than the values trending in a certain direction based on the time of year. Alternatively, this could be because material movement is mostly caused by operators during cylinder handling. This will be explored further in the next section.

6.4.2 Center of Gravity Values at Different Temperatures

This section investigates whether the dispersion of cylinder center of gravity data has any relationship with the ambient temperature. To perform this investigation, the full population of cylinders was segregated into four equal populations based on the ambient temperature when the cylinder was measured. The resulting standard deviation in x and y for each subpopulation was then calculated to understand the dispersion of the data.

Figure 6.10, 6.11, 6.12, and 6.13 show plots of the center of gravity in x and y for each of the four slices of temperature. Comparing the coldest set of data in Fig. 6.10 to the warmest set of data in Fig. 6.13 is particularly interesting. The data set just by visual

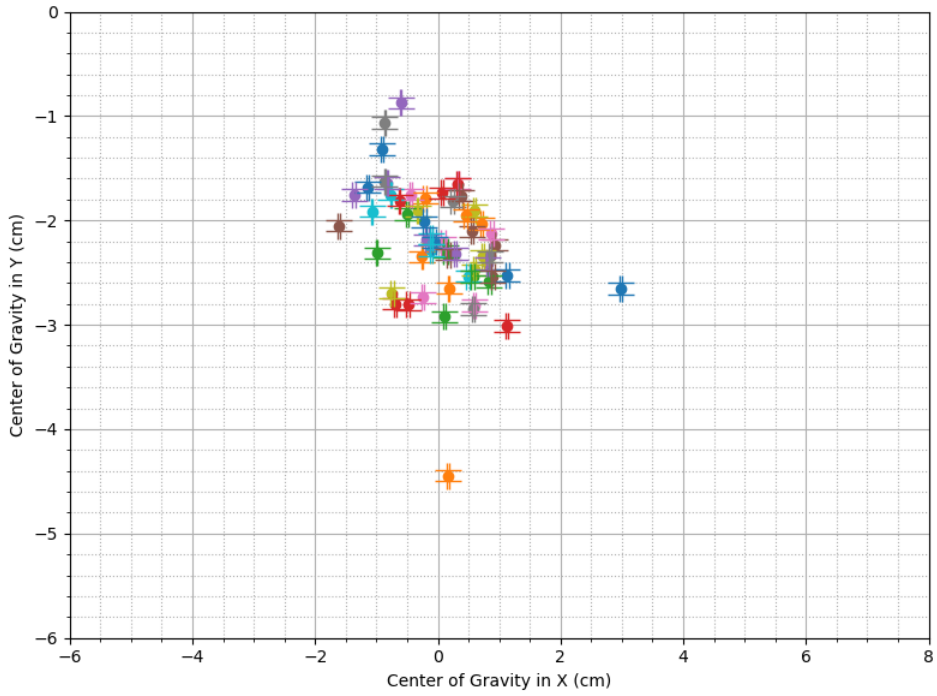


Figure 6.10: Center of gravity in x and y for temperatures from -3.0 to 13.0°C

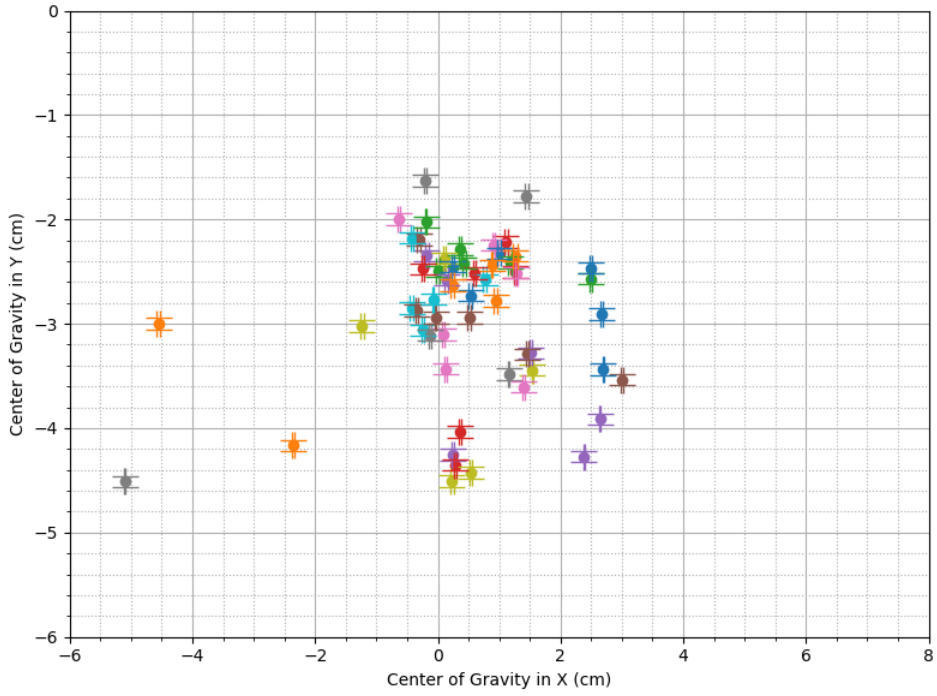


Figure 6.11: Center of gravity in x and y for temperatures from 13.0 to 21.0°C

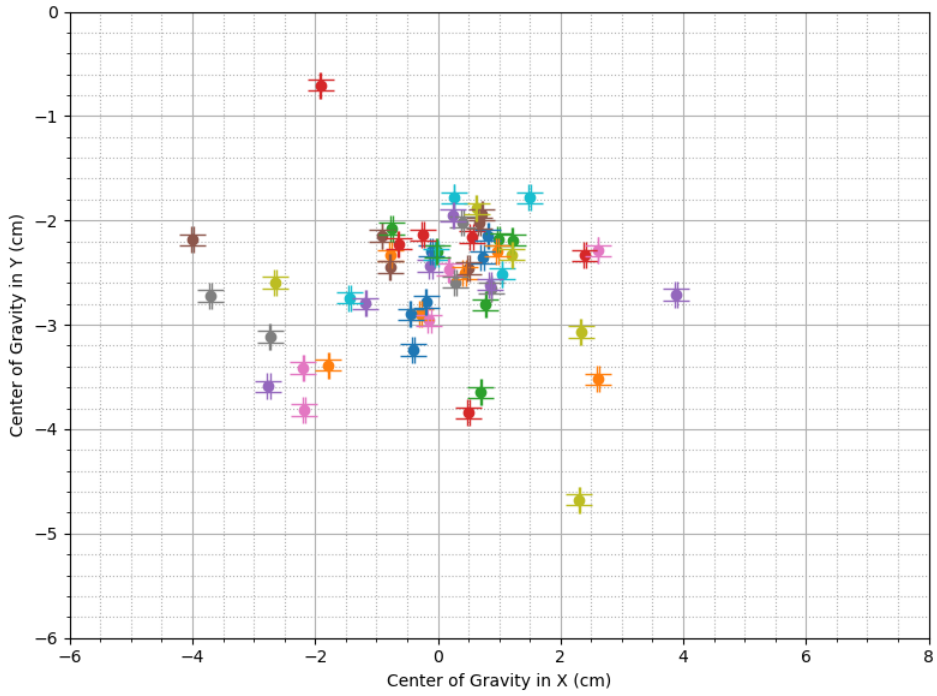


Figure 6.12: Center of gravity in x and y for temperatures from 21.0 to 27.0°C

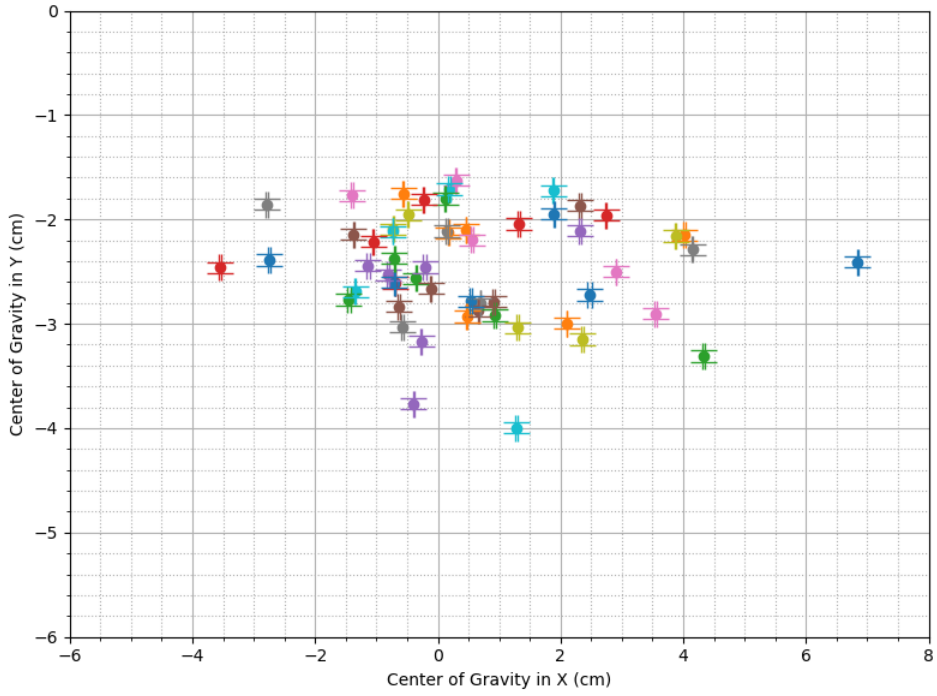


Figure 6.13: Center of gravity in x and y for temperatures from 27.0 to 41.0°C

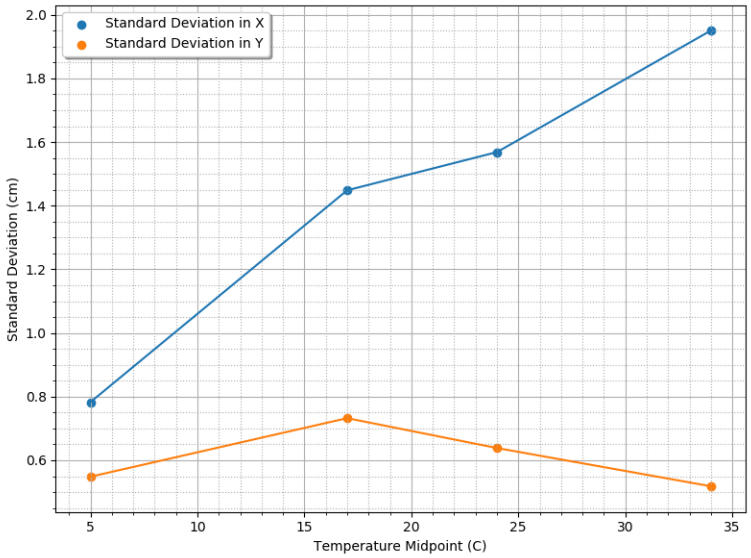


Figure 6.14: Standard deviation in x and y plotted versus the temperature midpoint for each subpopulation

inspection appears to be much more dispersed in x for the warmest subpopulation of data compared to the coldest.

The calculated standard deviation values for each of these subpopulations support this observation. Figure 6.14 shows how the standard deviation values change for each of the subpopulations. This analysis supports the visual observation that data gradually becomes more dispersed in x as the temperature increases, but interestingly that is not the case for y.

These results support the notion that the center of gravity of a cylinder seems to be influenced by the sublimation and desublimation of the UF_6 within the cylinder. The ambient temperature of a cylinder during its measurement may not be a perfect indicator of the internal temperature within a 30B cylinder on a given day, but it is reasonable to stipulate that as this temperature increases, a cylinder is more likely to be subjected to internal temperatures that would allow for UF_6 inside the cylinder to change state. Also, these results do not rule out the possibility that the material distribution inside the cylinder might also be changing because of routine operator handling.

Chapter 7

Conclusion

Uranium hexafluoride (UF_6) has been the chemical form of uranium used in the nuclear fuel cycle since the inception of the industry, and since 1971 an ANSI standard has defined the requirements for different kinds of storage cylinders for this material. The nuclear community has continued to speculate about the behavior of the UF_6 inside storage cylinders over time. Answering this question is not easily done because of the special handling requirements of UF_6. In particular, the violent reaction of UF_6 with water makes accessing the inside of a cylinder with a camera or other object to examine the material distribution complicated, time-consuming, and expensive.

It is generally accepted that the initial distribution of UF_6 inside a cylinder is highly dependent on the method used to fill the cylinder. Filling a cylinder with liquid UF_6 and allowing it to cool will generally result in most of the solid UF_6 crystals forming on the very bottom of the cylinder, with a very thin layer forming on the wall to the height that the cylinder was filled with liquid. On the other hand, filling a cylinder with gaseous UF_6 will typically result in an annular ring of UF_6 around the entire cylinder. This ring is then thought to gradually fall apart as the cylinder is handled, with a majority of material collecting at the bottom of the cylinder. Most of the questions about the behavior of UF_6 inside the cylinders relate to what happens to the material while the cylinders are stored outdoors in cylinder yards and are subject to wide swings in ambient temperature and radiative heating from the sun over the course of a year.

This work has sought to provide insight into the behavior of UF_6 inside 30B cylinders by using a weight measurement system with individually instrumented load cells to measure the center of gravity of the cylinder in two dimensions, x and y. A weighing system was chosen for this work because these systems are commonly used in nuclear facilities to perform weight measurements for nuclear material accountability or process control and monitoring, so it was easier to gain operator acceptance to collect this kind of data on 30B cylinders.

Weighing systems are commonly used to calculate the center of gravity of an object being measured in industries that need to predict the performance of a system that is in motion. Common applications include measuring the center of gravity of a truck pulling a load to understand how it will handle in an accident scenario, calculating the center of gravity and other parameters to understand aircraft performance at various phases of a flight, and calculating the center of gravity to aid in properly configuring a wheelchair for a medical patient.

The load cells used in this work are digital compression style load cells that measure the force applied using a strain gauge. A strain gauge is an instrument that can measure the deformation of an elastic material under stress using a thin foil resistor. The applied stress will lead to very small changes in resistance that can be quantified using a Wheatstone bridge circuit. In digital load cells, that response is then converted to a digital value and transmitted to a weight indicator.

The force applied to each individual load cell can then be used to calculate the center of gravity by treating each load cell as a point location in a discrete system. This approach was tested in a controlled laboratory setting using a mock 30B cylinder with a cutaway that allowed for known weight standards to be loaded at various locations. Data from testing with this system showed good agreement with a mathematical model that relied on the discrete system approach for calculating the center of gravity.

Laboratory testing also revealed that changes in the rotation of the cylinder under measurement can add a systematic bias to the y center of gravity value. This systematic bias would complicate any comparisons between cylinders. As a result of this, a correction

factor for the rotational angle of a cylinder was derived using a mathematical model of a 60% full UF_6 cylinder.

The experimental data set used for this work contains 240 measurements of 30B cylinders over 4 months in ambient temperatures that ranged from -9 °C to 41 °C. All of these cylinders were regularly stored outside and therefore subject to a range of weather conditions including rain, high winds, and snow/ice.

Controlling sources of experimental uncertainty was particularly important for this work because there was no way to gain ground truth knowledge of the distribution of UF_6 inside the 30B to compare measured values against. Potential sources of error for the platform scale include uncertainties associated with the force transducer, differences in how cylinders are placed on the scale, and random uncertainty from the electronics taking the measurement. Controls for these sources of uncertainty included collecting data on each cylinder for 1 min. and averaging the results, using engineering controls to limit the variability in cylinder positioning and capturing data to correct for any variability that could not be controlled, and propagating random uncertainties through all of the calculations used to find center of gravity values.

Another challenge is the fact that there is no way to deconvolve the center of gravity of the UF_6 cylinder from the center of gravity of the 30B cylinder itself without taking two measurements: one with the filled cylinder and one with just the 30B cylinder after it is washed. This was operationally infeasible during this data collection effort. In lieu of this, a small set of empty and heeled cylinders were measured to start to examine what the center of gravity of a 30B cylinder by itself might be. This data set was too small to gain any overarching understanding of the center of gravity of 30B cylinders or build any sort of empirical correction factor for full cylinders, but it did indicate that empty cylinders tend to have a center of gravity toward the front nameplate end of the cylinder, which is intuitively true because 30B cylinders have a larger steel lip on the front nameplate end of the cylinder than on the back.

One way to study the behavior of UF_6 inside the cylinder while reducing the impact of the 30B cylinder center of gravity is to take repeated measurements of the exact same cylinder over a long period of time. This work included repeat measurements

on five cylinders. One cylinder was measured repeatedly over 45 min. to establish an understanding of the random uncertainty of a center of gravity measurement on a 30B cylinder, whereas the other four cylinders were periodically measured over 4 months. The long term measurements from this population showed statistically significant movement of nuclear material over the 4 months.

The rest of the cylinders measured by the platform scale were only measured one time. These cylinders were used to determine whether there were any correlations between the cylinder center of gravity and attributes of the cylinder (e.g., enrichment, weight, fill date, etc.). This examination showed no strong correlations between the center of gravity of a cylinder and any attribute of the cylinder.

This large population was also used to try and determine whether or not changes in temperature might tend to cause center of gravity values to be more dispersed across the measurement population. To test this, the measured cylinders were separated into subpopulations based on the ambient temperature at the time of measurement. The standard deviation of the center of gravity in x and y for each subpopulation was then calculated. The results demonstrated that center of gravity values, particularly in x, are more highly dispersed as temperatures increase. This supports the theory that sublimation and desublimation resulting from the ambient temperature and radiative heating from the sun is a contributor to UF_6 material movement inside the cylinder when it is sitting outside in a storage yard.

7.1 Recommendations and Future Work

There are several ways that this type of work could be improved to provide more definitive results in the future. These recommendations include suggestions for changing the platform scale to reduce sources of systematic error, recommendations on other devices to include in any future measurement campaign to provide additional information on the behavior of UF_6, and suggestions on additional data sets that would help improve the conclusions from this work.

The main uncontrolled source of systematic error in this work was the level of the scale. An unleveled scale changes the force vector that is applied by the object being measured, which results in a bias to the measured center of gravity. Commercial leveling systems for scales exist and could be installed into the platform scale to help correct for any leveling issues.

Center of gravity data would be able to provide more definitive conclusions on the causes of material movement inside of the UF_6 cylinder if it were paired with another set of sensors attached to the UF_6 cylinders being measured. The goal of the sensors on the UF_6 cylinders would be to measure ambient weather conditions, light level, and motion of the cylinder over time. This information, coupled with repeated measurements on the platform scale, would allow for a better exploration of whether sublimation and desublimation inside the cylinder or operator handling tends to cause more material movement.

There are also some supplemental data sets that would improve the conclusions from this work. The most important set of data to collect would be measurements on a larger population of empty 30B cylinders. This kind of data would be useful for improving the conclusions from this work and could potentially be used to create a method to remove the empty cylinder contribution to the measured full cylinder center of gravity. This, in turn, would allow for a more in-depth analysis of the data collected in this work as well as any data collected in the future.

The other data set that would be very interesting to collect in the future would be one that included 48Y cylinders. Data exploring the material distribution on these cylinders has yet to be collected for a large population, so anything that leads to understanding about UF_6 behavior in a 48Y cylinder would be of benefit to the nuclear field.

Bibliography

[1] "Nuclear materials: Uranium hexafluoride, packagings for transport," ANSI Standard n14.1-2012, American National Standards Institute, 11 West 42nd Street, New York, NY 10036, Mar. 2012. viii, ix, 1, 8, 9, 10, 11, 16, 62

[2] "UF_6 phase diagram." https://web.evs.anl.gov/uranium/guide/prodhand/sld022.cfm. Accessed: 2019-08-03. ix, 2

[3] "UF_6 crystals in a glass vial." https://web.evs.anl.gov/uranium/guide/prodhand/images/DUF6PH19.jpg. Accessed: 2019-09-03. ix, 6

[4] "Video: The inside story (of a depleted uranium hexafluoride cylinder)." https://web.evs.anl.gov/uranium/guide/video/inside.cfm. Accessed: 2019-09-09. ix, 12, 13, 14, 15, 52

[5] R. D. McElroy, P. Hausladen, M. A. Blackston, and S. Croft, "UF_6 cylinder imaging by fast neutron transmission tomography," tech. rep., Oak Ridge National Laboratory (ORNL), Oak Ridge, TN (United States), 2014. ix, 16, 17

[6] R. Berndt, E. Franke, and P. Mortreau, "^{235}U enrichment or UF_6 mass determination on UF_6 cylinders with non-destructive analysis methods," *Nuclear Inst. and Methods in Physics Research, A*, vol. 612, no. 2, pp. 309–319, 2010. ix, 17, 18, 19, 52

[7] A. Fainberg, D. Gordon, E. Dermendjiev, D. Terrey, and R. Mitchell, "A portable load-cell based system for weighing UF_6 cylinders," IAEA-SM-260, Brookhaven National Laboratory, International Atomic Energy Agency, U.S. National Bureau of Standards, Nov. 1982. ix, 23

[8] R. Boynton, "Measuring weight and all three axes of the center of gravity of a rocket motor without having to re-position the motor," in *61st Annual Conference of the Society of Allied Weight Engineers*, (81 Fuller Way, Berlin, CT 06037 USA), May 2000. x, 26, 27, 28, 37, 63

[9] "UF_6 cylinder identification," WNTI Standard, World Nuclear Transport Institute, 2017. x, 31

[10] "Uranium hexafluoride: A manual of good handling practices," USEC-651 Rev. 7, United States Enrichment Corporation, Jan. 1995. 5, 6, 7, 8, 12, 16, 22, 47

[11] R. G. Cochran, E. E. Lewis, N. Tsoulfanidis, and W. Miller, *The nuclear fuel cycle: Analysis and management*. American Nuclear Society, 1990. 5

[12] J. Shoemaker, "Safety-related events at U.S. gaseous diffusion plants," in *Conference Proceedings for Uranium Hexafluoride-Safe Handling, Processing and Transporting*, pp. 37–46, May 1988. 5, 6, 7, 8

[13] M. Rao, A. Ellis, and D. Freels, "Characterization of the internal surfaces of two emptied 30A UF_6 storage cylinders," tech. rep., Oak Ridge K-25 Site, TN (United States), 1993. 7, 62

[14] H. Bayer and T. Grillenberger, "UF_6 release in a German fuel fabrication plant," in *Conference Proceedings for Uranium Hexafluoride-Safe Handling, Processing and Transporting*, pp. 61–65, May 1988. 7

[15] "Availability of uranium feed for the fissile materials disposition program," ORNL/TM-13417, Oak Ridge National Laboratory, Oak Ridge, TN 37831-6285, Nov. 1997. 10

[16] "American national standard for nuclear materials: Uranium hexafluoride, packagings for transport," ANSI Standard N14.1-2001, American National Standards Institute, 11 West 42nd Street, New York, NY 10036, Feb. 2001. 10

[17] B. Broadhead, "Criticality safety review of 2 1/2-, 10-, and 14-ton UF_6 cylinders," ORNL/TM-11947, Oak Ridge National Laboratory, Oak Ridge, TN 37831-6285, Oct. 1991. 14

[18] "Uranium hexafluoride: Handling procedures and container criteria," oro-651, rev. 3, Oak Ridge Operations Office, Oak Ridge, TN, Aug. 1972. 16

[19] A. A. Orlov, A. F. Tsimbalyuk, and R. V. Malyugin, "Desublimation for purification and transporting UF_6: Process description and modeling," *Separation & Purification Reviews*, vol. 46, no. 1, pp. 81–89, 2017. 16

[20] J. M. Whitaker, “Uranium enrichment plant characteristics: A training manual for the IAEA,” ORNL/TM-2005/43, Oak Ridge National Laboratory, Oak Ridge, TN 37831-6285, May 2005. 16

[21] “Enrichment process.” https://urenco.com/about/nuclear-fuel-supply-chain/enrichment-process. Accessed: 2019-09-10. 16

[22] P. A. Hausladen, M. A. Blackston, J. A. Mullens, S. McConchie, J. T. Mihalczo, P. R. Bingham, M. N. Ericson, and L. Fabris, “Induced-fission imaging of nuclear material,” in *INMM 51st Annual Meeting*, pp. 1–10, 2010. 16

[23] K. A. Miller, H. O. Menlove, M. T. Swinhoe, and J. B. Marlow, “The passive neutron enrichment meter for uranium cylinder assay,” tech. rep., Los Alamos National Laboratory (LANL), Los Alamos, NM (United States), 2011. 17

[24] S. Kiff, E. Brubaker, M. Gerling, P. Marleau, and W. Mengesha, “Using fast neutron signatures for improved UF_6 cylinder enrichment measurements,” SAND2013-8112, Sandia National Laboratory, P.O. Box 969, MS9406, Livermore, CA 94551-0969, Sept. 2013. 17

[25] K. Miller, H. Menlove, M. Swinhoe, and J. Marlow, “Technical assessment of the passive neutron enrichment meter (PNEM) for an unattended cylinder verification station (UCVS),” LA-UR-13-22913, Los Alamos National Laboratory, Apr. 2013. 18

[26] J. Jo, “Radio frequency identification devices: Effectiveness in improving safeguards at gas-centrifuge uranium-enrichment plants,” in *Institute of Nuclear Materials Management Conference in Tucson, AZ*, (P.O. Box 5000, Upton, NY 11973-5000), Feb. 2013. 20, 21

[27] R. D. Snow, J. R. Garner, and J. M. Whitaker, “Developing load cell monitoring on the mock UF_6 feed and withdrawal system,” ORNL/TM-2013/34, Oak Ridge National Laboratory, Oak Ridge, TN 37831-6285, Feb. 2013. 20

[28] J. Garner and M. Whitaker, "A Monte Carlo analysis of weight data from UF_6 cylinder feed and withdrawal stations," in *Institute of Nuclear Materials Management Annual Meeting*, (P.O. Box 2008, MS6315, Oak Ridge, TN 37831-6315), July 2015. 20

[29] J.-M. Reneaud, "UF_6 overfilling prevention at eurodif production," in *Second International Conference Proceedings for Uranium Hexafluoride Handling*, (Georges Besse Plant, Pierrelatte, France), pp. 63–71, Oct. 1991. 20

[30] "Manual on safe production, transport, handing and storage of uranium hexafluoride," IAEA-TECDOC-771, International Atomic Energy Agency, Nov. 1994. 20

[31] "Urenco: Virtual tour." https://urenco.com/about/tours. Accessed: 2019-10-05. 20, 22

[32] U.S. NRC, "10 CFR Part 74: Material control and accounting of special nuclear material." U.S. Code of Federal Regulations. 20

[33] U.S. NRC, "Nuclear material control and accountability: Records and reporting." https://www.nrc.gov/materials/fuel-cycle-fac/nuclear-mat-ctrl-acctng.html. Accessed: 2019-10-05. 21

[34] U. NRC, "Regulatory guide rg 5.41: Shipping, receiving, and internal transfer of special nuclear material at fuel cycle facilities," May 2017. 21

[35] N. C. Rowe, P. Fitzgerald, M. D. Laughter, R. Martyn, D. Richardson, C. A. Pickett, J. R. Younkin, and A. M. Shephard, "Authentication and interpretation of weight data collected from accountability scales at global nuclear fuels," in *INMM Pacific Northwest Chapter: Northwest International Conference on Global Nuclear Security – The Decade Ahead*, (Oak Ridge, TN 37830), Apr. 2010. 21

[36] J. Cooley and T. Huxford, "Development of a 20 ton capacity load cell based weighing system for iaea field use," in *Conference Proceedings for Uranium Hexafluoride-Safe Handling, Processing and Transporting*, pp. 75–80, May 1988. 23

[37] M. M. Curtis and D. R. Weier, “Testing the floor scale designated for pacific northwest national laboratory’s UF_6 cylinder portal monitor,” tech. rep., Pacific Northwest National Laboratory (PNNL), Richland, WA (United States), 2009. 24

[38] G. Previati, M. Gobbi, and G. Mastinu, “Improved measurement method for the identification of the centre of gravity location and of the inertia tensor of rigid bodies,” in *ASME 2008 International Design Engineering Technical Conferences and Computers and Information in Engineering Conference*, pp. 841–850, American Society of Mechanical Engineers Digital Collection, 2009. 24, 26, 28, 29

[39] S. Malaek and B. Soltan-Mohammed, “Mass distribution management and dynamic balancing of aircraft mass,” *Aircraft Design*, vol. 4, no. 1, pp. 51–61, 2001. 24, 25, 37, 40

[40] “Military specification: Flying qualities of piloted airplanes,” MIL-F-8785C, Nov. 1980. 25

[41] C. K. Nance, “Aircraft weight and center of gravity indicator,” May 1993. US Patent 5,214,586. 28

[42] “Load cell accuracy in relation to the conditions of use,” technical note vpgt-02, VPG Transducers, Jan. 2015. 28, 56, 58

[43] Y. Mikata, M. Yamanaka, K. Kameoka, A. Okunosono, and T. Kinoshita, “Measuring the center of gravity with truck scale,” in *SICE Annual Conference 2011*, pp. 405–410, IEEE, 2011. 28

[44] E. D. Lemaire, M. Lamontagne, H. W. Barclay, T. John, and G. Martel, “A technique for the determination of center of gravity and rolling resistance for tilt-seat wheelchairs,” *J Rehabil Res Dev*, vol. 28, no. 3, pp. 51–58, 1991. 28

[45] L. Tang and W.-B. Shangguan, “An improved pendulum method for the determination of the center of gravity and inertia tensor for irregular-shaped bodies,” *Measurement*, vol. 44, no. 10, pp. 1849–1859, 2011. 29

[46] K. Buck, "Analog or digital load cells?." https://www.carltonscale.com/analog-digital-load-cells/, Dec. 2017. Accessed: 2019-10-26. 32, 33

[47] I. Muller, R. M. de Brito, C. E. Pereira, and V. Brusamarello, "Load cells in force sensing analysis—theory and a novel application," *IEEE Instrumentation & Measurement Magazine*, vol. 13, no. 1, pp. 15–19, 2010. 33

[48] K. Hoffmann, *Applying the Wheatstone bridge circuit*. HBM Germany, 1974. 33, 34

[49] "Standard practices for calibration and verification for force-measuring instruments," ASTM E 74-18e1, ASTM International, West Conshohocken, PA, 2018. 35, 55

[50] J. R. Taylor, *Classical mechanics*. University Science Books, 2005. 35

[51] "80/20 Inc." https://8020.net/. Accessed: 2019-11-02. 37

[52] A. L. Ruina and R. Pratap, *Introduction to statics and dynamics*. Pre-print for Oxford University Press, 2002. 47

[53] "Circular segment." http://mathworld.wolfram.com/CircularSegment.html. Accessed: 2019-11-10. 48

[54] T. Bartel, "Uncertainty in NIST force measurements," *Journal of research of the National Institute of Standards and Technology*, vol. 110, no. 6, p. 589, 2005. 55, 56, 57, 58

[55] R. Boynton, "The seven secrets of accurate mass properties measurements," in *51st Annual Conference of the Society of Allied Weight Engineers*, (81 Fuller Way, Berlin, CT 06037 USA), May 1992. 56

[56] J. Schindelin, I. Arganda-Carreras, E. Frise, V. Kaynig, M. Longair, T. Pietzsch, S. Preibisch, C. Rueden, S. Saalfeld, B. Schmid, *et al.*, "Fiji: an open-source platform for biological-image analysis," *Nature Methods*, vol. 9, no. 7, p. 676, 2012. 60

[57] "sklearn MinMaxScaler." https://scikit-learn.org/stable/modules/generated/sklearn.preprocessing.MinMaxScaler.html. Accessed: 2019-11-12. 78

Appendix

A Detailed Plots of Repeated Cylinder Measurements

This appendix shows detailed plots of the five 30B cylinders filled with UF_6 which were repeatedly measured by the platform scale system. This population includes one cylinder that was measured multiple times in short succession as well as four cylinders that were measured periodically over about four months.

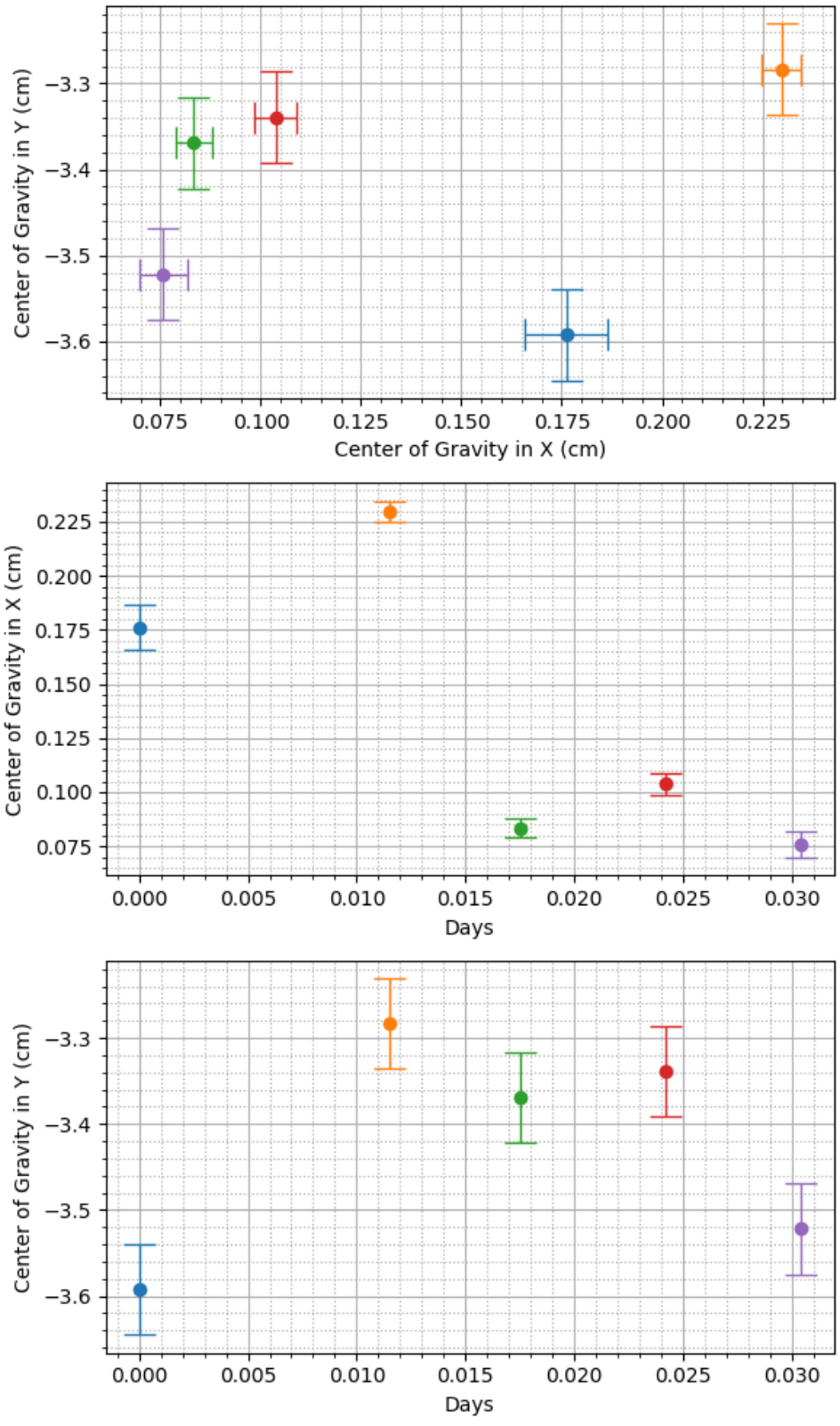


Figure A.1: Short-term repeat measurements of cylinder 13

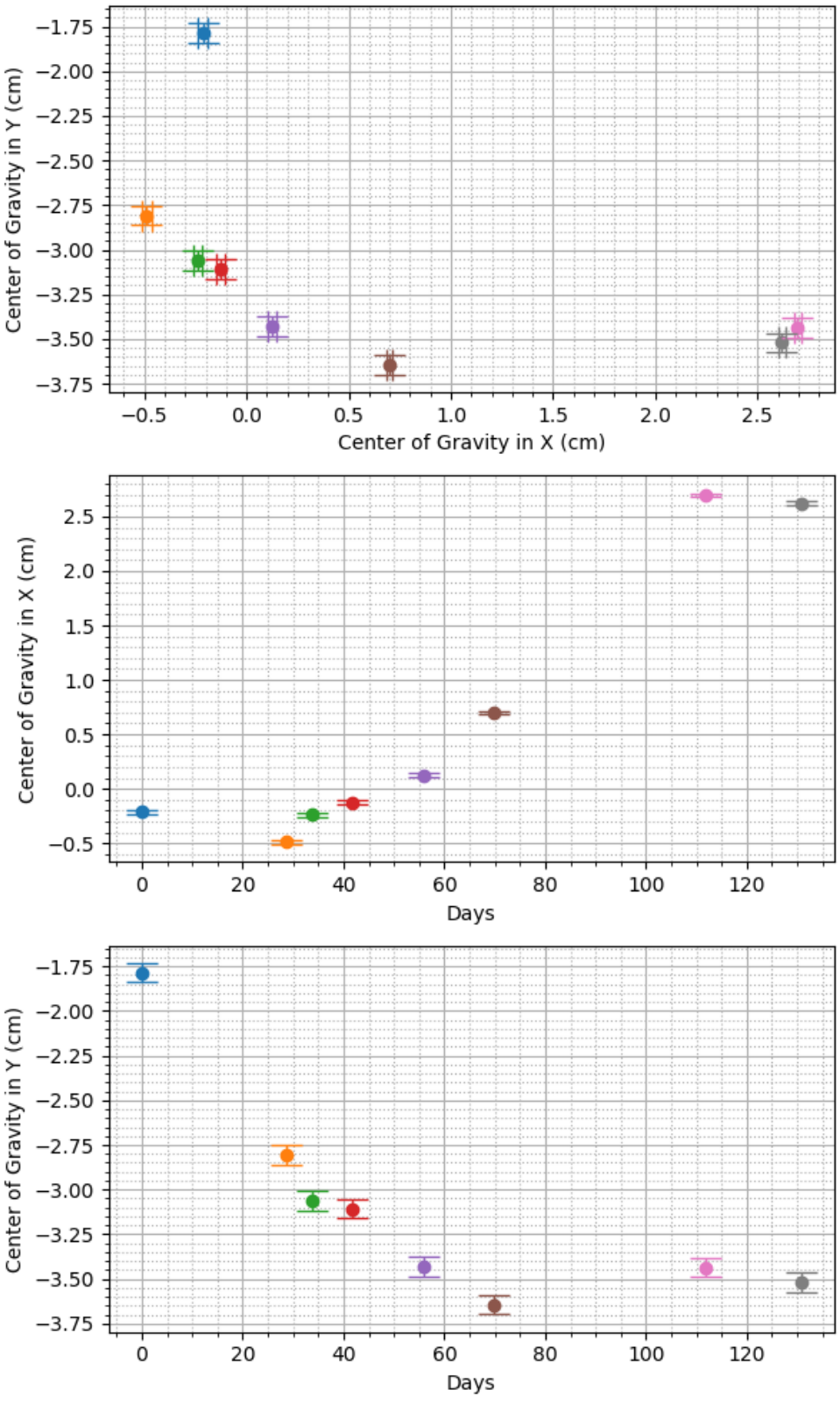


Figure A.2: Long-term repeat measurements of cylinder 26

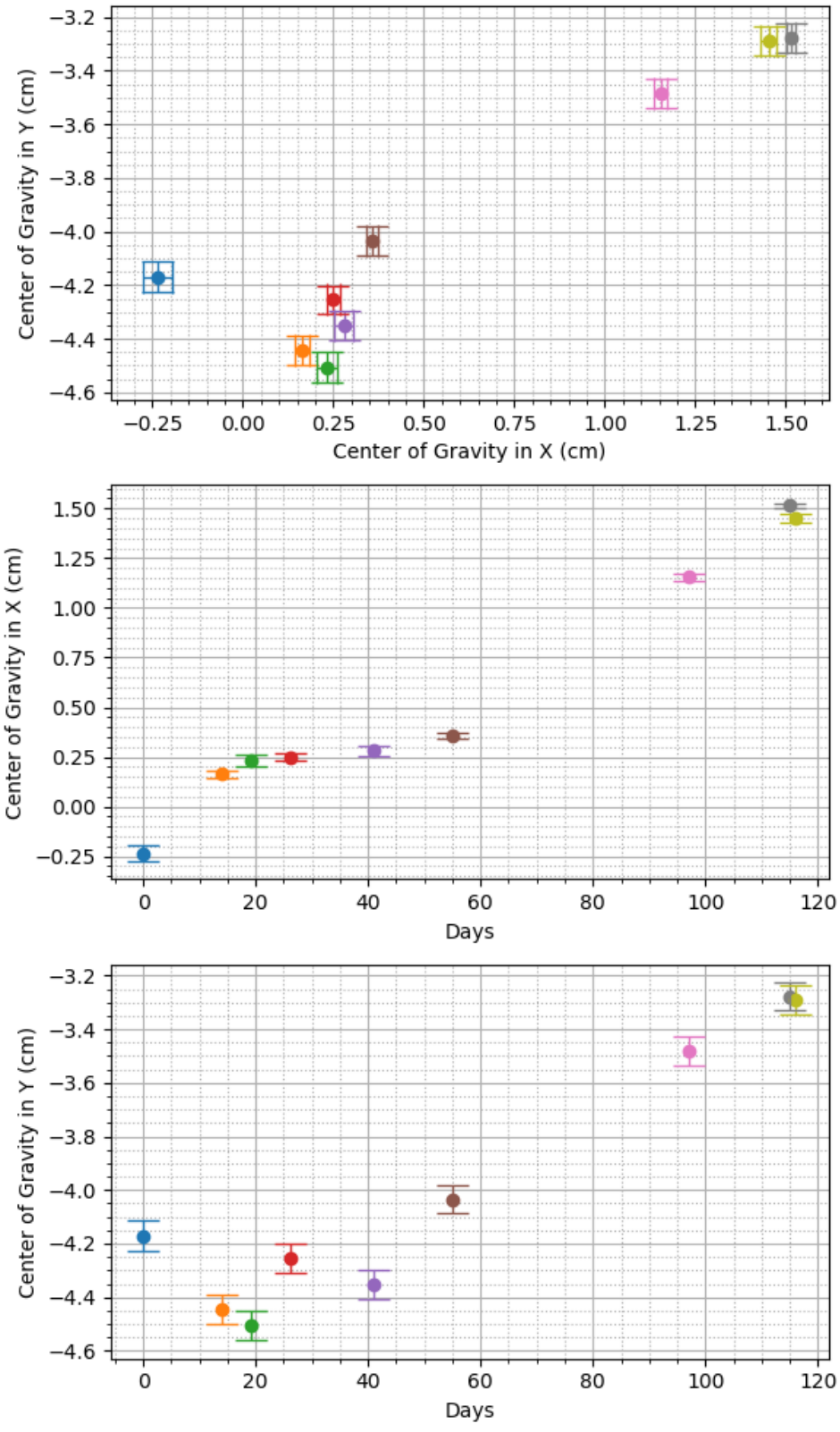


Figure A.3: Long-term repeat measurements of cylinder 65

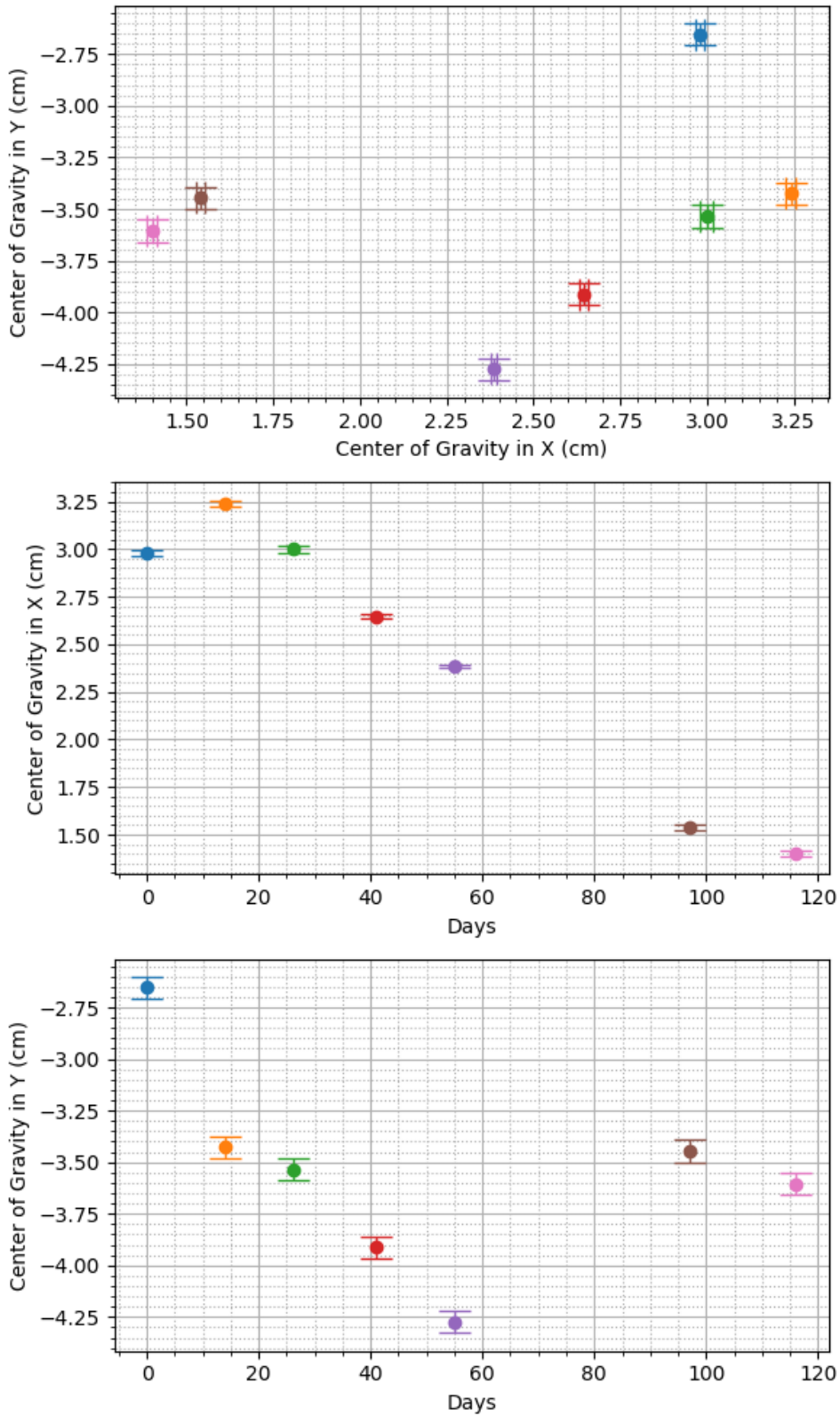


Figure A.4: Long-term repeat measurements of cylinder 66

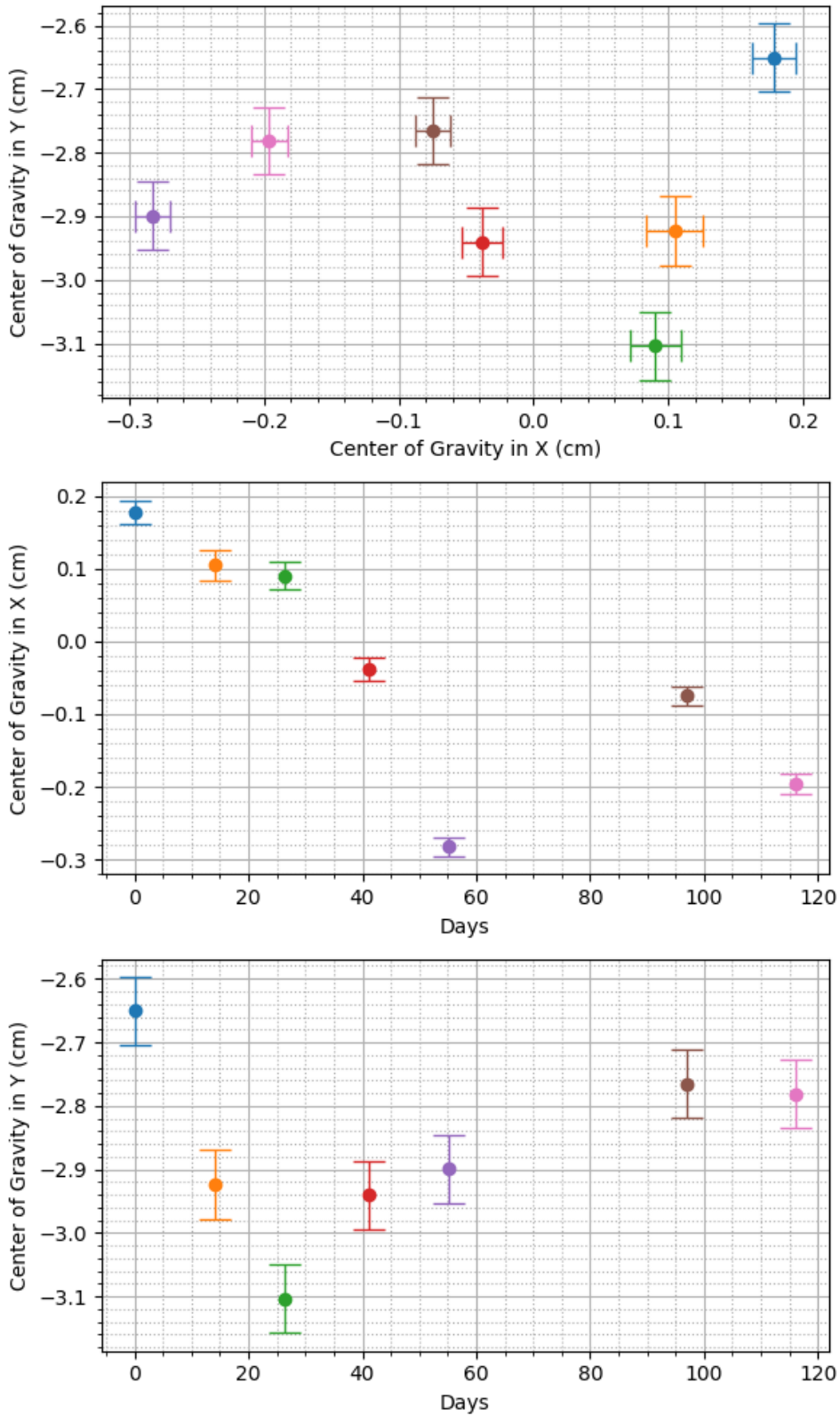


Figure A.5: Long-term repeat measurements of cylinder 67

Vita

Scott Stewart was born in 1989 to Darrell and Anita Stewart in Austin, Texas, and was raised in San Antonio, Texas. He attended Abilene Christian University in Abilene, Texas where he was selected as a Presidential Scholar. Scott graduated Magma Cum Laude from Abilene Christian with a Bachelors of Science in Physics with a minor in Public Service in 2011.

Scott was very involved in community initiatives in Abilene while studying for his undergraduate degree. This including working with local community organizations to build relationships between the university and underserved neighborhoods nearby. These efforts led to Scott receiving an award from the Breakfast Optimist Club as an Exemplary Student Leader in Abilene in 2010.

Scott was also fortunate to be included in research very early in his career by the physics faculty at Abilene Christian. This began with a summer internship at Los Alamos National Laboratory in 2008 and led to Scott being recognized as a University Scholar at Abilene Christian in 2010. Largely due to these early research experiences, Scott was encouraged to attend Texas A&M University for graduate school.

While at Texas A&M, Scott studied and received his Masters of Science in Nuclear Engineering degree in 2013. His thesis research was conducted jointly with faculty at Texas A&M and staff members at Los Alamos National Laboratory and focused on the development of a Nuclear Arms Control treaty verification system that used correlated neutrons from a pulsed interrogation system.

While at Texas A&M, Scott applied and was selected for the National Nuclear Security Administration Graduate Fellowship Program Class of 2013. While a graduate program fellow, Scott supported the Federal Program Manager for the NNSA Nuclear Material

Control and Accountability (NMC&A) program, and aided the program manager with targeted initiatives to improve NMC&A programs across the NNSA.

After completing the fellowship program in 2014, Scott began working at Oak Ridge National Laboratory as a Post-Master's Research Associate. Scott's work while in this role focused on developing software for remote and unattended systems for measuring nuclear material. He was converted to a full time research staff member at Oak Ridge National Laboratory in 2015.

Scott applied and was accepted into the Bredesen Center at the University of Tennessee to start his working towards the completion of a Doctorate of Philosophy in Energy Science and Engineering in 2016. He has continued to work full time at the laboratory while pursing his Ph.D. Scott's research focus continues to be on developing remote and unattended systems for measuring nuclear material. The need for analyzing fairly large datasets out of these systems has also led Scott to begin to focus his research on applying modern data analytics approaches to problems in the nuclear field.

When not working, Scott and his wife, Elena, enjoy going out into the backcountry to camp or backpack when at all possible. Both also enjoy playing board games with friends and suffering through CrossFit workouts together.